mTOR REGULATES CD4 AND CD8 EFFECTOR T CELL DIFFERENTIATION VIA SERUM- AND GLUCOCORTICOID-REGULATED KINASE 1 (SGK1)

by

Emily B. Heikamp

A dissertation submitted to Johns Hopkins University in conformity with the requirements for the degree of Doctor of Philosophy

Baltimore, Maryland
March 2015

ABSTRACT

The AGC kinases comprise approximately 10% of mammalian kinases, and are broadly involved in regulating metabolism, survival and differentiation[1]. While much is known about S6 Kinase and Akt, the precise downstream targets and functions of other enzymes in this family have yet to be determined. Serum- and glucocorticoid-regulated kinase 1 (SGK1) is an AGC kinase that plays a role in regulating membrane sodium channel expression in renal tubular cells in response to increases in serum osmolarity in an mTORC2-dependent manner[2]. We hypothesized that SGK1 might represent a novel mTORC2-depednent downstream regulator of T cell differentiation and function. Here we show that SGK1 is a critical regulator of CD4+ effector differentiation into Th1 and Th2 subsets. Specifically, upon activation by mTORC2, SGK1 promotes Th2 differentiation by negatively regulating the NEDD4-2 E3 ligase mediated destruction of JunB. Simultaneously, SGK1 represses the production of IFN-γ by controlling the expression of the long isoform of TCF-1. Consistent with these functions, mice in which SGK1 has been selectively deleted in T cells fail to generate a robust Th2 response and are resistant to experimentally induced asthma. Likewise, such mice generate robust levels of IFN-γ in response to vaccines and more readily reject tumors. Loss of SGK1 in CD8+ T cells leads to inappropriate expression of memory markers such as CD127 and eomesodermin on effector cells, and subsequently may lead to enhanced memory differentiation. Overall these results reveal a novel role for SGK1 in promoting a signaling program that simultaneously enhances IL-4 production and inhibits IFN-γ expression. Given the ubiquitous expression of SGK1 in mammalian cells, these findings provide novel insight into the ability of AGC kinases to regulate cellular function in response to the environment.

References

1 Pearce, L. R., Komander, D. & Alessi, D. R. The nuts and bolts of AGC protein kinases. *Nat Rev Mol Cell Biol* 11, 9-22, doi:10.1038/nrm2822 nrm2822 [pii] (2010).

2 Naray-Fejes-Toth, A., Helms, M. N., Stokes, J. B. & Fejes-Toth, G. Regulation of sodium transport in mammalian collecting duct cells by aldosterone-induced kinase, SGK1: structure/function studies. *Mol Cell Endocrinol* 217, 197-202, doi:10.1016/j.mce.2003.10.043 S030372070300399X [pii] (2004).

Readers: Jonathan Powell, M.D., Ph.D., Charles Drake, M.D., Ph.D.

Thesis Committee: Jonathan Powell, M.D., Ph.D., Charles Drake, M.D., Ph.D., Jyoti Sen, Ph.D, and Ben Ho Park, M.D., Ph.D.

PREFACE & ACKNOWLEDGEMENTS

Foremost, I would like to thank my mentor Dr. Jonathan Powell, for his support, guidance, and enthusiasm. I credit him with my development as an immunologist, and I'm truly grateful for all that he has taught me.

I would also like to thank the members of my thesis committee, Dr. Charles Drake, Dr. Ben Ho Park, and Dr. Jyoti Sen, who helped focus my work with their intellectual contributions, support, and encouragement.

I would also like to thank Dr. Charles Drake for reading this dissertation and offering helpful comments.

I would also like to thank the current and former members of the Powell laboratory: Angela Alme, Olesya Chornoguz, Sam Collins, Yukan Duan, Robert Hagan, Chris Gamper, Chen-Fang Lee, Ying-Chun Lo, Orestes Mavrothalassitis, Christian Meyer, Rose Parkinson, Kristen Pollizzi, Adam Waickman, and Jiayu Wen. Our lab manager, Chirag Patel, has provided immense support in assisting with experiments.

I'd also like to acknowledge the Graduate Program in Immunology, the Medical Scientist Training Program (MSTP), and the School of Medicine for funding and support.

Finally, I'd like to thank my family, especially my mom & dad, for their unwavering support through all my years of education.

TABLE OF CONTENTS

List of Figures

Chapter 1

Chapter 2

Chapter 3

CHAPTER 1: Introduction

T lymphocytes—both CD4+ and CD8+ T cells—are the workhorses of the adaptive immune response[1]. One of the hallmarks of adaptive immunity is the exquisite specificity of the T cell receptor (TCR) for its cognate antigen. During T cell development, through the process of V(D)J recombination, the TCR genetic locus is stochastically rearranged to generate a diverse repertoire of antigen receptors that can recognize up to $1x10^9$ different pathogens[2]. Despite the exquisite specificity of the TCR for its cognate antigen, however, this interaction does not impart any instructive information to guide T cell differentiation. Upon encountering antigen, naïve T cells must differentiate into various distinct lineages (**Fig 1**)[3]. These subsets possess particular functional capabilities that endow the cell to respond to the pathogen; however, recognition of the pathogen alone does not provide information about which subset is necessary for a productive immune response.

The two signal model of antigen recognition

The two signal model of T cell recognition posits that the outcome of antigen recognition (signal 1) is determined by a second signal derived from an antigen presenting cell (APC)[4]. First proposed by Lafferty & Cunningham[5] and Bretscher & Cohn[6] in the 1970s, the two signal model has evolved along with our understanding of the inflammatory mileu and metabolic demands of the adaptive immune response. Signal 2 is the actually the sum of multiple inputs: both costimulatory and inhibitory signals, cytokine receptor signals, environmental cues, and the availability of nutrients[7,8]. Thus, T cells must coordinate multiple inputs to produce a singular output in order to dictate the outcome of antigen

recognition. There is a growing appreciation that this process of signal integration is carried out by an evolutionarily conserved serine-threonine kinase called mTOR[8,9].

The mechanistic target of rapamycin (mTOR) is a central node in an intracellular signaling network that receives multiple inputs from cytokines, costimulatory receptors, environmental cues, and metabolic demands[10]. While it has long been appreciated that cytokines influence the immune response, there is an emerging paradigm that cellular metabolism is inextricably linked to T cell differentiation[11]. In this model, mTOR is proving to be a vital link between metabolism and immune function. Beyond T lymphocytes, mTOR regulates multiple types of immune cells, including neutrophils, mast cells, natural killer cells, γδ T cells, macrophages, dendritic cells (DCs), and B cells[8,12,13]. This dissertation will focus on the role of mTOR in guiding fate decisions of both CD4+ and CD8+ T lymphocytes.

mTOR signaling

First discovered in yeast[14,15], the mTOR kinase is the core catalytic component of a signaling complex that plays a role in regulating cell growth, metabolism and survival[16]. The C-terminus of mTOR is composed of two N-terminal HEAT (huntington, elongation factor 3, subunit of PP2A, and TOR) domains, which mediate protein-protein interactions (**Fig 2**). The FRB domain is the binding site for the 12 kDa FK506-binding protein (FKBP12), which binds the macrolide drug rapamycin. Originally discovered in soil samples from Easter Island (the local name being *Rapa nui*), rapamycin was found to be a poor antibiotic[17]. However, this macrolide drug was found to have potent immunosuppressive properties. Numerous analogs of rapamycin have since been developed, but the most potent inhibitors of mTOR are those drugs that bind to the kinase domain. The mTOR serine-threonine

kinase catalytic domain lies C-terminal to the FRB site. mTOR kinase inhibitors, such as pp242 and Torin1, function as ATP-competitive inhibitors at the catalytic domain to specifically and potently inhibit mTOR signaling[18,19].

Yeast express two TOR genes which play a critical role in coupling the availability of nutrients with cell growth only under favorable environmental conditions[20]. Interestingly, in higher organisms TOR exists as one gene product which can signal via two distinct complexes, TORC1 and TORC2 (**Fig 3**)[10]. In mammalian cells, TORC1 is responsible for regulating cell growth, metabolism, and cap-dependent protein translation, while TORC2 regulates cellular functions such as actin reorganization and survival[21]. In some mammalian cell lineages such as lymphocytes of the immune system, the nutrient-sensing TOR pathway has been co-opted to perform highly specialized functions, such as the integration of multiple signals in the immune microenvironment to direct cellular differentiation. Various inputs in the form of nutrients, costimulation, and cytokines feed into the mTOR pathway. In a coordinated fashion, these cell extrinsic differentiation cues are integrated by mTOR, which in turn activates diverse downstream pathways to determine cell fate.

mTORC1 signaling

The mTORC1 signaling complex is formed when mTOR associates with a particular set of adaptor proteins (**Fig 2**). Some of these accessory proteins act as scaffolds to promote binding of other proteins, while others function as key regulators of the signaling complex. The mTORC1 complex is composed of regulatory-associated protein of mTOR (raptor), mammalian lethal with Sec13 protein 8 (mLST8), and the proline-rich Akt substrate 40 kDa (PRAS40)[22-24]. mTORC1 is activated by its association with the small GTPase Rheb (ras

homologue enriched in brain), which itself is negatively regulated by the tuberous sclerosis complex 1/2 (TSC1/2)[25,26]. The adaptor protein and DEP-domain-containing mTOR-interacting protein (Deptor) can also negatively regulate mTORC1 activity[27].

Activation of mTORC1 is regulated by upstream signals, including oxygen tension, the availability of nutrients, and the overall energy status of the cell (**Fig 3**). A high AMP/ATP ratio (indicating low energy status) activates AMPK, which in turn activates TSC1/2, leading to repression of mTORC1[28,29]. Hypoxia also activates AMPK and ultimately leads to decreased mTORC1 activity[30]. By contrast, the availability of essential amino acids leads to activation of mTORC1 through activation of the heterotrimeric GTPases RagA-D, which interact with Raptor to provide a docking site for mTORC1 at lysosomal membranes[31-33]. Additionally, mTORC1 activity can be induced via cytokine and growth factor induced signaling, which is mediated via phosphoinositide 3-kinase (PI-3K) activation.

Upon activation of mTORC1, mTOR phosphorylates p70-S6 Kinase, leading to the phosphorylation of ribosomal S6 protein which allows for enhanced protein translation[34]. Phosphorylation of 4E-BP1 by mTOR releases eIF4E to participate in cap-dependent translation by recruiting eIF4G to the 5' mRNA cap[35]. Along with increasing protein translation, mTORC1 activity also upregulates gene expression programs necessary for glucose and lipid metabolism, mitochondria biogenesis and inhibition of autophagy.

mTORC2 signaling

mTORC2 is composed of mLST8 in addition to the scaffolding protein rapamycin-independent companion of TOR (rictor), mammalian stress-activated

protein kinase interacting protein (mSIN1), and the protein observed with rictor (Protor) (**Fig 2**)[22,23]. Recently, two studies have described positive and negative upstream regulators of mTORC2 activity. While physical association of mTORC2 with ribosomes in a PI-3K dependent manner promotes mTORC2 kinase activity, ER stress can inhibit mTORC2 activity via glycogen synthase kinase 3β (GSK3β) (**Fig 3**) [36,37]. Activation of mTORC2 leads to phosphorylation and activation of a number of downstream AGC kinases including Akt, protein kinase C (PKC), and serum- and glucocorticoid- regulated kinase 1 (SGK1)[38-40].

AGC Kinase signaling

AGC kinases—named for their homology to cAMP dependent protein kinase A, cGMP dependent kinase G, and protein kinase C—are a family of highly conserved serine/threonine kinases[41]. S6 Kinase, Akt and SGK1 are all AGC kinases in the mTOR signaling network that have similar sequence motifs and domain structures. Each of these AGC kinases contains two regulatory domains: an activation or T-loop domain, and a hydrophobic motif[41]. Akt contains two additional regulatory domains, which include a turn motif and a pleckstrin homology (PH) domain. Constitutive phosphorylation of the turn motif occurs soon after Akt is synthesized, and this is thought to stabilize the protein and protect the hydrophobic motif from dephosphorylation[39]. The PH domain of Akt interacts with high affinity with hydrolyzed phospholipids, including phosphatidylinositol-3,4,5-triphosphate (PIP3) and its breakdown product phosphatidylinositol-3,4-bishosphate (PIP2)[42]. This interaction recruits Akt to the plasma membrane of the cell and induces a conformational change in the protein so it can be phosphorylated at its T loop domain by 3-phosphoinositide-dependent kinase 1 (PDK1)[43,44] . This phosphorylation at threonine 308 only partially activates Akt, but phosphorylation of the hydrophobic motif is necessary for

full activation. The hydrophobic motif of both Akt and SGK1 are phosphorylated by mTORC2 at serine 473 and 422, respectively. Like Akt, SGK1 is also phosphorylated by PDK1 at its T loop domain by PDK1.

While Akt and SGK1 are highly homologous, there are key differences in the way these enzymes are activated. In addition, Akt and SGK1 have partially overlapping but nonredundant functions and substrate specificities downstream of mTORC2. For example, the N-myc downregulated gene 1 (NDRG1) and the ubiquitin E3 ligase neural precursor cell expressed, developmentally down-regulated 4-2 **(**NEDD4-2) are both exclusive target of SGK1[44,45]. Since relatively more is known about Akt, there have been over 130 substrates identified for this AGC kinase[41]. On the other hand, Akt and SGK1 share some targets. For example, the forkhead box transcription factors (FOXO) are shared substrates of both SGK1 and Akt[46]. For example, Akt seems to favor phosphorylation of Foxo1 at serine 253, while SGK1 favors serine 315[46]. On the other hand, both Akt and SGK1 readily phosphorylate threonine 32 in Foxo1[46]. The different substrate specificities of Akt and SGK1 thus impart a unique functional repertoire to these AGC kinases downstream of mTORC2.

mTOR in the immune system

The immune microenvironment plays a critical role in directing the outcome of antigen recognition. By integrating multiple signals from the immune microenvironment, mTOR exists at the interface between extracellular signals and T cell fate decisions. Both mTORC1 and mTORC2 are activated downstream of TCR signaling, and the magnitude of activation is correlated with the duration of TCR stimulation and the dose of antigen[47]. Costimulatory

signaling from CD28 feeds into the mTOR pathway by activating PI-3K and Akt[48,49]. By contrast, negative regulators of TCR signaling, such as the programmed cell death protein 1 (PD1), inhibit mTOR signaling[50].

Given its central role in T cell metabolism and differentiation, deletion of mTOR at the double positive stage of T cell development using CD4-Cre does not disrupt T cell homeostasis[47]. Mice lacking mTOR have a normal compartment of naïve CD4+ and CD8+ T cells, as well as T regulatory (Treg) cells. Interestingly, loss of mTOR in CD4+ T cells results in an inability to differentiate to any of the T helper effector lineages (Th1, Th2, or Th17)[47]. Instead, cells lacking mTOR adopt a default regulatory phenotype[47]. The mTOR deficient T cells display constitutively high expression of FoxP3 and hyperphosphorylation of Smad3, even in the absence of exogenous TGF-β[47].

Subsequently we have employed genetic models to study the consequences of selectively ablating mTORC1 or mTORC2 activity in T cells[51]. To generate an mTORC1 knockout, we deleted the small GTPase Rheb in CD4 T cells (*T-Rheb-/-*)[51]. To generate an mTORC2 knockout, we deleted the adaptor protein Rictor in CD4 T cells (*T-Rictor-/-*)[51]. We found that *T-Rheb-/-* mice could not adopt a Th1 or Th17 phenotype [51]. In an experimental autoimmune encephalomyelitis model of disease (EAE), *T-Rheb-/-* mice were protected from the classical Th1/Th17-mediated autoimmune paralysis, but instead developed a Th2-mediated autoimmune cerebellar ataxia (atypical EAE). By contrast, *T-Rictor-/-* mice have defective Th2 differentiation, characterized by decreased IL4 production and diminished STAT6 phosphorylation[51]. Interestingly, deletion of either mTORC1 or mTORC2 activity

does not lead to an increase in T_{reg} differentiation, suggesting that both mTOR complexes must be inhibited in order to promote a regulatory cell fate[51].

In CD8+ T cells, several studies have shown that mTOR dictates effector versus memory differentiation[52-54]. Unpublished work from our laboratory using genetic mouse models suggests that mTORC1 is necessary for effector differentiation, while mTORC2 is necessary for memory differentiation. Studies using rapamycin have previously shown that mTOR inhibition can lead to both enhanced effector and memory differentiation[52]. In a mouse model of Lymphocytic Choriomeningitis Virus (LCMV), rapamycin was shown to increase the number of virus-specific CD8 T cells by promoting survival of memory T cells during the contraction phase of the immune response[52]. However, since prolonged exposure to rapamycin can inhibit both mTORC1 and mTORC2, it is unclear from these studies what is the mechanism underlying enhanced effector and memory generation.

There is still much work to be done in order to understand how signaling events downstream of mTOR regulate T cell differentiation and metabolism. We propose that differential signaling via mTORC1 and mTORC2 leads to the upregulation of distinct gene expression programs characteristic of a particular immune and metabolic phenotype. Our strategy has been to employ mouse genetic models to elucidate the role of each TOR complex in driving metabolic and fate decisions. More recently, we have become interested in kinases downstream of mTOR that are responsible for activating transcriptional networks to influence T cell fate.

The remainder of this dissertation will focus on one such protein that is activated downstream of mTORC2 called the serum- and glucocorticoid regulated kinase 1 (SGK1). Until recently, very little was known about the role of SGK1 in the immune system. The focus of this work will be on the role of SGK1 in CD4+ T cell differentiation into Th1 and Th2 subsets (**Chapter 2**) and the role of SGK1 in CD8+ T cell effector and memory differentiation (**Chapter 3**).

Figure Legends

Figure 1. CD4+ and CD8+ T cell differentiation. Upon TCR stimulation in the presence of costimulation, naïve CD4+ or CD8+ T cells differentiate into distinct various lineages. For CD4+ T cells, cytokines such as IFN-γ and IL-12 direct differentiation toward a Th1 phenotype, which is characterized by the lineage-spefici transcription factor Tbet and STAT4. Th2 differentiation occurs in the presence of IL-4, and this lineage is characterized by the GATA-3 and STAT6 transcription factors. Cytokines like IL-6 and TGF-β promote Th17 development, with expression of ROR-γT and STAT3. If CD4+ T cells are stimulated in the presence of TGF-β alone, however, these cells adopt a regulatory T cell fate (Treg), which is characterized by FoxP3 expression. For CD8+ T cells, differentiation can result in at least two distinct subsets: effector (T_{EFF}) and memory (T_{MEM}) cells. How these populations arise is controversial, but they can be distinguished phenotypically based on cell surface markers and transcription factor expression. While T_{EFF} are KLRG1HI, CD127low and express the transcription factor Tbet, T_{MEM} cells are KLRG1low, CD127 high and express the transcription factor eomesodermin.

Figure 2. Structure of mTOR, TORC1 and TORC2 signaling complexes. (A) mTOR is an evolutionarily conserved 289 kDA serine-threonine protein kinase that is composed of two N-terminal HEAT (huntington, elongation factor 3, subunit of PP2A, and TOR) domains, which mediate protein-protein interactions, adjacent to a FRAP, ATM, and TRRAP (FAT) domain. The FRB domain is where the small 12 kDa FK506-binding protein (FKBP12) bound to the macrolide drug rapamycin binds to mTOR to inhibit its activity. The mTOR Kinase catalytic domain lies C-terminal to the FRB site, and this is where mTOR kinase inhibitors bind. The Carboxy FAT domain maintains structural integrity of this large protein kinase. **(B)** mTOR associates with two distinct sets of adapter proteins to form two intracellular signaling complexes with unique substrate specificity. The TORC1 signaling complex is composed of the regulatory-associated protein of mTOR (raptor) and mammalian lethal with Sec13 protein 8 (mLST8), which are both adapter proteins that mediate protein-protein interactions via their WD-40 domains. The proline-rich Akt substrate 40 kDa (PRAS40) and DEP-domain-containing mTOR-interacting protein (Deptor) inhibit mTORC1 activity. The mTORC2 complex can also associate with Deptor and mLST8, but this complex is distinguished by the adapter protein raptor-independent companion of TOR (rictor) and protein observed with rictor (protor). Another unique component of mTORC2 is mSin1, which contains a plekstrin homology domain that is thought to target TORC2 to the membrane, where it can activate myristolated Akt.

Figure 3. Overview of the mTOR signaling pathway. The mammalian target of rapamycin (mTOR) associates with distinct sets of adaptor proteins to form the mTORC1 and mTORC2 signaling complexes. Growth factors, cytokines and comstimulation activate mTORC1 via PI3K activation, while amino acids activate the Ragulator complex (RagA-D).

Oxygen and energy availability control mTORC1 via the regulation of AMPK. The canonical downstream targets of mTORC1 include 4E-BP1 and S6 Kinase. mTORC2 is activated by its association with ribosomes and inhibited by endoplasmic reticulum (ER) stress. SGK1, PKC, and Akt are activated downstream of mTORC2, but Akt also negatively regulates TSC1/2 upstream of mTORC1.

References

1 Murphy, K., Travers, P., Walport, M. & Janeway, C. *Janeway's immunobiology*. 8th edn, (Garland Science, 2012).

2 Schatz, D. G. & Ji, Y. Recombination centres and the orchestration of V(D)J recombination. *Nat Rev Immunol* **11**, 251-263, doi:10.1038/nri2941 nri2941 [pii] (2011).

3 Yamane, H. & Paul, W. E. Early signaling events that underlie fate decisions of naive CD4(+) T cells toward distinct T-helper cell subsets. *Immunol Rev* **252**, 12-23, doi:10.1111/imr.12032 (2013).

4 Bretscher, P. A. A two-step, two-signal model for the primary activation of precursor helper T cells. *Proc Natl Acad Sci U S A* **96**, 185-190 (1999).

5 Lafferty, K. J. & Cunningham, A. J. A new analysis of allogeneic interactions. *Aust J Exp Biol Med Sci* **53**, 27-42 (1975).

6 Bretscher, P. & Cohn, M. A theory of self-nonself discrimination. *Science* **169**, 1042-1049 (1970).

7 Schwartz, R. H. Costimulation of T lymphocytes: the role of CD28, CTLA-4, and B7/BB1 in interleukin-2 production and immunotherapy. *Cell* **71**, 1065-1068, doi:S0092-8674(05)80055-8 [pii] (1992).

8 Powell, J. D., Pollizzi, K. N., Heikamp, E. B. & Horton, M. R. Regulation of immune responses by mTOR. *Annu Rev Immunol* **30**, 39-68, doi:10.1146/annurev-immunol-020711-075024 (2012).

9 Chi, H. Regulation and function of mTOR signalling in T cell fate decisions. *Nat Rev Immunol* **12**, 325-338, doi:10.1038/nri3198
nri3198 [pii] (2012).

10 Zoncu, R., Efeyan, A. & Sabatini, D. M. mTOR: from growth signal integration to cancer, diabetes and ageing. *Nat Rev Mol Cell Biol* **12**, 21-35, doi:nrm3025 [pii]
10.1038/nrm3025 (2011).

11 Gerriets, V. A. & Rathmell, J. C. Metabolic pathways in T cell fate and function. *Trends Immunol* **33**, 168-173, doi:10.1016/j.it.2012.01.010
S1471-4906(12)00019-1 [pii] (2012).

12 Weichhart, T. & Saemann, M. D. The multiple facets of mTOR in immunity. *Trends Immunol* **30**, 218-226, doi:10.1016/j.it.2009.02.002
S1471-4906(09)00062-3 [pii] (2009).

13 Thomson, A. W., Turnquist, H. R. & Raimondi, G. Immunoregulatory functions of mTOR inhibition. *Nat Rev Immunol* **9**, 324-337, doi:10.1038/nri2546
nri2546 [pii] (2009).

14 Brown, E. J. *et al.* A mammalian protein targeted by G1-arresting rapamycin-receptor complex. *Nature* **369**, 756-758, doi:10.1038/369756a0 (1994).

15 Sabatini, D. M., Erdjument-Bromage, H., Lui, M., Tempst, P. & Snyder, S. H. RAFT1: a mammalian protein that binds to FKBP12 in a rapamycin-dependent fashion and is homologous to yeast TORs. *Cell* **78**, 35-43, doi:0092-8674(94)90570-3 [pii] (1994).

16 Laplante, M. & Sabatini, D. M. mTOR Signaling. *Cold Spring Harb Perspect Biol* **4**, doi:10.1101/cshperspect.a011593 a011593 [pii] cshperspect.a011593 [pii] (2012).

17 Vezina, C., Kudelski, A. & Sehgal, S. N. Rapamycin (AY-22,989), a new antifungal antibiotic. I. Taxonomy of the producing streptomycete and isolation of the active principle. *J Antibiot (Tokyo)* **28**, 721-726 (1975).

18 Thoreen, C. C. *et al.* An ATP-competitive mammalian target of rapamycin inhibitor reveals rapamycin-resistant functions of mTORC1. *J Biol Chem* **284**, 8023-8032, doi:10.1074/jbc.M900301200 M900301200 [pii] (2009).

19 Feldman, M. E. *et al.* Active-site inhibitors of mTOR target rapamycin-resistant outputs of mTORC1 and mTORC2. *PLoS Biol* **7**, e38, doi:08-PLBI-RA-4959 [pii] 10.1371/journal.pbio.1000038 (2009).

20 Dann, S. G. & Thomas, G. The amino acid sensitive TOR pathway from yeast to mammals. *FEBS Lett* **580**, 2821-2829, doi:S0014-5793(06)00508-4 [pii] 10.1016/j.febslet.2006.04.068 (2006).

21 Laplante, M. & Sabatini, D. M. mTOR signaling in growth control and disease. *Cell* **149**, 274-293, doi:10.1016/j.cell.2012.03.017 S0092-8674(12)00351-0 [pii] (2012).

22 Laplante, M. & Sabatini, D. M. mTOR signaling at a glance. *J Cell Sci* **122**, 3589-3594, doi:10.1242/jcs.051011
122/20/3589 [pii] (2009).

23 Yecies, J. L. & Manning, B. D. Transcriptional control of cellular metabolism by mTOR signaling. *Cancer Res* **71**, 2815-2820, doi:0008-5472.CAN-10-4158 [pii]
10.1158/0008-5472.CAN-10-4158 (2011).

24 Wang, L., Harris, T. E., Roth, R. A. & Lawrence, J. C., Jr. PRAS40 regulates mTORC1 kinase activity by functioning as a direct inhibitor of substrate binding. *J Biol Chem* **282**, 20036-20044, doi:M702376200 [pii]
10.1074/jbc.M702376200 (2007).

25 Yamagata, K. *et al.* rheb, a growth factor- and synaptic activity-regulated gene, encodes a novel Ras-related protein. *J Biol Chem* **269**, 16333-16339 (1994).

26 Zhang, Y. *et al.* Rheb is a direct target of the tuberous sclerosis tumour suppressor proteins. *Nat Cell Biol* **5**, 578-581, doi:10.1038/ncb999
ncb999 [pii] (2003).

27 Peterson, T. R. *et al.* DEPTOR is an mTOR inhibitor frequently overexpressed in multiple myeloma cells and required for their survival. *Cell* **137**, 873-886, doi:S0092-8674(09)00389-4 [pii]
10.1016/j.cell.2009.03.046 (2009).

28 Sengupta, S., Peterson, T. R. & Sabatini, D. M. Regulation of the mTOR complex 1 pathway by nutrients, growth factors, and stress. *Mol Cell* **40**, 310-322, doi:S1097-2765(10)00754-9 [pii]
10.1016/j.molcel.2010.09.026 (2010).

29 Gwinn, D. M. *et al.* AMPK phosphorylation of raptor mediates a metabolic checkpoint. *Mol Cell* **30**, 214-226, doi:S1097-2765(08)00169-X [pii]
10.1016/j.molcel.2008.03.003 (2008).

30 Schneider, A., Younis, R. H. & Gutkind, J. S. Hypoxia-induced energy stress inhibits the mTOR pathway by activating an AMPK/REDD1 signaling axis in head and neck squamous cell carcinoma. *Neoplasia* **10**, 1295-1302 (2008).

31 Sancak, Y. *et al.* The Rag GTPases bind raptor and mediate amino acid signaling to mTORC1. *Science* **320**, 1496-1501, doi:1157535 [pii]
10.1126/science.1157535 (2008).

32 Kim, E., Goraksha-Hicks, P., Li, L., Neufeld, T. P. & Guan, K. L. Regulation of TORC1 by Rag GTPases in nutrient response. *Nat Cell Biol* **10**, 935-945, doi:ncb1753 [pii]
10.1038/ncb1753 (2008).

33 Sancak, Y. *et al.* Ragulator-Rag complex targets mTORC1 to the lysosomal surface and is necessary for its activation by amino acids. *Cell* **141**, 290-303, doi:S0092-8674(10)00177-7 [pii]
10.1016/j.cell.2010.02.024 (2010).

34 Holz, M. K. & Blenis, J. Identification of S6 kinase 1 as a novel mammalian target of rapamycin (mTOR)-phosphorylating kinase. *J Biol Chem* **280**, 26089-26093, doi:M504045200 [pii]
10.1074/jbc.M504045200 (2005).

35 Holz, M. K., Ballif, B. A., Gygi, S. P. & Blenis, J. mTOR and S6K1 mediate assembly of the translation preinitiation complex through dynamic protein interchange and ordered phosphorylation events. *Cell* **123**, 569-580, doi:S0092-8674(05)01157-8 [pii]

10.1016/j.cell.2005.10.024 (2005).

36 Zinzalla, V., Stracka, D., Oppliger, W. & Hall, M. N. Activation of mTORC2 by association with the ribosome. *Cell* **144**, 757-768, doi:S0092-8674(11)00128-0 [pii] 10.1016/j.cell.2011.02.014 (2011).

37 Chen, C. H. *et al.* ER stress inhibits mTORC2 and Akt signaling through GSK-3beta-mediated phosphorylation of rictor. *Sci Signal* **4**, ra10, doi:10.1126/scisignal.2001731 4/161/ra10 [pii] (2011).

38 Guertin, D. A. *et al.* Ablation in mice of the mTORC components raptor, rictor, or mLST8 reveals that mTORC2 is required for signaling to Akt-FOXO and PKCalpha, but not S6K1. *Dev Cell* **11**, 859-871, doi:S1534-5807(06)00459-X [pii] 10.1016/j.devcel.2006.10.007 (2006).

39 Ikenoue, T., Inoki, K., Yang, Q., Zhou, X. & Guan, K. L. Essential function of TORC2 in PKC and Akt turn motif phosphorylation, maturation and signalling. *EMBO J* **27**, 1919-1931, doi:10.1038/emboj.2008.119 emboj2008119 [pii] (2008).

40 Garcia-Martinez, J. M. & Alessi, D. R. mTOR complex 2 (mTORC2) controls hydrophobic motif phosphorylation and activation of serum- and glucocorticoid-induced protein kinase 1 (SGK1). *Biochem J* **416**, 375-385, doi:BJ20081668 [pii] 10.1042/BJ20081668 (2008).

41 Pearce, L. R., Komander, D. & Alessi, D. R. The nuts and bolts of AGC protein kinases. *Nat Rev Mol Cell Biol* **11**, 9-22, doi:10.1038/nrm2822 nrm2822 [pii] (2010).

42 Kohn, A. D., Takeuchi, F. & Roth, R. A. Akt, a pleckstrin homology domain containing kinase, is activated primarily by phosphorylation. *J Biol Chem* **271**, 21920-21926 (1996).

43 Currie, R. A. *et al.* Role of phosphatidylinositol 3,4,5-trisphosphate in regulating the activity and localization of 3-phosphoinositide-dependent protein kinase-1. *Biochem J* **337 (Pt 3)**, 575-583 (1999).

44 Murray, J. T. *et al.* Exploitation of KESTREL to identify NDRG family members as physiological substrates for SGK1 and GSK3. *Biochem J* **384**, 477-488, doi:BJ20041057 [pii]
10.1042/BJ20041057 (2004).

45 Debonneville, C. *et al.* Phosphorylation of Nedd4-2 by Sgk1 regulates epithelial Na(+) channel cell surface expression. *EMBO J* **20**, 7052-7059, doi:10.1093/emboj/20.24.7052 (2001).

46 Brunet, A. *et al.* Protein kinase SGK mediates survival signals by phosphorylating the forkhead transcription factor FKHRL1 (FOXO3a). *Mol Cell Biol* **21**, 952-965, doi:10.1128/MCB.21.3.952-965.2001 (2001).

47 Delgoffe, G. M. *et al.* The mTOR kinase differentially regulates effector and regulatory T cell lineage commitment. *Immunity* **30**, 832-844, doi:S1074-7613(09)00237-4 [pii]
10.1016/j.immuni.2009.04.014 (2009).

48 Colombetti, S., Basso, V., Mueller, D. L. & Mondino, A. Prolonged TCR/CD28 engagement drives IL-2-independent T cell clonal expansion through signaling mediated by the mammalian target of rapamycin. *J Immunol* **176**, 2730-2738, doi:176/5/2730 [pii] (2006).

49 Zheng, Y. *et al.* A role for mammalian target of rapamycin in regulating T cell activation versus anergy. *J Immunol* **178**, 2163-2170, doi:178/4/2163 [pii] (2007).

50 Francisco, L. M. *et al.* PD-L1 regulates the development, maintenance, and function of induced regulatory T cells. *J Exp Med* **206**, 3015-3029, doi:10.1084/jem.20090847 jem.20090847 [pii] (2009).

51 Delgoffe, G. M. *et al.* The kinase mTOR regulates the differentiation of helper T cells through the selective activation of signaling by mTORC1 and mTORC2. *Nat Immunol* **12**, 295-303, doi:ni.2005 [pii] 10.1038/ni.2005 (2011).

52 Araki, K. *et al.* mTOR regulates memory CD8 T-cell differentiation. *Nature* **460**, 108-112, doi:nature08155 [pii] 10.1038/nature08155 (2009).

53 Pearce, E. L. *et al.* Enhancing CD8 T-cell memory by modulating fatty acid metabolism. *Nature* **460**, 103-107, doi:nature08097 [pii] 10.1038/nature08097 (2009).

54 Rao, R. R., Li, Q., Odunsi, K. & Shrikant, P. A. The mTOR kinase determines effector versus memory CD8+ T cell fate by regulating the expression of transcription factors T-bet and Eomesodermin. *Immunity* **32**, 67-78, doi:S1074-7613(09)00545-7 [pii] 10.1016/j.immuni.2009.10.010 (2010).

Figure 1

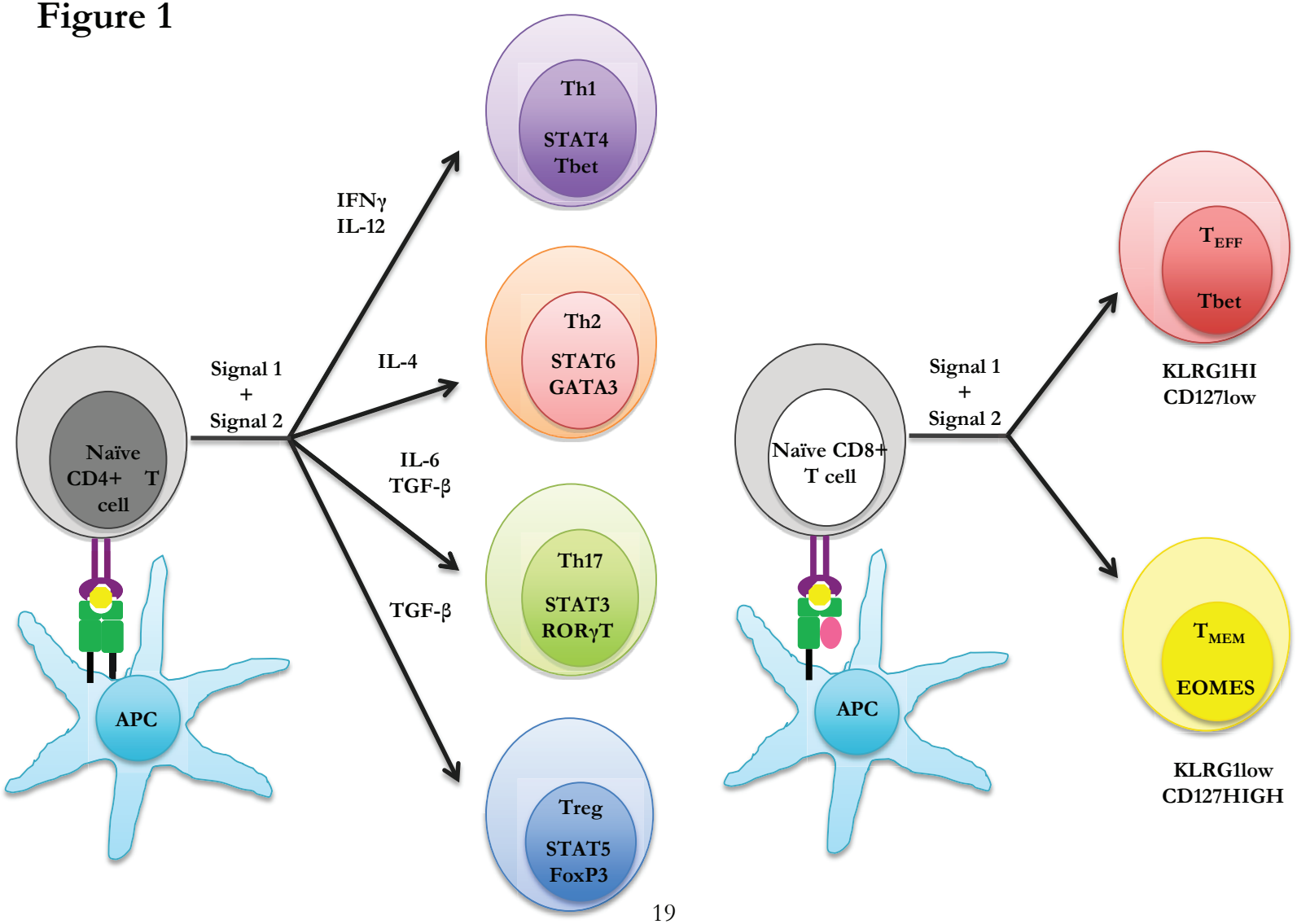
Th1
STAT4
Tbet
IFNγ
IL-12
Th2
STAT6
GATA3
IL-4
Signal 1
+
Signal 2
Naïve
CD4+ T
cell
IL-6
TGF-β
Th17
STAT3
RORγT
TGF-β
APC
Treg
STAT5
FoxP3
Naïve CD8+
T cell
Signal 1
+
Signal 2
APC
T_{EFF}
Tbet
KLRG1HI
CD127low
T_{MEM}
EOMES
KLRG1low
CD127HIGH

Figure 2

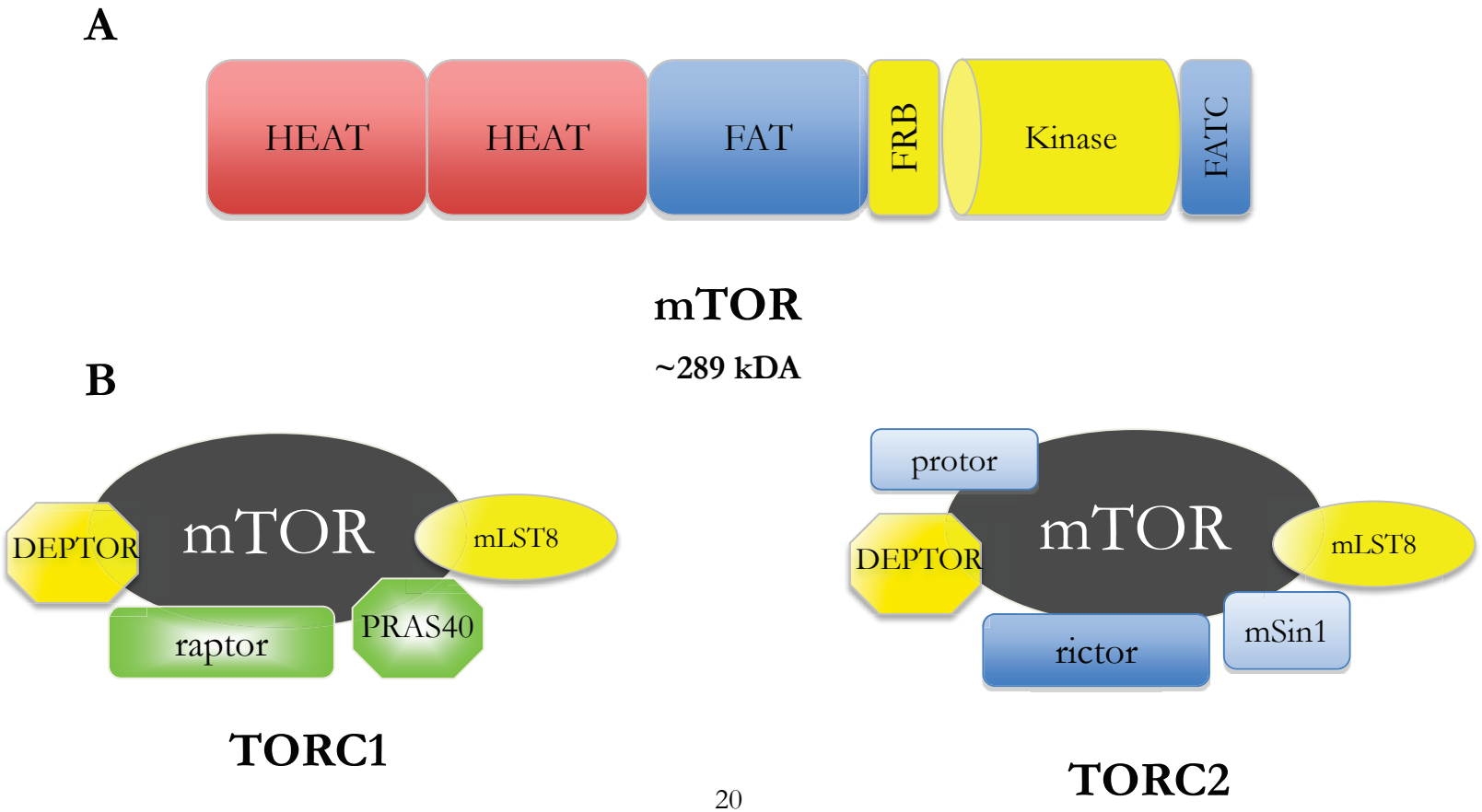
A
HEAT
HEAT
FAT
FRB
Kinase
FATC
mTOR
~289 kDA
B
DEPTOR
mTOR
mLST8
raptor
PRAS40
TORC1
protor
DEPTOR
mTOR
mLST8
rictor
mSin1
TORC2

Figure 3

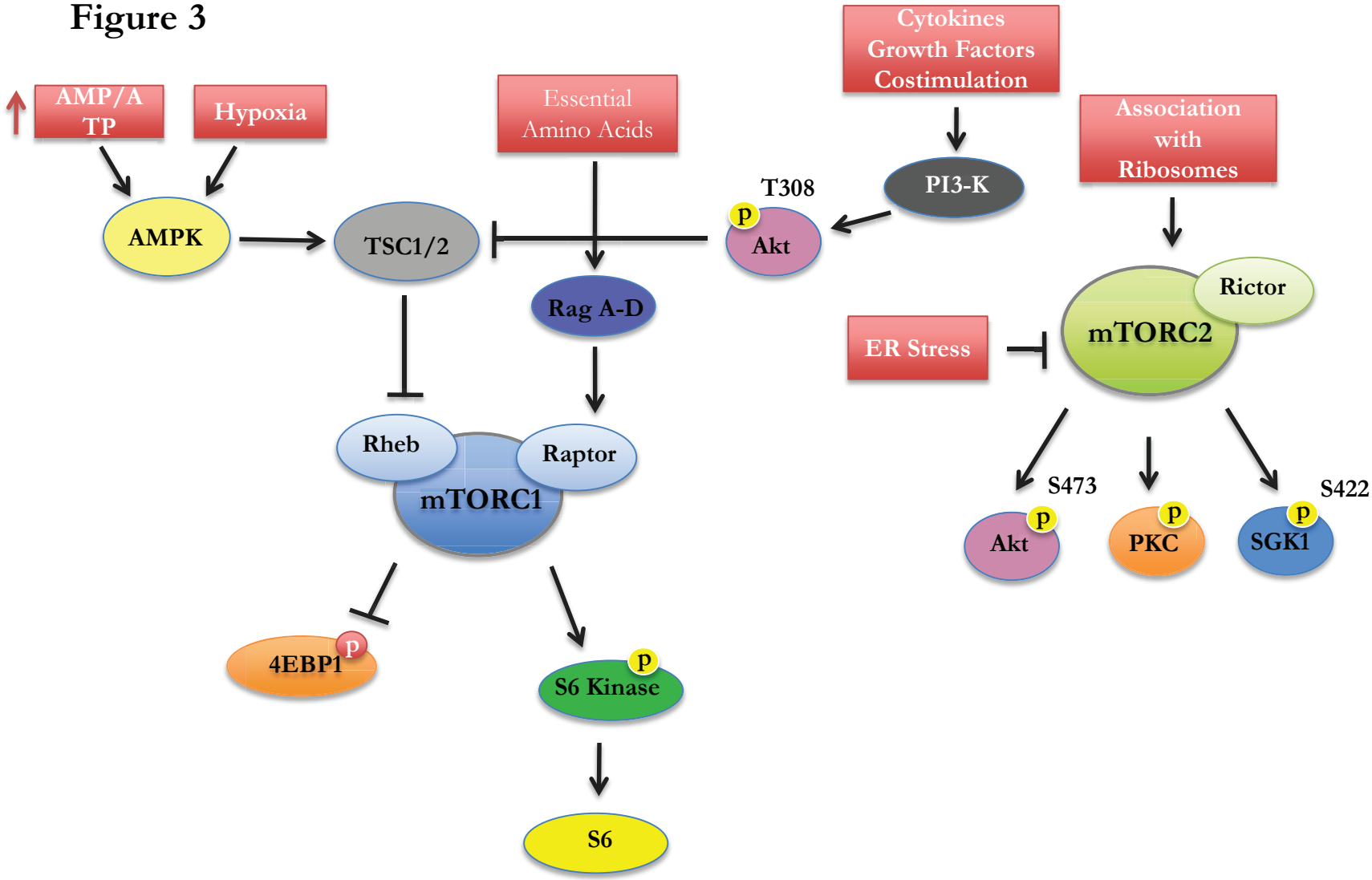
AMP/ATP
Hypoxia
AMPK
TSC1/2
Essential Amino Acids
Rag A-D
Rheb
Raptor
mTORC1
4EBP1
P
S6 Kinase
P
S6
Cytokines
Growth Factors
Costimulation
PI3-K
T308
P
Akt
Association with Ribosomes
Rictor
mTORC2
ER Stress
S473
Akt
P
PKC
P
S422
SGK1
P

CHAPTER 2: The AGC kinase serum- and glucocorticoid-regulated kinase 1 (SGK1) regulates T_H1 and T_H2 differentiation downstream of mTORC2

Introduction

AGC kinases are serine/threonine protein kinases that are broadly involved in regulating numerous aspects of cell physiology, including growth, survival and metabolism[1]. The serum- and glucocorticoid-regulated kinase 1 (SGK1) is an AGC kinase that is activated by sequential phosphorylation of two highly conserved regulatory motifs. The T-loop domain is phosphorylated at threonine 256 by the kinase PDK1 (ref. 2), and the hydrophobic motif is phosphorylated at serine 422 by mTORC2 (refs. 3,4). Compared to other AGC kinases that are also downstream of mTOR, such as Akt and S6 kinase, relatively little is known about SGK1. Downstream targets of SGK1 include E3 ubiquitin ligases such as NEDD4-2 (refs. 5,6), transcription factors such as Foxo[7,8], and other kinases like GSK-3b[9]. In the kidney, SGK1 phosphorylates and inhibits NEDD4-2 to prevent degradation of the epithelial Na^+ channel, thus allowing sodium to be reclaimed in the urine when serum concentrations of sodium are low[5,10,11]. Recently, it has been shown that SGK1 mRNA is upregulated by sodium in lymphocytes, and that mice that are fed a high salt diet develop more severe T_H17-mediated autoimmune encephalomyelitis[12,13]. Loss of SGK1 in T cells leads to a selective defect in pathogenic T_H17 differentiation, due to decreased expression of the interleukin 23 (IL-23) receptor[12]. The role of SGK1 in other T cell lineages, however, has yet to be determined.

We became interested in SGK1 because it is a downstream target of mTOR, which serves as a critical node in a highly conserved signaling pathway that integrates multiple

inputs from the environment[14,15]. In the immune system, mTOR integrates various signals, such as cytokines and costimulatory molecules, to influence T cell differentiation[15]. mTOR can associate with two distinct protein complexes (mTORC1 and mTORC2) to drive the selective differentiation of $CD4^+$ T cells. Genetic deletion of mTOR in $CD4^+$ T cells has shown that loss of both mTORC1 and mTORC2 signaling results in a default T regulatory (Treg) phenotype upon T cell activation[16,17]. Loss of either mTORC1 or mTORC2 leads to selective deficits in distinct T cell lineages. For example, genetic deletion of the mTORC2 adapter protein Rictor in $CD4^+$ T cells results in defective T_H2 differentiation, characterized by an inability to produce IL-4 (refs. 18,19). Despite the critical role of mTOR in regulating T effector and Treg cell differentiation, the precise downstream targets of mTOR that control differentiation into distinct helper T cell subsets have yet to be elucidated.

Because SGK1 is a downstream target of mTORC2, we hypothesized that it might be involved in mTORC2 regulation of T_H2 lineage commitment. To this end, we generated mice in which SGK1 was selectively deleted in T cells by crossing *Sgk1*$^{fl/fl}$ mice[11] with *Cd4*-Cre expressing mice (hereafter referred to as T-*Sgk1*$^{-/-}$ mice). We show that loss of SGK1 led to decreased production of IL-4 and inappropriate release of interferon-g (IFN-g) under T_H2 polarizing conditions *in vitro*. In a mouse model of allergic asthma, we found that loss of SGK1 resulted in diminished T_H2 responses and protection against disease. Mechanistically, we show that SGK1 promoted T_H2 differentiation by preventing ubiquitination and destruction of the transcription factor JunB by NEDD4-2 and its adaptor protein Ndfip. Alternatively, we found that T-*Sgk1*$^{-/-}$ mice produced increased amounts of IFN-g under T_H1 polarizing conditions *in vivo*, which was associated with both stronger anti-tumor and anti-viral immune responses. The ability of SGK1 to inhibit T_H1 differentiation was

mediated in part by its ability to regulate the expression of the long isoform of TCF-1 via b-catenin and GSK-3b. Overall, our findings define distinct signaling pathways downstream of SGK1 that provide new evidence as to how mTOR controls helper T cell differentiation.

Methods

Mice. Mice were kept in accordance with guidelines of the Johns Hopkins University Institutional Animal Care and Use Committee. Mice with *lox*P-flanked *Sgk1* alleles were described previously[11], and mice with *lox*P-flanked *Rictor* alleles were provided by M. Magnuson[40]. C57BL/6, *Cd4*-Cre and OT-II mice were obtained from Jackson Laboratories and bred to Thy-1.1 backgrounds. 5C.C7 mice were from Taconic Farms.

Antibodies and reagents. The following antibodies for flow cytometry were from BD Biosciences: anti-B220 (RA3-6B2), anti-CD3 (2C11), anti-CD4 (RM4-5), anti-CD8 (Ly-3), anti-CD25 (PC61), anti-CD44 (IM7), anti-CD124 (mIL4R-M1), anti-IFN-g (XMG1.2), anti-IL-17a (TC11-18H10), and anti-human CD8 (RPA-T8). Anti-CD62L (MEL-14), anti-IL-13 (eBio13A), anti-IL-5 (TRFK5), anti-T-bet (eBio4B10) and anti-Foxp3 (FJK-16s) were from eBioscience.

The following antibodies for immunoblotting were from Cell Signaling Technologies: Antibody to Rictor (2140), NDRG1 phosphorylated at Thr346 (5482), total NDRG1 (9408), antibody to Akt phosphorylated at S473 (4060), pan-Akt (4685), NEDD4-2 phosphorylated at Ser342 (4080), total NEDD4-2 (4013), TCF-1 (2206), antibody to b-catenin (9562), antibody to phosphorylated b-catenin (9561), antibody to phosphorylated STAT6 (9361). Anti-T-bet (4B10) and anti-GATA-3 (TWAJ) were from eBioscience. Anti-JunB (210) was

from Santa Cruz Biotechnology. Anti-ubiquitin was and actin were from Sigma. MG132 was from Sigma, PP242 was from Calbiochem, and CFSE was from Invitrogen.

T cell stimulation and polarization. $CD4^+$ T cells were purified by negative selection using a $CD4^+$ isolation kit and MACS Cell Separation (Miltenyi Biotec). For polarizing experiments, T cells were stimulated with irradiated autologous APCs or with plate-bound anti-CD3 and soluble anti-CD28. For APC-free stimulations, flat-bottomed plates were coated with anti-CD3 (3 mg/ml) diluted in PBS, and soluble anti-CD28 (2 mg/ml) was added to the cultures. For stimulation with APCs, T cells were cultured with irradiated APCs and anti-CD3 (1 mg/ml), followed by rest and expansion for 5 days. For rechallenge, live cells were harvested by Ficoll gradient, washed, and then stimulated with plate-bound anti-CD3 (1 mg/ml) and soluble anti-CD28 (2 mg/ml). Polarizing conditions were as follows: T_H0, anti-IL-4 (5 mg/ml) and anti-IFN-g (5 mg/ml), with IL-2 (1 ng/ml) during the rest period; T_H1, IL-12 (5 ng/ml), IFN-g (100 ng/ml) and anti-IL-4 (5 mg/ml), with IL-2 (1 ng/ml) during the rest period; T_H2, IL-4 (10 ng/ml), anti-IL-12 (5 mg/ml) and anti-IFN-g (5 mg/ml), with IL-2 (1 ng/ml) during the rest period; T_H17, IL-6 (30 ng/ml), TGF-β (3 ng/ml), anti-IFN-g (5 mg/ml), anti-IL-4 (5 mg/ml), and IL-23 (10 ng/ml) during the rest period. Stimulatory anti-CD3 (2C11) and anti-CD28 (37.51), as well as neutralizing anti-IFN-g (XMG1.2) and anti-IL-4 (11B11) were purified from hybridoma supernatants prepared in-house. Neutralizing anti-IL-12p40 (C17.8) was from eBioscience. Cytokines were from Peprotech.

Adoptive transfer. 1×10^6 naïve $CD4^+$ T cells specific for the OVA MHC class II epitope (OVA aa329-337) congenically marked with Thy1.1 were transferred intravenously to Thy1.2 C57BL/6 recipients by retro orbital injection. 1×10^6 pfu Vac-OVA was simultaneously administered by either retro orbital injection or intraperitoneal injection.

House Dust Mite Asthma Model. On days 0 and 7, mice were primed by intraperitoneal injection of 10 mg of house dust mite (HDM) extract (*D. pteronyssinus*, Greer Labs) in PBS. On days 14 and 21, mice were challenged via inhalation of 50 mg HDM extract per nostril. On day 24, mice are sacrificed for analysis. Lymphocytes from bronchoalveolar lavage (BAL) and mediastinal lymph nodes were stimulated *ex vivo* with PMA (phorbol 12-myristate 13-acetate) and ionomycin for 4 h. Lung lymphocytes were stimulated *ex vivo* with 30 mg HDM extract for 72 h, and supernatant from cultures were analyzed by ELISA. Differential cellular analysis of BAL was done via cytospin and Diff-quick staining. For histological analysis, lungs were formalin fixed, embedded in paraffin, and stained with hematoxylin and eosin, or periodic acid-Schiff (PAS), and scored by previously reported methods[41]. Peribronchiolar and perivascular inflammation was determined by a semi-quantitatively graded scale from 0-3, where a score of 0 = absent inflammation, 1 = mild, 2 = moderate, 3 = severe. Goblet cell hyperplasia was assessed by PAS staining of histologic sections, and was semi-quantitatively graded on a scale from 0-3, where a score of 0 = no or rare PAS-positive cells, 1 = less than 10% PAS-positive cells observed at 10X, 2 = between 10% and 25% PAS-positive cells observed at 10X, and 3 = greater than 25% PAS-positive cells observed at 4X. A composite score was determined by multiplying the graded score and the percent of airways or vessels that exhibited a given pathological finding. All scoring was performed by a pathologist (P.

Illei), who was blinded to the identity of the samples, and all slides were examined in a random order.

Influenza Model. On day 0, mice were challenged with intranasal influenza strain PR8 (Charles River) by injecting 600 egg infective dose (EID) per nostril for a final dose of 1200 EID. On day 8, mice were sacrificed. Lymphocytes from the lung were harvested by gentle mechanical and chemical digestion of lung parenchyma with collagenase and DNAse and stimulated *ex vivo* with PMA and ionomycin for 4 h. Experimental samples from groups were excluded from the final analysis if flow analysis of T lymphocytes from lungs demonstrated more than 70% $CD44^-$ and no detectable MHC class I or class II NP tetramer-positive cells, suggesting inadequate influenza inoculation.

B16 melanoma model. Mice were injected with 2×10^5 B16-OVA cells intravenously on day 0 and lungs were harvested 21 days later. Lung lymphocytes were stimulated *ex vivo* with PMA and ionomycin (Sigma) at a concentration of 50 ng/ml and 500 ng/ml, respectively. For survival experiments, mice were injected with 1×10^6 pfu VAC-OVA intraperitoneally on day 0, followed by intravenous injection with 2×10^5 B16-OVA cells on day 7.

Ovalbumin (OVA) airway sensitization model. OVA (Sigma-Aldrich) was adsorbed by gentle shaking for 30 min onto Imject Alum adjuvant (Pierce) to a final concentration of 250 mg/ml. Mice were primed by intraperitoneal injection of 50 mg of OVA-Alum in 200 ml. On day 7, mice were boosted by the same protocol. On days 15, 16, and 17, mice were challenged with intranasal OVA by injecting 25 mg OVA in PBS per nostril. On day 18, mice were sacrificed.

Intracellular staining. Brefeldin A (GolgiPlug; BD Biosciences) or monensin (GolgiStop; BD Biosciences) was used for cytokine staining. Cell were stained for surface antigens, fixed and made permeable with either the BD Cytofix/Cytoperm or the eBioscience Fixation/Permeabilization kit, then stained for intracellular cytokines. For intracellular staining of phosphorylated proteins, cells were fixed with 2.0% formalin and permeabilized with methanol.

Flow Cytometric Analysis. Flow cytometric data was acquired using a BD FACS Calibur or LSR II, and analyzed using FlowJo7.6 (Tree Star Inc, Ashland, OR). Gates were determined by using unstimulated controls or isotype controls where appropriate.
Cells were sorted using a BD FACS Aria at the Flow Cytometry Core at the Sidney Kimmel Comprehensive Cancer Center, JHMI.

Immunoblot analysis. For immunoblot analysis of mTOR substrates, $CD4^+$ T cells were stimulated in regular medium with anti-CD3 (1 mg/ml), anti-CD28 (2 mg/ml) and antibody to hamster immunoglobulin IgG1 (0.75 mg/ml; G94-56; BD Biosciences). T cells were harvested by centrifugation and resuspended in ice-cold lysis buffer (20 mM Tris (pH 7.5), 150 mM NaCl, 1 mM EDTA, 1 mM EGTA, 1% Triton X-100, 2.5 mM sodium pyrophosphate, 1 mM b-glycerolphosphate (glycerol-2-phosphate), 1 mM sodium orthovanadate, 1 mM PMSF, 1× protease inhibitors (Roche) and lysed at 4 °C for 30 min. Lysates were cleared of debris by high-speed centrifugation. Equal protein mass from each condition was mixed with 4× LDS buffer (Invitrogen) and boiled for 10 min. Lysates were

then loaded into NuPAGE gels (10% Bis–Tris gels, Invitrogen) and run at 150 V for 90 min. Protein was transferred to polyvinylidene fluoride (*PVDF*) membranes with transfer buffer (1× NuPAGE Transfer Buffer (Invitrogen) with 20% methanol) at 30 V for 90 min. Membranes were blocked in 5% nonfat dry milk (NFDM) for 60 min, washed briefly with Tris-buffered saline (pH=8) + 0.1% Tween-20 (TBST) and probed with primary antibody in 4% bovine serum albumin in TBST overnight at 4 °C. Membranes were washed with TBST three times for 10 min and probed with secondary antibody conjugated to horseradish peroxidase (HRP) in NFDM. Membranes were washed 2 times in TBST for 5 min, and then once in Tris-buffered saline once for 5 min. Enhanced chemiluminescent plus substrate (GE Healthcare) was used to detect HRP-labeled antibodies. Blots were developed using a Biospectrum Multispectrum Imaging System and images were acquired and analyzed using VisionWorks, LS Image Acquisition and Analysis software (UVP).

Enzyme-linked immunosorbent assay. IL-2, IL-4, IL-5, and IL-13 were analyzed by enzyme-linked immunosorbent assay as described by the manufacturer (eBioscience). Total serum IgE was measured using the following reagents from BD: anti-mouse IgE capture antibody (553413), mouse IgE standard (557080), and anti-mouse IgE biotinylated detection antibody (553419). HDM and OVA-specific antibodies were analyzed by enzyme-linked immunosorbent assay in Nunc-Immuno plates which had been coated overnight at 4 °C with 100 ml HDM (25 mg/ml in PBS) or OVA (20 mg/ml in PBS) and blocked for 1 h at 25 °C with assay diluent (eBioscience). Wells were washed several times and mouse serum samples diluted in assay diluent were added for 2 h or overnight. Wells were washed and then biotinylated anti-mouse immunoglobulin IgG1a (553441; BD) or IgG2a (553455; BD) diluted to a concentration of 0.5 mg/ml in assay diluent was added for 1 h. Wells were

washed and then streptavidin-conjugated HRP (eBioscience) was added for 30 min. Wells were washed seven times, and then incubated for 15 min with tetramethylbenzidine substrate, or until the reaction approached saturation. Linear regression analysis or absorbance levels were used to determine antibody titers or relative differences.

Real-time PCR. RNA was isolated and reverse transcribed into cDNA using the SuperScript III First-Strand Synthesis System for RT-PCR (Invitrogen) according to the manufacturer's protocol. Primers for short and long isoforms of TCF-1 were from Sigma, and primers to detect NEDD4-2 and Ndfip were from Applied Biosystems. Primers used to detect TCF-1 long isoforms were the following: 5′-CAATCTGCTCATGCCCTACC-3′ (forward) and 5′-GCCTGTGAACTCCTTGCTTC-3′ (reverse). Relative amounts of long and short isoforms were quantified using real-time PCR with a SYBR green fluorescent probe (Applied Biosystems). Quantitative RT-PCR was performed using a Step One Plus Real Time PCR System (Applied Biosystems).

Retroviral transduction. T cells were stimulated with plate-bound anti-CD3 and soluble anti-CD28 (as described above) overnight prior to spinfection with supernatants from 293T Phoenix cells. The Phoenix helper-free retroviral ecotropic packaging cell line (Nolan Laboratory) was transfected using Lipofectamine 2000 (Invitrogen) with plasmids encoding MSCV retrovirus containing full-length TCF-1 and a human CD8 reporter. MSCV constructs were provided by J. Sen.

siRNA knockdown. T cells were stimulated with plate-bound anti-CD3 and soluble anti-CD28 (as described above) for 48 h prior to transfection. ON-TARGET siRNA reagents for

scrambled control and NEDD4-2 and Ndfip specific RNA-mediated interference were from Dharmacon. Nucleofection reagents were from Lonza.

Statistical analysis. Prism version 5.0 (GraphPad Software) was used to perform statistical analyses, including unpaired Student's *t*-test, 2-way Analysis of Variance (ANOVA), and Log-rank (Mantel Cox) survival analysis. A *P*-value <0.05 was considered to be statistically significant.

Results

SGK1 is activated upon antigen recognition in T cells

Sgk1 RNA is expressed in resting naïve T cells (**Supplementary Fig. 1a**). We wanted to determine whether SGK1 is activated upon T cell stimulation by measuring the phosphorylation of the SGK1 substrate N-myc downregulated gene 1 (p-NDRG1 T346)[20]. Activation of T cells led to an increase in SGK1 activity (**Fig. 1a**). The kinetics of SGK1 activation paralleled the mTORC2-dependent activation of Akt (p-Akt S473). Next, we investigated whether SGK1 activity was modulated by polarizing cytokines upon T cell activation. Consistent with a recent report[12], SGK1 mRNA was expressed under all polarizing conditions *in vitro*, but expression was highest under T_H17 conditions (**Supplementary Fig. 1b**). Interestingly, we found that SGK1 activity was acutely induced to a similar degree under all polarizing conditions (**Fig. 1b**).

In light of the role of mTOR in regulating SGK1 activity in HEK293T, MCF-7 and HeLa cells[3,21], we sought to determine whether SGK1 was also activated in an mTOR-dependent manner in T cells (**Supplementary Fig. 2a**). Phosphorylation of NDRG1 increased upon T cell stimulation, but this effect was abrogated in the presence of the mTOR kinase inhibitor PP242 (**Fig. 1c**)[22]. Consistent with these results, inhibition of Akt phosphorylation (p-Akt S473) was also observed, indicating successful blockade of mTORC2 activity[23,24,25] (**Fig. 1c**). Likewise, the deletion of the mTORC2 component Rictor mitigated both Akt and SGK1 activation (**Fig. 2a, Supplementary Fig. 2b,c**). Having established that SGK1 signaling is mTORC2-dependent in T cells, we wanted to determine if SGK1 might function downstream of mTORC2 to regulate helper T cell differentiation. To address this question, mice were generated in which SGK1 was selectively deleted in T cells by breeding *Sgk1*$^{fl/fl}$ mice[11] with mice transgenic for Cre under control of the *Cd4* promoter and enhancer regions (T-*Sgk1*$^{-/-}$ mice) (**Supplementary Fig. 1a**). Upon stimulation, phosphorylation of NDRG1 was markedly decreased in T-*Sgk1*$^{-/-}$ CD4^{+} T cells **(Fig. 2a)**. Alternatively, the selective deletion of SGK1 in T cells did not affect Akt or S6 phosphorylation (**Supplementary Fig. 2b,c**).

The role of SGK1 in the maturation of peripheral T cells has never been described. Thymic development was essentially not different between wild-type and T-*Sgk1*$^{-/-}$ mice (**Supplementary Fig. 3a)** and there were no differences in the percent of CD3^{+}, B220^{+}, CD4^{+} and CD8^{+} cells in the spleen and lymph nodes compared to wild-type mice (**Fig. 2b-e).** Subtle differences in absolute T cell numbers and expression of activation markers were observed (**Supplementary Fig. 3b-g**). Finally there was a slight increase in Foxp3^{+} T cells in the spleens of T-*Sgk1*$^{-/-}$ mice when compared to wild-type mice (6.23% vs 7.50%) however

these differences were not observed in the lymph nodes (**Supplementary Fig. 3h**). T-*Sgk1*$^{-/-}$ CD4$^+$ T cells displayed a slightly reduced rate of proliferation (**Fig. 2f**). Nevertheless, T-*Sgk1*$^{-/-}$ CD4$^+$ T cells produce similar amounts of IL-2 compared to wild-type cells (**Fig. 2g**). Thus, the deletion of SGK1 does not greatly impact the composition of the peripheral T cell compartment.

SGK1 regulates T_H1 and T_H2 differentiation

In light of the ability of mTORC2 to regulate T_H2 generation[18,19], we wanted to determine whether loss of SGK1 affected T_H1 and T_H2 differentiation. CD4$^+$ T cells from wild-type and T-*Sgk1*$^{-/-}$ mice were polarized under T_H0, T_H1, or T_H2 conditions and interrogated for IL-4 production. As expected, wild-type T cells polarized under T_H2 conditions produced IL-4 upon re-challenge (**Fig. 3a**). However, T cells from T-*Sgk1*$^{-/-}$ mice failed to produce robust amounts of IL-4. Furthermore, loss of SGK1 resulted in decreased production of the T_H2 cytokines IL-5 and IL-13 (**Fig. 3b,c**).

Next, we examined the ability of T cells from T-*Sgk1*$^{-/-}$ mice to produce IFN-g and to be polarized to T_H1 effector cells. Without any polarizing cytokines, T cells from C57BL/6 mice will preferentially differentiate into T_H1 cells (**Fig. 3d**). CD4$^+$ T cells from both wild-type and T-*Sgk1*$^{-/-}$ mice activated and cultured under non-polarizing (T_H0) or T_H1 polarizing conditions led to the generation of IFN-g producing cells. However, T cells from T-*Sgk1*$^{-/-}$ mice robustly expressed IFN-g even when they were differentiated under T_H2 conditions (**Fig. 3d**). Thus, T cells lacking SGK1 fail to produce IL-4, IL-5, and IL-13, but

instead inappropriately produce IFN-g under T_H2 polarizing conditions. Consistent with recent studies (ref. 12,13), SGK1 does not affect T_H17 polarization (**Supplementary Fig. 4**).

Next, we examined the lineage-specific transcription factors T-bet and GATA-3. As expected, wild-type T cells cultured under T_H1 conditions expressed abundant T-bet, while cells cultured under T_H2 conditions robustly expressed GATA-3 (**Fig. 3e**). Alternatively, T cells derived from T-*Sgk1*$^{-/-}$ mice expressed abundant T-bet when cultured under either T_H1 or T_H2 conditions. Such cells also failed to express GATA-3 under T_H2 polarizing conditions. Overall, these observations demonstrate a role for SGK1 in reciprocally regulating T_H1 and T_H2 differentiation. During $CD4^+$ T cell effector differentiation, SGK1 activation simultaneously enhances IL-4 production and inhibits IFN-g production.

SGK1 regulates T_H2 differentiation by stabilizing JunB

We sought to define a biochemical mechanism by which SGK1 regulates T_H1 and T_H2 differentiation. We did not observe a defect in IL-4 receptor expression or IL-4-induced STAT6 phosphorylation in the absence of SGK1 (*data not shown*). Previous studies on the role of SGK1 in renal epithelial cells have demonstrated that SGK1 negatively regulates the HECT-type E3 ligase by phosphorylation at serine 342 and serine 448 (refs. 5,10). A closely related homolog of NEDD4-2 is the ubiquitin ligase Itch, which has been shown to interact with the NEDD4 family–interacting protein 1 (Ndfip1) adapter protein to mediate polyubiquitination of JunB[26,27]. JunB has been shown to be essential for T_H2 development[26,28]. We sought to determine if the defect in T_H2 differentiation that we observed in T-*Sgk1*$^{-/-}$ mice could be in part due to increased ubiquitination and destruction

of JunB by NEDD4-2. As previously shown[28], JunB abundance was higher in wild-type T cells cultured under T_H2 conditions compared to those cultured under T_H1 conditions (**Fig. 4a**). In SGK1-deficient T cells, we observed that JunB protein abundance was decreased under both T_H1 and T_H2 polarizing conditions (**Fig. 4a**). These findings correlated with the phosphorylation status of NEDD4-2 at S342. That is, inhibition of NEDD4-2 (as measured by p-NEDD4-2 S342) was greatest under T_H2 conditions and decreased in the absence of SGK1 (**Fig. 4a**).

We next investigated the ability of SGK1 to regulate NEDD4-2 *in vivo*. To this end, we adoptively transferred congenically marked Thy1.1$^+$, ovalbumin (OVA)-specific CD4$^+$ T cells from wild-type or T-*Sgk1*$^{-/-}$ mice into naïve hosts that were subsequently immunized with OVA in alum to induce a T_H2 response. Similar to the *in* vitro results, we observed p-NEDD4-2 S342 phosphorylation and inhibition upon stimulation of wild-type adoptively transferred cells (**Fig. 4b**). By contrast, NEDD4-2 was not phosphorylated and inhibited in T-*Sgk1*$^{-/-}$ adoptively transferred cells.

Our data are consistent with the hypothesis that NEDD4-2 degrades JunB protein in T cells lacking SGK1 even under T_H2 conditions, both *in vitro* and *in vivo*. To further test this hypothesis, wild-type and T-*Sgk1*$^{-/-}$ T CD4$^+$ cells were activated under T_H2 conditions in the presence of the proteasome inhibitor MG132. JunB abundance was markedly decreased in the T cells lacking SGK1 when compared to the wild-type T cells (**Fig. 4c**). However, expression of JunB protein was restored in T-*Sgk1*$^{-/-}$ cells in the presence of MG132, suggesting that Jun B is expressed in T-*Sgk1*$^{-/-}$ T cells but is subsequently degraded. To confirm that JunB degradation was due to increased ubiquitination we immunoprecipitated JunB in wild-type and T-*Sgk1*$^{-/-}$ CD4+ T cells and immunoblotted for

ubiquitin. We found that JunB was not ubiquitinated under T_H2 conditions in wild-type cells, but JunB ubiquitination was markedly enhanced in the absence of SGK1 (**Fig. 4d**).

Next, we wanted to determine whether we could rescue the ability of T-*Sgk1*$^{-/-}$ $CD4^+$ T cells to make IL-4 under T_H2 conditions by knocking down NEDD4-2 or Ndfip using siRNA. Knocking down either NEDD4-2 or Ndfip led to partial rescue of IL-4 production in the T-*Sgk1*$^{-/-}$ T_H2 polarized T cells (**Fig. 4e**). Knockdown was confirmed by measuring the expression of NEDD4-2 and Ndfip mRNA (**Supplementary Fig. 5a,b**). Additionally, NEDD4-2 knockdown was confirmed at the protein level, which correlated with the re-accumulation of JunB protein (**Fig. 4f**). It was difficult to confirm knockdown of Ndfip at the protein level because the available antibodies are not robust, however knockdown of Ndfip also resulted in the re-accumulation of JunB protein (*data not shown*). Altogether, these results suggest that SGK1 activation promotes T_H2 differentiation in part by negatively regulating E3 ligases that target JunB for destruction.

T-*Sgk1*$^{-/-}$ mice are resistant to Th2-mediated asthma

Since we had defined the role of SGK1 in regulating the differentiation of helper T cells *in vitro*, we wanted to confirm this paradigm in an *in vivo* model. We chose to study the OVA-alum allergic asthma model because T_H2 cells are involved in the early pathogenesis of this disease[29]. Therefore, we hypothesized that T-*Sgk1*$^{-/-}$ mice would be resistant to allergic asthma. Wild-type mice mounted a stereotypic T_H2 response to this allergic stimulus, characterized by IL-4 in bronchoalveolar lavage (BAL) and IgE in serum. However, BAL and serum from T-*Sgk1*$^{-/-}$ mice contained significantly less IL-4 and IgE (**Supplementary**

Fig. 6a,b). Alternatively, we detected OVA-specific IgG2a, characteristic of a T_H1 response in the serum of T-*Sgk1*$^{-/-}$ mice (**Supplementary Fig. 6c**). Along these lines, lung lymphocytes from T-*Sgk1*$^{-/-}$ mice inappropriately produced IFN-g when stimulated *ex vivo* (**Supplementary Fig. 6d**). Thus in this *in vivo* model of T_H2-mediated inflammation, loss of SGK1 in T cells abrogated the T_H2 response and instead produced an inappropriate T_H1 response to an allergic stimulus.

In light of these findings we wanted to determine if deleting SGK1 in T cells could prevent allergen-induced lung pathology. To this end we challenged wild-type and T-*Sgk1*$^{-/-}$ mice with house dust mite (HDM) extract. Similar to our findings in the OVA-alum adjuvant model, we observed a marked decrease in the T_H2 response of T-*Sgk1*$^{-/-}$ mice when challenged with HDM extract. Expression of IL-4, IL-13 and IL-5 in the lungs of T-*Sgk1*$^{-/-}$ mice was markedly diminished when compared to wild-type mice (**Fig. 5a–c**). Likewise, we observed a decrease in the expression of these cytokines by $CD4^+$ T cells in the mediastinal lymph nodes of T-*Sgk1*$^{-/-}$ mice (**Fig. 5d–g**). We observed a significant decrease in the absolute number of $CD4^+$ T cells in the lymph nodes of T-*Sgk1*$^{-/-}$ mice, however, the there was no significant decrease observed in the lungs and BAL fluid between wild-type and T-*Sgk1*$^{-/-}$ mice (**Supplementary Fig. 6e,f**). Consistent with our model, $CD4^+$ T cells in the lungs, BAL and lymph nodes of T-*Sgk1*$^{-/-}$ mice produced significantly more IFN-g compared to wild-type mice (**Fig. 5h,i**). Furthermore, the T-*Sgk1*$^{-/-}$ mice displayed decreased total IgE, in addition to decreased HDM-specific IgE and IgG1 (**Fig. 5j–l**). Finally, the lungs of the T-*Sgk1*$^{-/-}$ mice demonstrated markedly decreased goblet cell hyperplasia and decreased peribronchiolar and perivascular inflammation when compared to

the lungs of the wild-type mice (**Fig. 5m–q**). Thus, loss of SGK1 in T cell protects against allergen-induced T_H2-mediated lung disease.

SGK1 negatively regulates IFN-g production via TCF-1

The SGK1–NEDD4-2–Ndfip–JunB axis provides a selective mechanism as to why T-*Sgk1*$^{-/-}$ CD4$^+$ T cells do not differentiate towards a T_H2 phenotype. However, it does not adequately explain why CD4$^+$ T cells produce IFN-g under T_H2 conditions in the absence of SGK1. It has previously been reported that the glycogen synthase kinase-3β (GSK-3b) is inhibited by the AGC kinases Akt and SGK1 (ref. 9). In turn, GSK-3b phosphorylates b-catenin and targets this protein for degradation[30,31]. We observed a marked decrease in expression of b-catenin in T-*Sgk1*$^{-/-}$ T cells (**Fig. 6a**). b-catenin is critical during T_H2 differentiation because it promotes early GATA-3 expression by binding at the proximal promoter[32]. In the absence of SGK1, GSK-3b remains highly active and thus there is very little total b-catenin. On the other hand, inhibiting GSK-3b in the T-*Sgk1*$^{-/-}$ T cells with LiCl leads to an increase in total b-catenin (**Fig. 6a).**

The transcription factor T cell factor 1 (TCF-1) is both a downstream target of b-catenin and a transcriptional co-activator with b-catenin[31-33]. Similar to T-*Sgk1*$^{-/-}$ mice, mice deficient in TCF-1 produce more IFN-g even under T_H2 polarizing conditions[32]. Specifically, the long isoforms of TCF-1 contain an additional b-catenin binding domain, and these long isoforms promote T_H2 polarization by increasing expression of GATA-3 and repressing expression of IFN-g[32]. We hypothesized that there would be decreased expression of the long form of TCF-1 in the T cells lacking SGK1. Wild-type and T-*Sgk1*$^{-/-}$ CD4$^+$ T cells

were polarized under T_H1 and T_H2 conditions and assayed for TCF-1 protein. We found that the long isoforms of TCF-1 were decreased in T-*Sgk1*$^{-/-}$ under both T_H1 and T_H2 polarizing conditions, but there was no difference in expression of the short isoforms of this protein (**Fig. 6b**).

To determine if SGK1 regulates TCF-1 expression at the transcriptional level, we designed primers that flank the b-catenin binding domain to specifically detect the long isoform of TCF-1. In the absence of SGK1, we observed decreased transcription of the long isoforms of TCF-1 at 72 h post-TCR activation, and a complete absence of transcripts at 8 days post-stimulation (**Fig. 6c**). To further test this hypothesis, we sought to rescue the phenotype of T-*Sgk1*$^{-/-}$ $CD4^+$ T cells by retroviral transduction with a vector encoding the long isoform of TCF-1 (FL-TCF-1) and a human CD8 reporter (**Fig. 6d**). We sorted transduced cells for human CD8, then restimulated the cells and assayed for the production of IFN-g by intracellular staining. Wild-type T cells polarized under T_H2 conditions failed to express IFN-g. T cells from the T-*Sgk1*$^{-/-}$ mice, transduced with the empty vector (EV), expressed significant amounts of IFN-g under T_H2 conditions. Alternatively, IFN-g expression was mitigated when the T-*Sgk1*$^{-/-}$ T cells were transfected with FL-TCF-1 (**Fig. 6d**). These data support a model whereby under T_H2 conditions SGK1 inhibits the GSK-3b-mediated degradation of b-catenin, leading in turn to increased expression of the long form of TCF-1 and inhibition of IFN-g (**Supplementary Fig. 7**).

T-*Sgk1*$^{-/-}$ mice mount robust T_H1-mediated immune responses

The ability of SGK1 to regulate T_H2 responses is in part due to its ability to negatively regulate IFN-g. We wondered whether we would also see an increase in IFN-g *in vivo* under strongly polarizing T_H1 conditions in the T-*Sgk1*$^{-/-}$ mice. To this end, congenically marked Thy1.1$^+$, OVA-specific wild-type and T-*Sgk1*$^{-/-}$ CD4$^+$ T cells were adoptively transferred into Thy1.2$^+$ wild-type mice that were infected intravenously with OVA-expressing vaccinia virus (Vac-OVA) which induces robust T_H1 immune responses. Vaccinia infection led to a marked increase in the numbers of OVA-specific IFN-g producing cells from wild-type mice. However, the T_H1 response by the T cells from the *Sgk1*$^{-/-}$ mice demonstrated an increase in both the percentage of IFN-g producing cells and the amount of IFN-g produced on a per cell basis (**Fig. 7a**). To confirm this observation, we challenged wild-type and T-*Sgk1*$^{-/-}$ mice with the PR8 strain of influenza virus, which also promotes a strong T_H1-mediated immune response. Similar to what we observed for vaccinia virus, CD4$^+$ T cells from T-*Sgk1*$^{-/-}$ mice produced more IFN-g in response to influenza virus infection compared to wild-type mice (**Fig. 7b).**

To further assess the T_H1 response by T-*Sgk1*$^{-/-}$ cells *in vivo* we employed a model of T_H1-mediated tumor rejection, since T_H1-polarized CD4$^+$ T cells have previously been shown to have an important role in anti-tumor immunity[34]. To address this hypothesis, we injected wild-type and T-*Sgk1*$^{-/-}$ mice with 2×10^5 B16 melanoma cells intravenously, and harvested lungs 21 days later. Loss of SGK1 in T cells resulted in less than half as many lung tumors as compared to wild-type mice (**Fig. 7c, Supplementary Fig. 8**). While it is quite possible that the decrease in tumor burden could have been promoted by CD8$^+$ T cells, it is clear that the more effective response by the T-*Sgk1*$^{-/-}$ mice was associated with an increase in CD4$^+$ IFN-g producing T cells in the lungs (**Fig. 7d**). Next, we sought to further boost

tumor immunity in T-*Sgk1*$^{-/-}$ mice by vaccination. Mice were immunized with vaccinia virus expressing OVA seven days prior to intravenous injection of B16 melanoma cells expressing OVA, and survival was monitored as the primary outcome. We found that T-*Sgk1*$^{-/-}$ mice had significantly prolonged survival compared to wild-type mice in response to a tumor vaccine **(Fig. 7e**). Thus, the targeted deletion of SGK1 in T cells leads to enhanced tumor immunity, characterized by more IFN-g production and robust immunologic rejection of tumors.

Discussion

A critical task of both the adaptive and innate immune system is to integrate cues from the immune microenvironment and then respond appropriately. Recently, it has become clear that the evolutionarily conserved serine/threonine kinase mTOR plays a central role in this process[15]. The outcome of mTOR activation is determined by the regulation of selective downstream signaling pathways and substrates. To this end, we have identified the AGC kinase SGK1 as an mTORC2 activated substrate that selectively regulates T_H1 and T_H2 helper T cell differentiation. T cells lacking SGK1 demonstrate a markedly diminished ability to differentiate into T_H2 cells both *in vitro* and *in vivo*. Furthermore, under T_H2 polarizing conditions the T-*Sgk1*$^{-/-}$ T cells inappropriately produced IFN-γ. Thus, under T_H2 conditions SGK1 simultaneously promotes T_H2 differentiation while also inhibiting the production of T_H1 cytokines. Likewise, *in vivo* we observed increased IFN-γ production by the T-*Sgk1*$^{-/-}$ T cells in the setting of viral infection and anti-tumor immunity. Of note, under T_H1 polarizing conditions *in vitro,* the T-*Sgk1*$^{-/-}$ cells produced equivalent levels of IFN-γ as wild-type T cells. Perhaps this indicates that under

strongly polarizing conditions *in vitro*, the ability of SGK1 to inhibit the T_H1 response is inconsequential. However, *in vivo*, under inflammatory conditions that predominantly favor T_H1 polarization, SGK1 signaling appears to limit the magnitude of the T_H1 immune response.

Our studies provide a mechanism by which mTOR (specifically mTORC2) activation regulates T_H1 and T_H2 differentiation. Recently, it has been reported that SGK1 plays a role in promoting the stability of pathogenic T_H17 cells[12]. Notably, in this study, as in ours, T_H17 differentiation was similar in both wild-type and T-*Sgk1*$^{-/-}$ T cells. However, it was shown that SGK1 plays a role in controlling the expression of the IL-23 receptor. As a result, T cells lacking SGK1 respond poorly to IL-23 and T-*Sgk1*$^{-/-}$ mice are resistant to the development of experimental autoimmune encephalitis (EAE). Furthermore, it was shown that an increase in the extracellular concentration of sodium leads to increased IL-23-mediated T_H17 differentiation and that this effect was abrogated in T-*Sgk1*$^{-/-}$ T cells. This report and another link these findings to the ability of increased dietary salt to exacerbate EAE[12,13].

Previous studies on the role of SGK1 in the kidney provided clues as to how this AGC kinase may be functioning in T cells[11]. In order to reclaim sodium in the urine, SGK1 prevents degradation of sodium channels by phosphorylating and inhibiting the NEDD4-2 E3 ubiquitin ligase[5,6]. Similarly, we found that SGK1 promoted T_H2 differentiation by phosphorylating and inhibiting NEDD4-2, thus preventing degradation of JunB. These findings are consistent with previous reports that mice lacking Ndfip or Itch display a hyper-T_H2 phenotype[26,27]. In these studies loss of Ndfip or Itch led to accumulation of JunB and

increased expression of IL-4. Overall, our studies serve to strengthen the link between mTOR-SGK1 and the regulation of cellular differentiation and function by E3-ligases. Just as these connections have been shown to be important in T cells and renal epithelial cells, we propose that these pathways will prove to be important for a diversity of cellular functions.

Our findings identify SGK1 as a potential target for the treatment of T_H2-mediated autoimmune and allergic diseases, such as asthma. Currently, non-specific immunosuppressive agents such as steroids play an important role in the treatment of acute asthma flares as well as in preventing recurrences[35-37]. Our data suggest that the selective inhibition of SGK1 might represent an immunomodulatory approach to treating and preventing the sequelae of asthma and other allergic diseases without globally inhibiting the immune system. Interestingly, small molecule inhibitors of SGK1 have already been developed[38,39]. Additionally, inhibiting SGK1 may be of therapeutic value in terms of enhancing T_H1-mediated immune responses, for example, in the setting of viral infections or as an adjunct to tumor immunotherapy. That is, while an asthmatic might take an SGK1 inhibitor to prevent the development of T_H2-mediated inflammation, the same small molecule inhibitor might be given to a patient in the midst of receiving cancer immunotherapy in order to enhance the anti-tumor response.

Figure Legends

Figure 1. SGK1 is activated downstream of TCR signaling in an mTOR-dependent manner. (a) Immunoblot (IB) of naïve lymphocytes from 5C.C7 mice that were rested for 1 h prior to stimulation with anti-CD3 and anti-CD28. Cells were lysed, and the activity of SGK1 was measured by blotting for phosphorylated NDRG1 (p-T346). The activity of mTORC2 was measured by blotting for phosphorylated Akt (p-S473). Total protein and actin are included as loading controls. **(b)** IB of $CD4^+$ T cells isolated from 5C.C7 mice, as described in a, and stimulated for 3 h in the presence of polarizing cytokines. Cells were lysed and immunoblotted for SGK1 and Akt activity. **(c)** IB of naïve 5C.C7 lymphocytes, as described above. Where indicated, the mTOR kinase inhibitor PP242 (1 mM) was added to the cells upon stimulation. Total protein and actin are included as loading controls. Data are representative of 3-5 independent experiments (**a-c**).

Figure 2. SGK1 is activated downstream of mTORC2 in T cells. (a) IB of wild-type (WT), T-*Rictor*$^{-/-}$**,** and T-*Sgk1*$^{-/-}$ $CD4^+$ T cells that were stimulated as in **Fig. 1a**. Cells were lysed and the activity of Akt and SGK1 was measured as above. Total protein and actin are included as loading controls. **(b-e)** Flow cytometric phenotyping data compiled from multiple mice (n = 6) showing percentages of $B220^+$, $CD3^+$, $CD4^+$ and $CD8^+$ cells from WT and T-*Sgk1*$^{-/-}$ spleen (b-c) and lymph nodes (d-e). CD4+ and CD8+ subsets in (c) and (e) were gated on $CD3^+$. **(f)** $CD4^+$ T cells were isolated from WT or T-*Sgk1*$^{-/-}$ mice, stained with carboxyfluorescein succinimidyl ester (CFSE), and stimulated with irradiated syngeneic APCs and 1 mg/mL anti-CD3 for 24, 48, 72 or 96 h. Unstimulated (US) cells are shown as a control. **(g)** Naïve $CD4^+$ T cells were isolated and stimulated overnight with 0.3, 1.0, or 3.0

mg/ml plate-bound anti-CD3 and 2.0 mg/ml soluble anti-CD28. Supernatants were harvested to determine IL-2 production by ELISA. ND = not detectable. Data are representative of 3 independent experiments **(a-g)** and samples were analyzed in triplicate in each experiment **(g)**. Statistical significance determined by Student's *t*-test, NS=No Significance, error bars s.e.m.

Figure 3. SGK1 reciprocally regulates T_H1 and T_H2 differentiation downstream of mTORC2. (a) IL-4 production of activated $CD4^+$ T cells by ELISA. Naïve $CD4^+$ T cells from WT and T-*Sgk1*$^{-/-}$ mice were isolated based on expression of CD44 and CD62L. Cells were stimulated with irradiated autologous APCs under T_H0, T_H1 or T_H2 polarizing conditions as indicated in the **Methods**. (**b,c**) As in **a**, but supernatants were assayed for IL-5 (**b**) or IL-13 (**c**) production by ELISA. (Statistical significance calculated by ANOVA, $*P < 0.001$, error bars s.e.m.) **(d)** IFN-g production of activated $CD4^+$ T cells by intracellular staining. Cells were stimulated and rested as in **a** prior to activation with overnight plate-bound anti-CD3 and soluble anti-CD28 in the presence of Golgi plug. Numbers represent percentages of cells in each quadrant. **(e)** IB of activated $CD4^+$ T cells for lineage-specific transcription factors. Cells were stimulated with plate-bound anti-CD3 and anti-CD28 for 48 h then rested for 5 days in IL-2. Live cells were harvested, lysed and immunoblotted for T-bet and GATA-3. Actin is included as a loading control. Right, flow cytometric data showing intracellular staining for the transcription factors T-bet and GATA-3. Cells were fixed and permeabilised to determine expression of T-bet and GATA-3 by flow cytometry. Mean Fluorescence Intensity (MFI) is displayed on each respective flow plot. Data are representative of 4 independent experiments **(a-e)** and samples were analyzed in triplicate in each experiment **(a-c)**.

Figure 4. SGK1 promotes Th2 differentiation by negatively regulating NEDD4-2. (a) IB of cell extracts from WT and T-*Sgk1*$^{-/-}$ CD4^{+} T cells that were stimulated *in vitro* under either T_H1 or T_H2 polarizing conditions. Cells were lysed and blotted for the expression of JunB and the activity of the E3 ligase NEDD4-2 (by measuring p-S342). Total NEDD4-2 and actin are included as loading controls. ImageJ software was used to calculate band density from 3 independent experiments, and band density was normalized to loading controls and to WT T_H1 conditions. (Statistical significance calculated by ANOVA, $^{**}P < 0.001$, error bars s.e.m.) **(b)** Intracellular staining of Thy1.1^{+} adoptively transferred cells for phosphorylated NEDD4-2. OT-II CD4^{+} T cells bearing the Thy1.1 congenic marker were adoptively transferred into WT Thy1.2^{+} recipients immunized with OVA adsorbed onto alum to induce a Th2 immune response. Spleens were harvested on day 4, restimulated with OVA Class II peptide, and intracellular staining was performed for phosphorylated NEDD4-2. Plots depict MFI of indicated samples. (Statistical significance calculated by ANOVA, $^{*}P = 0.0183$. **(c)** IB of cell extracts of WT and T-*Sgk1*$^{-/-}$ treated with MG132. Cells were polarized under T_H2 conditions as in **a**, but with the addition of the proteasome inhibitor MG132 during the final 2 h of stimulation. Lysates were blotted for JunB, and actin is included as a loading control. **(d)** Immunoprecipitates (IPs) of JunB from WT and T-*Sgk1*$^{-/-}$ CD4^{+} T cells polarized with IL-4 and treated with MG132. As in **c**, but lysates were subject to IP with JunB antibody. IPs were blotted for ubiquitin and immunoprecipitated JunB is included as a loading control. **(e)** IL-4 production of CD4^{+} T cells transfected with siRNA targeting NEDD4-2 or Ndfip. A non-specific pool of siRNA (scrambled, Scr) was used as a control. Cells were stimulated under T_H2 polarizing conditions for 48 h prior to transfection with siRNA then expanded in IL-2 for 5 d. Cells were restimulated overnight

with anti-CD3 and anti-CD28 and supernatants were harvested to determine cytokine production. **(f)** $CD4^+$ T cells from WT or T-*Sgk1*$^{-/-}$ mice were treated as in (**e**) then lysed for immunoblot to show knockdown of NEDD4-2 and rescue of JunB protein. (Data not shown for Ndfip.) (Statistical significance calculated by ANOVA, $^{**}P < 0.001$, error bars s.e.m.) Data are representative of 3 independent experiments (**a–d**), 4 independent experiments (**e**) or 2 independent experiments (**f**).

Figure 5. Loss of SGK1 activity in $CD4^+$ T cells mitigates T_H2-mediated disease in an allergen induced asthma model. (a–c) IL-4, IL-13 and IL-5 production from lung lymphocytes from mice that had been sensitized intraperitoneally and re-challenged intranasally on days 14 and 21 with HDM extract to induce allergic airway inflammation. Lung lymphocytes were stimulated for 3 days *ex vivo* with HDM extract, and supernatants were harvested and analyzed by ELISA for cytokine production. **(d–g)** IL-4, IL-13 and IL-5 production from mediastinal lymph nodes from mice that had been immunized as in **a–c**. Lymphocytes were stimulated *ex vivo* with PMA and ionomycin for 4 h, then fixed, permeabilised and analyzed by intracellular staining and flow cytometry for cytokine production. **(h)** Lymphocytes were harvested from lung parenchyma or BAL, stimulated *ex vivo* with PMA and ionomycin for 4 h, and analyzed for production of IFN-g by intracellular staining and flow cytometry as described above. **(i)** As in **h**, but lymphocytes were harvested from mediastinal lymph nodes. **(j–l)** Total IgE (**j**), HDM specific IgE (**k**), and HDM specific IgG1 (**l**) in serum from mice that were sensitized and rechallenged with HDM extract as described above. Antibody titers were extrapolated from a standard curve (if available) or absorbance is shown for a dilution of serum for which all samples were in the range of the assay. **(m,n)** Representative lung sections after periodic acid-Schiff (PAS) (m) or

hematoxylin and eosin (H&E) (n) staining for saline control (mock) and HDM-treated mice. Pathologic changes in WT mice include goblet cell hyperplasia **(m)** and perivascular and peribronchiolar inflammation **(n)**. Images from HDM treated mice are shown at 10x (top, middle rows) and at 20x magnification (bottom row). **(o-p)** Histologic scoring data of PAS^+ cells in large bronchioles **(o)** and small bronchioles **(p)** from HDM-treated mice. **(q)** Histologic scoring data of perivascular and peribronchiolar inflammation as seen in H&E stained lung sections as described above. Data are representative of 3 independent experiments (a-i), 4 independent experiments (j-l) or 2 independent experiments (m-q), n = 5–11 mice per group. (Statistical significance determined by Student's t-test (a-q), **** $P <$ 0.0001, ***$P < 0.001$, **$P < 0.01$, *$P < 0.05$, error bars s.e.m.)

Figure 6. SGK1 negatively regulates T_H1 differentiation via the long isoform of TCF-1. (a) IB of cell extracts from WT and T-*Sgk1*$^{-/-}$ $CD4^+$ T cells stimulated under T_H2 polarizing conditions and treated overnight with 25 mM LiCl. Lysates were blotted for p-b-catenin (S33/47/T41) and total b-catenin. Total GSK-3b is included as a loading control. (**b**) IB of cell extracts from WT and T-*Sgk1*$^{-/-}$ $CD4^+$ T cells that were stimulated *in vitro* under either T_H1 or T_H2 polarizing conditions. Cells were lysed and blotted for TCF-1. Actin is included as a loading control. Two exposures are shown to appreciate differences in long and short isoforms of TCF-1, short exposure (top), long exposure (bottom). **(c)** Expression of long isoform of TCF-1 in activated $CD4^+$ T cells at early and late time points during differentiation. $CD4^+$ T cells were purified from WT and T-*Sgk1*$^{-/-}$ mice by magnetic separation, stimulated with anti-CD3 anti-CD28 magnetic beads for 2 d in T_H1 or T_H2 conditions then rested in IL-2 for 6 d. Fold induction of long isoform of TCF-1 normalized 18S rRNA and to WT T_H1 polarizing conditions at 72 h and 8 days post stimulation, as

analyzed by quantitative polymerase chain reaction. **(d)** Flow cytometric analysis of $CD4^+$ T cells polarized under T_H2 conditions and transduced to overexpress the long isoform of TCF-1 (FL-TCF-1) with an MSCV retrovirus containing a human CD8 marker. Following transduction, cells were rested then sorted for human CD8 surface expression. Cells were restimulated and analyzed for production of IFN-γ by intracellular staining. Cells were gated on low, intermediate, and high expression of human CD8. Histogram overlays of human CD8 high cells are shown to emphasize differences in IFN-γ production among cells with similar multiplicity of infection. Data are representative of 3 independent experiments **(a-c)** or 4 independent experiments **(d),** and samples were analyzed in triplicate in each experiment **(c)**. (Statistical significance calculated by ANOVA, $P<0.001$, error bars s.e.m.)

Figure 7. Loss of SGK1 enhances T_H1-mediated viral and tumor immunity. (a) IFN-g production from adoptively transferred OT-II cells that were restimulated *ex vivo* with PMA and ionomycin. OT-II cells were adoptively transferred into mice that had been simultaneously immunized intravenously with 1×10^6 pfu VAC-OVA. Positive gates for IFN-g were set using a no stimulation control such that <1.0% of cells were allowed in the positive gate. Plots gated on adoptively transferred cells (left) and bar graph depicts MFI (right). $n = 10$ mice per group. **(b)** IFN-g production from lung lymphocytes of mice infected intranasally with the PR8 strain of influenza. On day 8, lung lymphocytes were harvested and stimulated for 4 h *ex vivo* with PMA and ionomycin then fixed, permeabilized and analyzed by intracellular staining and flow cytometry for IFN-g production. **(c)** Number of B16 melanoma lung metastases. WT and T-*Sgk1*$^{-/-}$ mice were injected intravenously with 2×10^5 B16 melanoma cells, and lungs were harvested 21 days later. The number of lung metastases were counted and expressed as mean + s.e.m. **(d)** As in **b**, lung lymphocytes were

harvested and stimulated for 4 hours *ex vivo* with PMA and ionomycin and analyzed by intracellular staining for production of IFN-g by $CD4^+$ T cells. **(e)** Kaplan-Meier analysis of WT and T-*Sgk1*$^{-/-}$ mice vaccinated with 1×10^6 pfu VAC-OVA 7 days prior to challenge with 2×10^5 B16 melanoma cells expressing OVA (B16-OVA). T-*Sgk1*$^{-/-}$ mice have prolonged survival ($P<0.0001$, n = 5–7 mice per group). Data are representative of 2–3 independent experiments, n = 5–15 mice per group. Statistical significance determined by Student's *t*-test (**a–d**) or Log-rank (Mantel Cox) survival analysis (**e**), $^{****}P < 0.0001$, $^{***}P < 0.001$, $^{**}P < 0.01$, $^{*}P < 0.05$, error bars s.e.m.

Supplementary Figure Legends

Supplementary Figure 1. *Sgk1* mRNA is expressed in $CD4^+$ and $CD8^+$ T cells and is upregulated in response to cytokines. **(a)** $CD4^+$ and $CD8^+$ T cells were isolated from wild-type and T-*Sgk1*$^{-/-}$ mice by magnetic separation, and RNA was isolated. Sgk1 mRNA levels were determined by polymerase chain reaction using the following excision primers: forward primer 5-CTCAGTCTCTTTTGGGCTCTTT-3 and the reverse primer 5-TTTCTTCTTCAGGATGGCTTTC-3, as described in the **Methods**. GAPDH is included as a loading control. Data is representative of 3 independent experiments. **(b)** $CD4^+$ T cells were isolated from 5C.C7 mice using magnetic separation, and cells were stimulated with anti-CD3 and anti-CD28 for 1 hour under polarizing conditions. RNA was isolated and reverse transcribed into cDNA to measure expression of *Sgk1* by RT-PCR. Expression is normalized to the unstimulated control and to 18s rRNA expression.

Supplementary Figure 2. mTORC2 is required for activation of SGK1. **(a)** Model depicting downstream targets of mTORC2. Activation of mTORC2 leads to phosphorylation of Akt (p-S473) and SGK1 (p-S422). Activation of SGK1 leads to

phosphorylation of its downstream target NDRG1 (p-T346). **(b)** ImageJ software was used to calculate band density from 3 independent experiments shown in **Fig. 2a**, and band density was normalized to loading controls and to WT unstimulated (US) conditions. **(c)** Flow cytometric analysis of CD4+ T cells isolated from WT, T-*Rictor*$^{-/-}$, and T-*Sgk1*$^{-/-}$ mice and stimulated with anti-CD3 and anti-CD28 for 1,3, or 6 hours. Cells were permeabilised with methanol and interrogated for phosphorylation of Akt (S473) using flow cytometry. Numbers in upper right corner of each plot indicate mean fluorescent index (MFI) of p-Akt or total Akt. Below, MFI of p-Akt from flow cytometry plots above were normalized to the MFI of total Akt. Data are representative of 3 independent experiments (a-c), statistical significance calculated by ANOVA, ns=no significance, error bars s.e.m.).

Supplementary Figure 3. Characterization of lymphocyte development and maturation of T-*Sgk1*$^{-/-}$ mice. **(a)** Flow cytometric phenotyping data compiled from multiple mice (n=6) of double negative ($CD4^-CD8^-$), double positive ($CD4^+CD8^+$), or single positive ($CD4^+$ or $CD8^+$) thymocytes, **(b,c)** absolute numbers of $B220^+$, $CD3^+$, $CD4^+$, and $CD8^+$ cells in the spleen and lymph nodes, **(d-g)** expression of CD44 and CD62L on both $CD4^+$ and $CD8^+$ subsets in the spleen and lymph nodes, **(h)** expression of Treg phenotypic markers ($CD3^+$ $CD4^+$ $CD25^+$ $FoxP3^+$) in spleen and lymph nodes. Data are compiled from 6 mice and are representative of 3 independent experiments. Statistical significance determined by Student's t-test, NS=No Significance, $*P<0.05$ $**P<0.01$, error bars s.e.m.

Supplementary Figure 4. SGK1 is not required for T_H17 differentiation *in vitro*. Intracellular staining of $CD4^+$ T cells that were polarized for 48 hours under T_H0 or T_H17 (IL-6 and TGF-β) conditions, then rested and restimulated as in Fig. 3D. Data is representative of 3 independent experiments.

Supplementary Figure 5. Knockdown of NEDD4-2 and Ndfip by siRNA. Quantitative PCR analysis of NEDD4-2 **(a)** and Ndfip **(b)** mRNA in CD4+ T cells from WT and T-*Sgk1*$^{-/-}$ mice. RNA was harvested from cells 24 hours after transfection with siRNA for analysis by real time PCR. Gene expression is normalized to 18s rRNA and to the WT scrambled control. Data is representative of two independent experiments, and samples were analyzed in triplicate for each experiment. Statistical significance calculated by ANOVA, **P*<0.001, error bars s.e.m.)

Supplementary Figure 6. Decreased Th2 mediated immunity *in vivo* in T-*Sgk1*$^{-/-}$ mice in asthma models. **(a)** IL-4 production in bronchoalveolar lavage (BAL) harvested from mice that had been sensitized with OVA in alum i.p., then rechallenged with intranasal OVA on days 15, 16, and 17, followed by sacrifice on day 18. Lungs were lavaged with PBS and analyzed by ELISA. **(b)** Total IgE in serum. **(c)** OVA-specific IgG2a in serum. **(d)** IFN-γ production by lung lymphocytes, as measured by intracellular staining and flow cytometry. As in A, lung lymphocytes were harvested from diseased mice and stimulated for 4 hours *ex vivo* with PMA and ionomycin. **(e)** Analysis of $CD4^+$ lymphocytes found in the lungs and mediastinal lymph nodes of mice that were sensitized and challenged with HDM extract as described in Fig 5. Graph depicts absolute number of $CD4^+$ T cells recovered from each compartment. **(f)** BAL was analyzed by cytospin and Diff-quick staining for the presence of lymphocytes in WT and T-*Sgk1*$^{-/-}$ mice that were sensitized and challenged with HDM extract as described in Fig 5. Data are representative of 3 independent experiments, and n=5-11 mice per group, **P*<0.05, ***P*<0.01, ****P*<0.001. (Statistical significance calculated by ANOVA (d) or Student's t test, error bars s.e.m.)

Supplementary Figure 7. Model depicting regulation of TCF-1 by SGK1. In WT T cells, activation of mTORC2 downstream of TCR signaling results in activation of SGK1. In turn,

SGK1 phosphorylates and inhibits GSK-3β. When GSK-3β is inactive, its target β-catenin cannot be degraded. Active β-catenin cooperates with the long isoforms of TCF-1 to promote transcription of TCF-1, which inhibits expression of IFN-γ. In T-*Sgk1*$^{-/-}$ cells, GSK-3β is active and thus targets β-catenin for destruction. Loss of β-catenin leads to decreased expression of TCF-1 long isoforms, and thus increased expression of IFN-γ.

Supplementary Figure 8. Reduced melanoma tumor burden in T-*Sgk1*$^{-/-}$ mice. Representative images from one of 3 independent experiments showing reduced melanoma tumor burden in the lungs of T-*Sgk1*$^{-/-}$ mice as compared to WT mice.

References

1 Pearce, L. R., Komander, D. & Alessi, D. R. The nuts and bolts of AGC protein kinases. *Nat Rev Mol Cell Biol* **11**, 9-22, doi:10.1038/nrm2822 nrm2822 [pii] (2010).

2 Biondi, R. M., Kieloch, A., Currie, R. A., Deak, M. & Alessi, D. R. The PIF-binding pocket in PDK1 is essential for activation of S6K and SGK, but not PKB. *EMBO J* **20**, 4380-4390, doi:10.1093/emboj/20.16.4380 (2001).

3 Garcia-Martinez, J. M. & Alessi, D. R. mTOR complex 2 (mTORC2) controls hydrophobic motif phosphorylation and activation of serum- and glucocorticoid-induced protein kinase 1 (SGK1). *Biochem J* **416**, 375-385, doi:BJ20081668 [pii] 10.1042/BJ20081668 (2008).

4 Yan, L., Mieulet, V. & Lamb, R. F. mTORC2 is the hydrophobic motif kinase for SGK1. *Biochem J* **416**, e19-21, doi:BJ20082202 [pii] 10.1042/BJ20082202 (2008).

5 Debonneville, C. *et al.* Phosphorylation of Nedd4-2 by Sgk1 regulates epithelial Na(+) channel cell surface expression. *EMBO J* **20**, 7052-7059, doi:10.1093/emboj/20.24.7052 (2001).

6 Ichimura, T. *et al.* 14-3-3 proteins modulate the expression of epithelial Na+ channels by phosphorylation-dependent interaction with Nedd4-2 ubiquitin ligase. *J Biol Chem* **280**, 13187-13194, doi:M412884200 [pii] 10.1074/jbc.M412884200 (2005).

7 Di Pietro, N. *et al.* Serum- and glucocorticoid-inducible kinase 1 (SGK1) regulates adipocyte differentiation via forkhead box O1. *Mol Endocrinol* **24**, 370-380, doi:me.2009-0265 [pii] 10.1210/me.2009-0265 (2010).

8 Brunet, A. *et al.* Protein kinase SGK mediates survival signals by phosphorylating the forkhead transcription factor FKHRL1 (FOXO3a). *Mol Cell Biol* **21**, 952-965, doi:10.1128/MCB.21.3.952-965.2001 (2001).

9 Sakoda, H. *et al.* Differing roles of Akt and serum- and glucocorticoid-regulated kinase in glucose metabolism, DNA synthesis, and oncogenic activity. *J Biol Chem* **278**, 25802-25807, doi:10.1074/jbc.M301127200 M301127200 [pii] (2003).

10 Wiemuth, D. *et al.* Interaction of serum- and glucocorticoid regulated kinase 1 (SGK1) with the WW-domains of Nedd4-2 is required for epithelial sodium channel regulation. *PLoS One* **5**, e12163, doi:e12163 [pii] 10.1371/journal.pone.0012163 (2010).

11 Fejes-Toth, G., Frindt, G., Naray-Fejes-Toth, A. & Palmer, L. G. Epithelial Na+ channel activation and processing in mice lacking SGK1. *Am J Physiol Renal Physiol* **294**, F1298-1305, doi:00579.2007 [pii] 10.1152/ajprenal.00579.2007 (2008).

12 Wu, C. *et al.* Induction of pathogenic T17 cells by inducible salt-sensing kinase SGK1. *Nature*, doi:10.1038/nature11984 nature11984 [pii] (2013).

13 Kleinewietfeld, M. *et al.* Sodium chloride drives autoimmune disease by the induction of pathogenic T17 cells. *Nature*, doi:10.1038/nature11868 nature11868 [pii] (2013).

14 Zoncu, R., Efeyan, A. & Sabatini, D. M. mTOR: from growth signal integration to cancer, diabetes and ageing. *Nat Rev Mol Cell Biol* **12**, 21-35, doi:nrm3025 [pii] 10.1038/nrm3025 (2011).

15 Powell, J. D., Pollizzi, K. N., Heikamp, E. B. & Horton, M. R. Regulation of Immune Responses by mTOR. *Annu Rev Immunol* **30**, 39-68, doi:10.1146/annurev-immunol-020711-075024 (2012).

16 Delgoffe, G. M. *et al.* The mTOR kinase differentially regulates effector and regulatory T cell lineage commitment. *Immunity* **30**, 832-844, doi:S1074-7613(09)00237-4 [pii] 10.1016/j.immuni.2009.04.014 (2009).

17 Zhang, S. *et al.* Constitutive reductions in mTOR alter cell size, immune cell development, and antibody production. *Blood* **117**, 1228-1238, doi:10.1182/blood-2010-05-287821blood-2010-05-287821 [pii] (2011).

18 Delgoffe, G. M. *et al.* The kinase mTOR regulates the differentiation of helper T cells through the selective activation of signaling by mTORC1 and mTORC2. *Nat Immunol* **12**, 295-303, doi:ni.2005 [pii] 10.1038/ni.2005 (2011).

19 Lee, K. *et al.* Mammalian target of rapamycin protein complex 2 regulates differentiation of Th1 and Th2 cell subsets via distinct signaling pathways. *Immunity* **32**, 743-753, doi:S1074-7613(10)00205-0 [pii] 10.1016/j.immuni.2010.06.002 (2010).

20 Murray, J. T. *et al.* Exploitation of KESTREL to identify NDRG family members as physiological substrates for SGK1 and GSK3. *Biochem J* **384**, 477-488, doi:BJ20041057 [pii] 10.1042/BJ20041057 (2004).

21 Lu, M., Wang, J., Ives, H. E. & Pearce, D. mSIN1 protein mediates SGK1 protein interaction with mTORC2 protein complex and is required for selective activation of

the epithelial sodium channel. *J Biol Chem* **286**, 30647-30654, doi:10.1074/jbc.M111.257592 M111.257592 [pii] (2011).

22 Feldman, M. E. *et al.* Active-site inhibitors of mTOR target rapamycin-resistant outputs of mTORC1 and mTORC2. *PLoS Biol* **7**, e38, doi:10.1371/journal.pbio.100003808-PLBI-RA-4959 [pii] (2009).

23 Sarbassov, D. D., Guertin, D. A., Ali, S. M. & Sabatini, D. M. Phosphorylation and regulation of Akt/PKB by the rictor-mTOR complex. *Science* **307**, 1098-1101 (2005).

24 Guertin, D. A. *et al.* Ablation in mice of the mTORC components raptor, rictor, or mLST8 reveals that mTORC2 is required for signaling to Akt-FOXO and PKCalpha, but not S6K1. *Dev Cell* **11**, 859-871, doi:S1534-5807(06)00459-X [pii] 10.1016/j.devcel.2006.10.007 (2006).

25 Jacinto, E. *et al.* SIN1/MIP1 maintains rictor-mTOR complex integrity and regulates Akt phosphorylation and substrate specificity. *Cell* **127**, 125-137, doi:S0092-8674(06)01147-0 [pii] 10.1016/j.cell.2006.08.033 (2006).

26 Oliver, P. M. *et al.* Ndfip1 protein promotes the function of itch ubiquitin ligase to prevent T cell activation and T helper 2 cell-mediated inflammation. *Immunity* **25**, 929-940, doi:S1074-7613(06)00509-7 [pii] 10.1016/j.immuni.2006.10.012 (2006).

27 Fang, D. *et al.* Dysregulation of T lymphocyte function in itchy mice: a role for Itch in TH2 differentiation. *Nat Immunol* **3**, 281-287, doi:10.1038/ni763 ni763 [pii] (2002).

28 Li, B., Tournier, C., Davis, R. J. & Flavell, R. A. Regulation of IL-4 expression by the transcription factor JunB during T helper cell differentiation. *EMBO J* **18**, 420-432, doi:10.1093/emboj/18.2.420 (1999).

29 Huang, T. J. *et al.* Allergen-specific Th1 cells counteract efferent Th2 cell-dependent bronchial hyperresponsiveness and eosinophilic inflammation partly via IFN-gamma. *J Immunol* **166**, 207-217 (2001).

30 Liu, C. *et al.* Control of beta-catenin phosphorylation/degradation by a dual-kinase mechanism. *Cell* **108**, 837-847, doi:S0092867402006852 [pii] (2002).

31 Yu, Q., Sharma, A. & Sen, J. M. TCF1 and beta-catenin regulate T cell development and function. *Immunol Res* **47**, 45-55, doi:10.1007/s12026-009-8137-2 (2010).

32 Yu, Q. *et al.* T cell factor 1 initiates the T helper type 2 fate by inducing the transcription factor GATA-3 and repressing interferon-gamma. *Nat Immunol* **10**, 992-999, doi:ni.1762 [pii] 10.1038/ni.1762 (2009).

33 Roose, J. *et al.* Synergy between tumor suppressor APC and the beta-catenin-Tcf4 target Tcf1. *Science* **285**, 1923-1926, doi:7843 [pii] (1999).

34 Quezada, S. A. *et al.* Tumor-reactive CD4(+) T cells develop cytotoxic activity and eradicate large established melanoma after transfer into lymphopenic hosts. *J Exp Med* **207**, 637-650, doi:10.1084/jem.20091918 jem.20091918 [pii] (2010).

35 Suissa, S., Ernst, P., Benayoun, S., Baltzan, M. & Cai, B. Low-dose inhaled corticosteroids and the prevention of death from asthma. *N Engl J Med* **343**, 332-336, doi:10.1056/NEJM200008033430504 (2000).

36 Fanta, C. H. Asthma. *N Engl J Med* **360**, 1002-1014, doi:10.1056/NEJMra0804579 360/10/1002 [pii] (2009).

37 Littenberg, B. & Gluck, E. H. A controlled trial of methylprednisolone in the emergency treatment of acute asthma. *N Engl J Med* **314**, 150-152, doi:10.1056/NEJM198601163140304 (1986).

38 Sherk, A. B. *et al.* Development of a small-molecule serum- and glucocorticoid-regulated kinase-1 antagonist and its evaluation as a prostate cancer therapeutic. *Cancer Res* **68**, 7475-7483, doi:10.1158/0008-5472.CAN-08-1047 68/18/7475 [pii] (2008).

39 Ackermann, T. F. *et al.* EMD638683, a novel SGK inhibitor with antihypertensive potency. *Cell Physiol Biochem* **28**, 137-146, doi:10.1159/000331722 000331722 [pii] (2011).

40 Kumar, A. *et al.* Muscle-specific deletion of rictor impairs insulin-stimulated glucose transport and enhances Basal glycogen synthase activity. *Mol Cell Biol* **28**, 61-70, doi:MCB.01405-07 [pii] 10.1128/MCB.01405-07 (2008).

41 Daan de Boer, J. *et al.* Lipopolysaccharide inhibits Th2 lung inflammation induced by house dust mite allergens in mice. *Am J Respir Cell Mol Biol* **48**, 382-389, doi:10.1165/rcmb.2012-0331OCrcmb.2012-0331OC [pii] (2013).

Figure 1

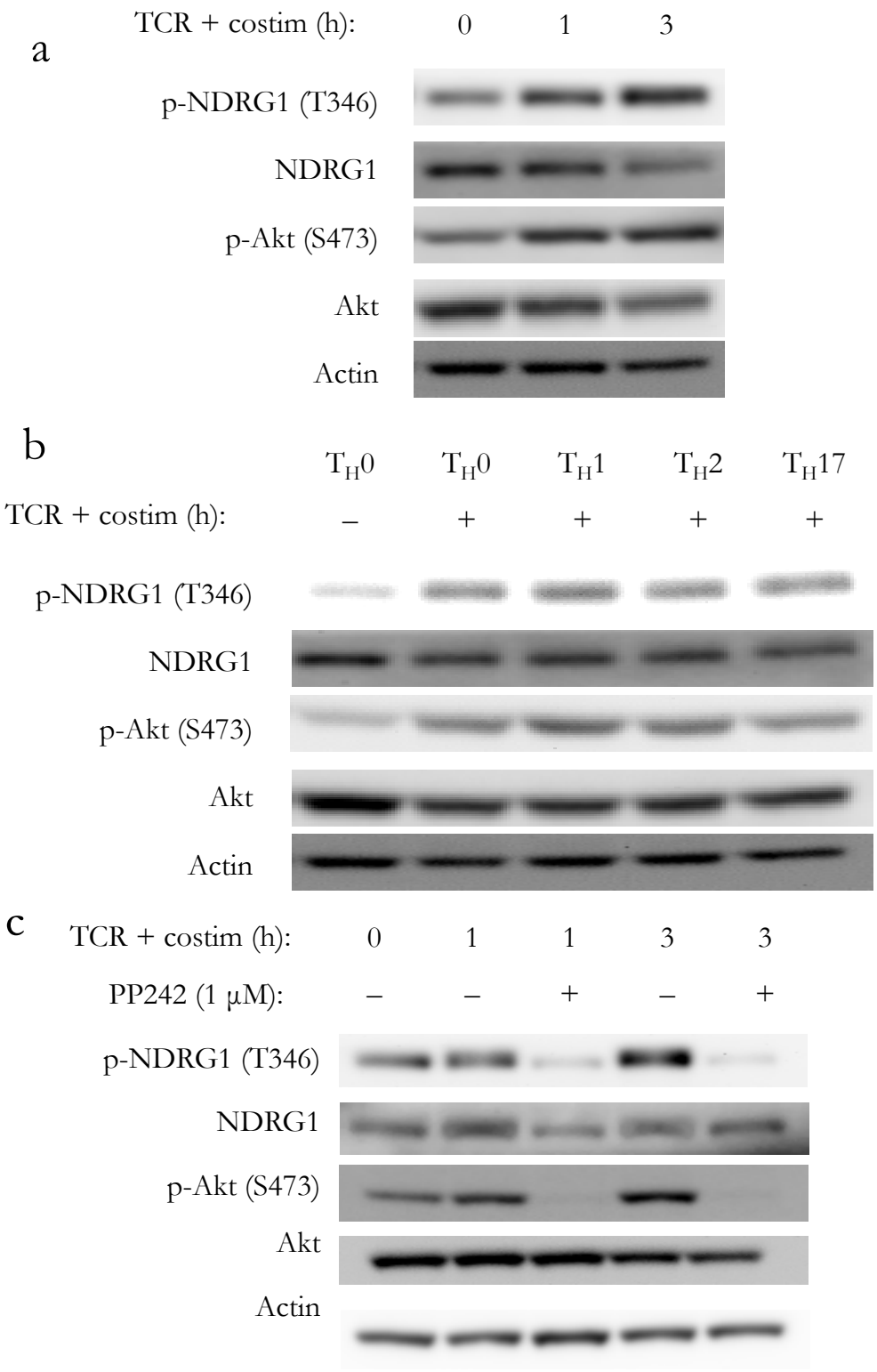
a
TCR + costim (h): 0 1 3
p-NDRG1 (T346)
NDRG1
p-Akt (S473)
Akt
Actin
b
T_H0 T_H0 T_H1 T_H2 T_H17
TCR + costim (h): – + + + +
p-NDRG1 (T346)
NDRG1
p-Akt (S473)
Akt
Actin
c
TCR + costim (h): 0 1 1 3 3
PP242 (1 μM): – – + – +
p-NDRG1 (T346)
NDRG1
p-Akt (S473)
Akt
Actin

Figure 2

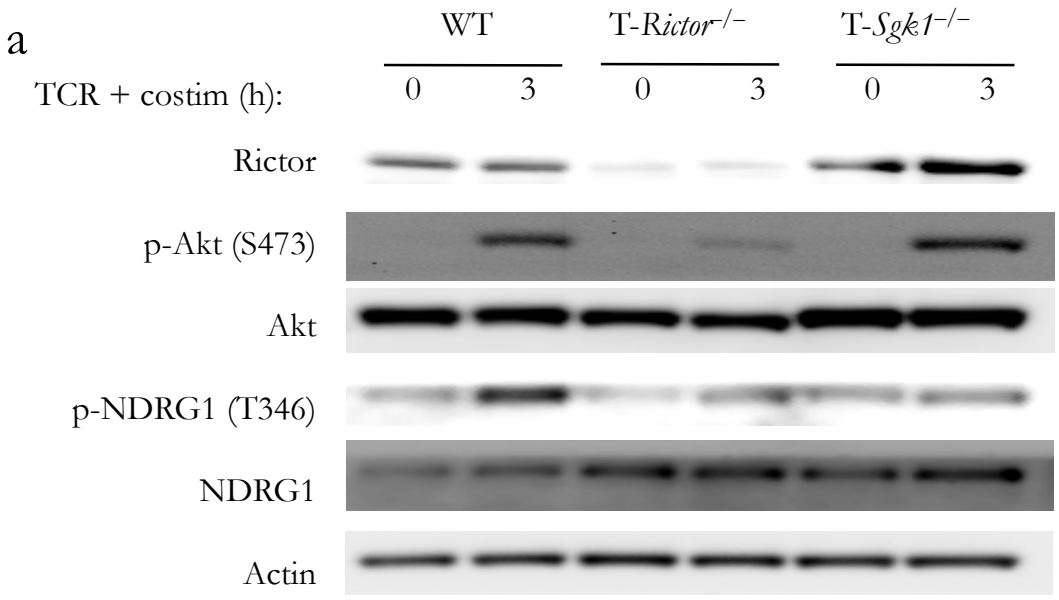
a
WT
T-Rictor−/−
T-Sgk1−/−
TCR + costim (h):
0
3
0
3
0
3
Rictor
p-Akt (S473)
Akt
p-NDRG1 (T346)
NDRG1
Actin

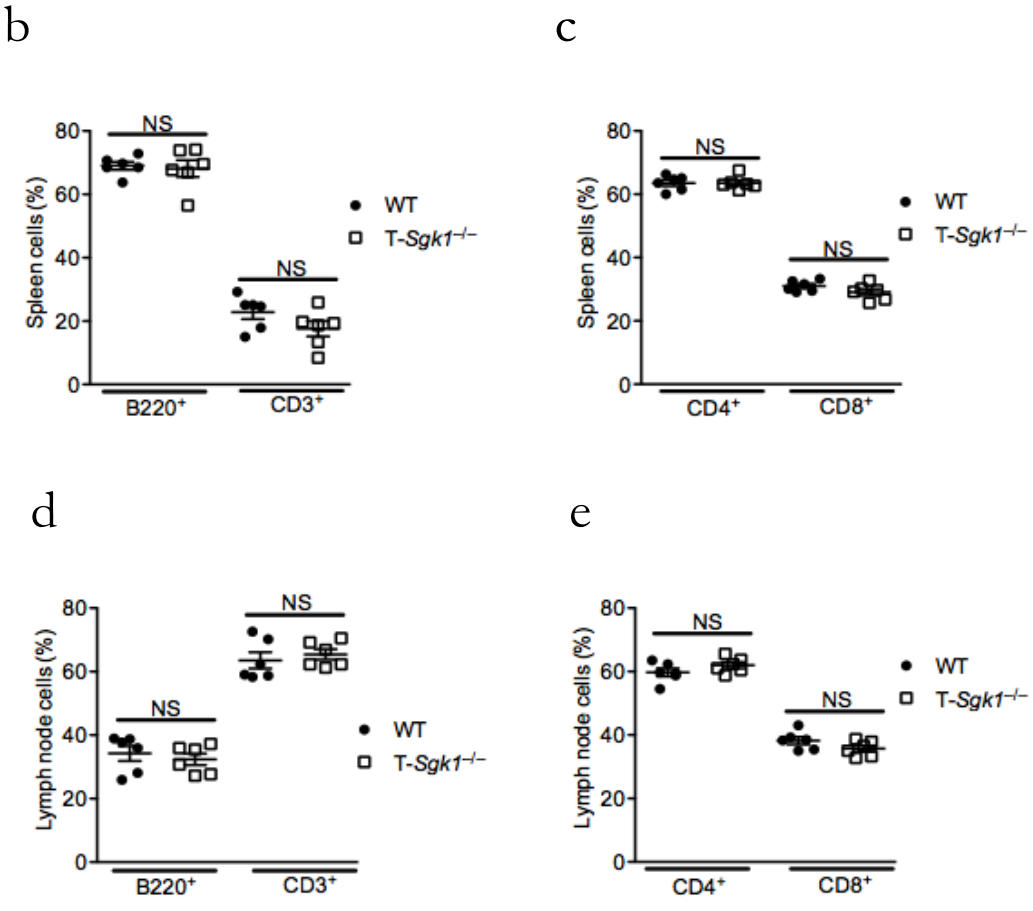
b
c
Spleen cells (%)
NS
NS
WT
T-Sgk1−/−
B220+
CD3+
CD4+
CD8+
d
e
Lymph node cells (%)

Figure 2, cont'd

f

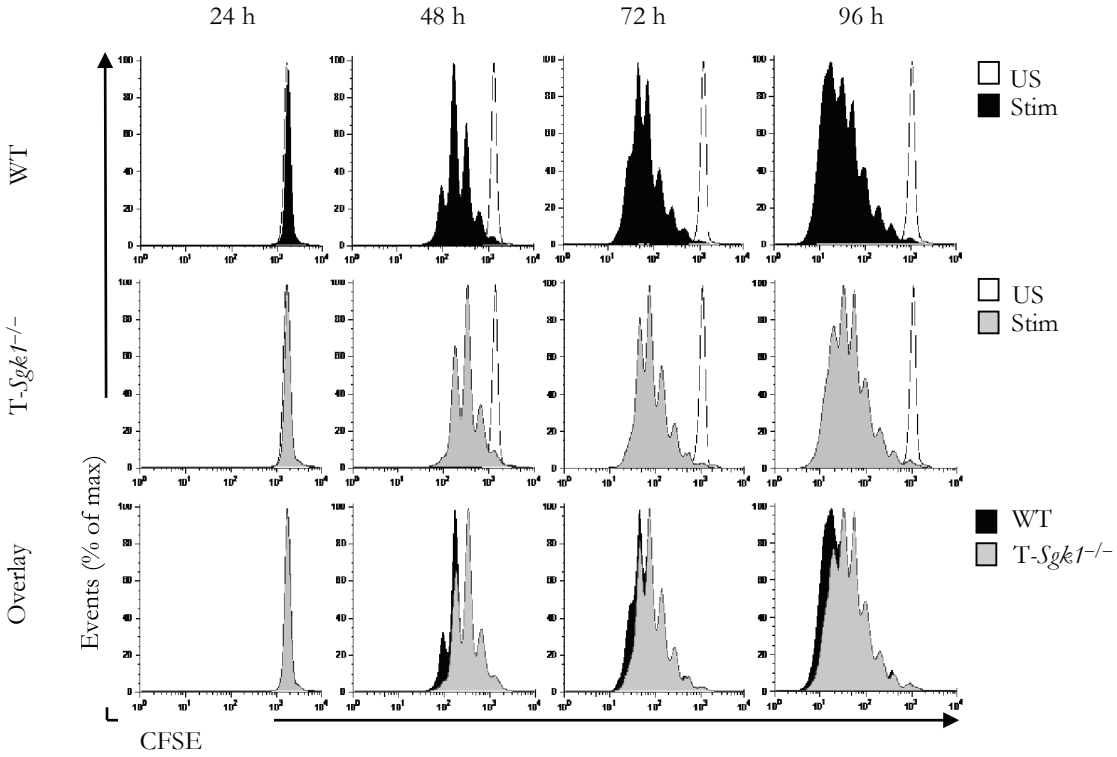

g

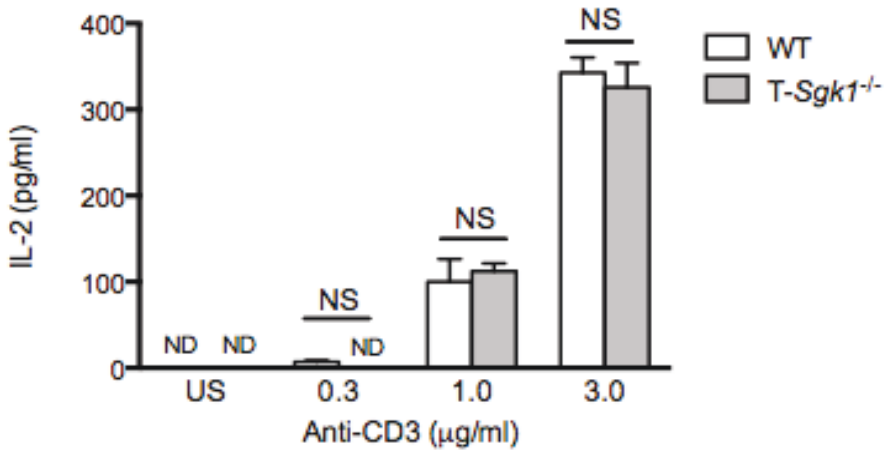

Figure 3

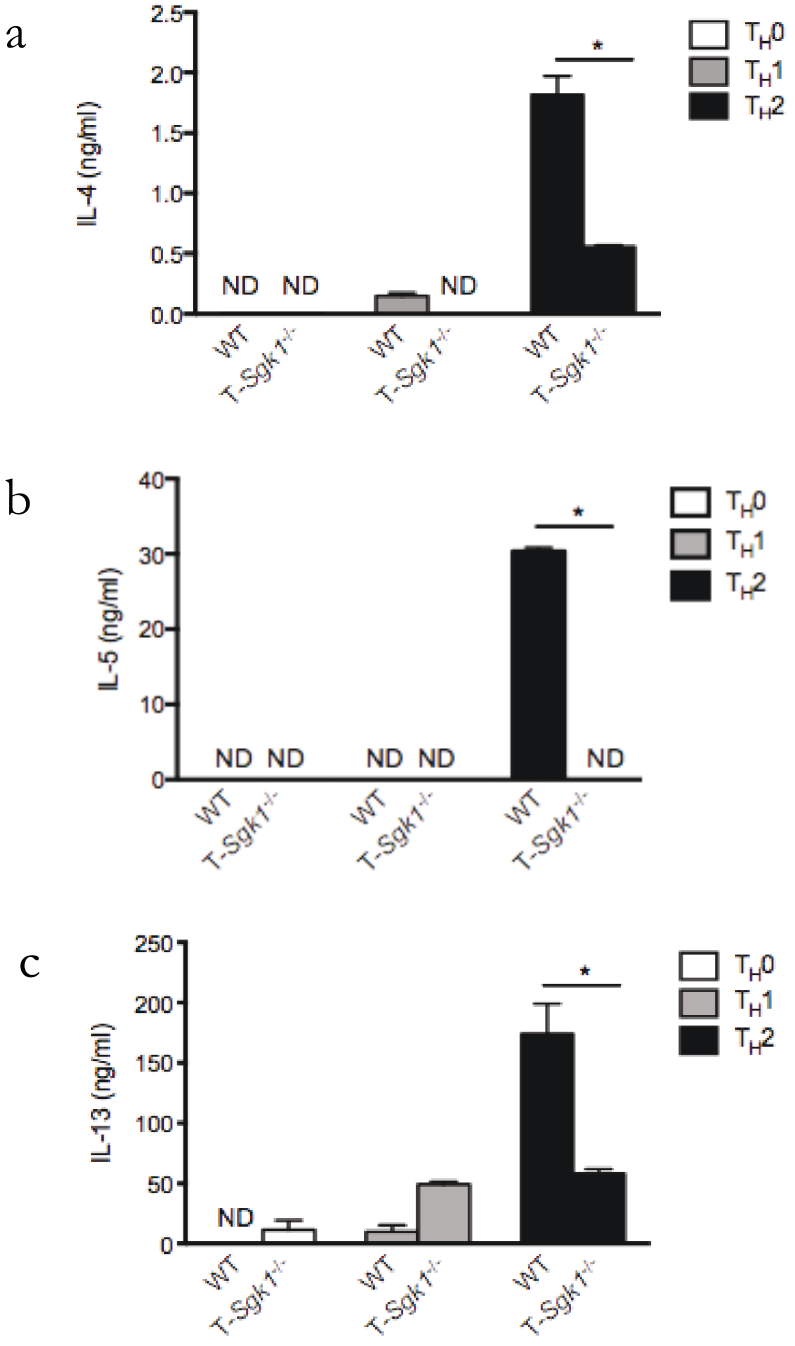
a
IL-4 (ng/ml)
2.5
2.0
1.5
1.0
0.5
0.0
ND ND
ND
*
T_H0
T_H1
T_H2
WT
T-Sgk1-/-
WT
T-Sgk1-/-
WT
T-Sgk1-/-
b
IL-5 (ng/ml)
40
30
20
10
0
ND ND
ND ND
ND
*
T_H0
T_H1
T_H2
WT
T-Sgk1-/-
WT
T-Sgk1-/-
WT
T-Sgk1-/-
c
IL-13 (ng/ml)
250
200
150
100
50
0
ND
*
T_H0
T_H1
T_H2
WT
T-Sgk1-/-
WT
T-Sgk1-/-
WT
T-Sgk1-/-

Figure 3, cont'd

d

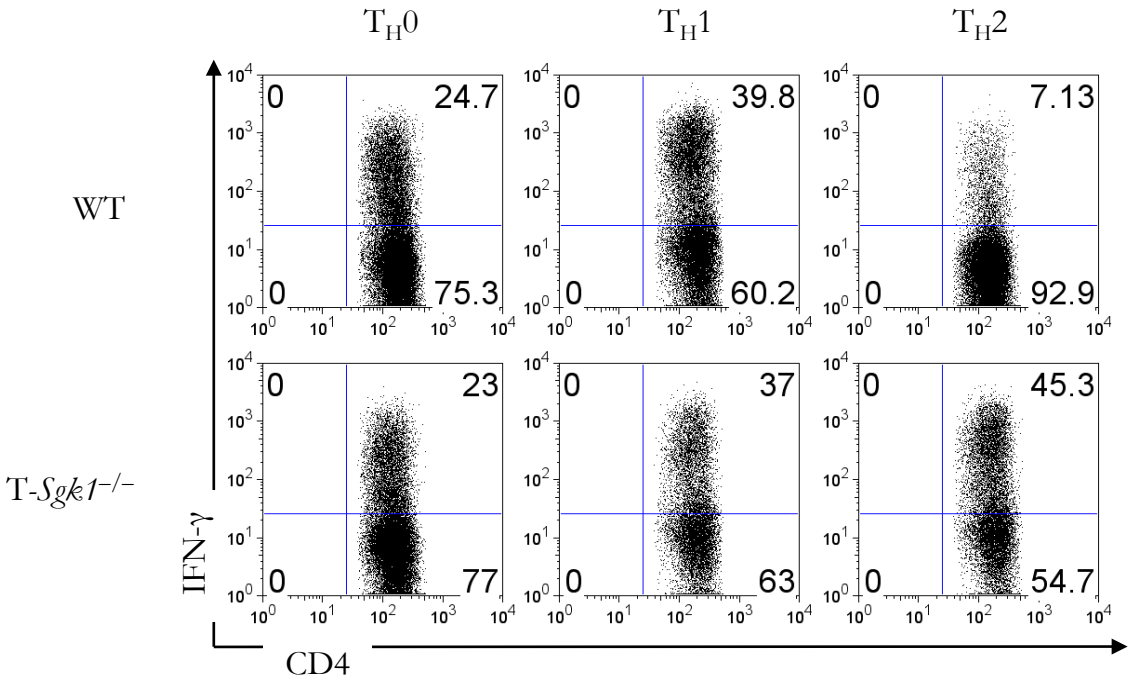

Figure 3, cont'd

e

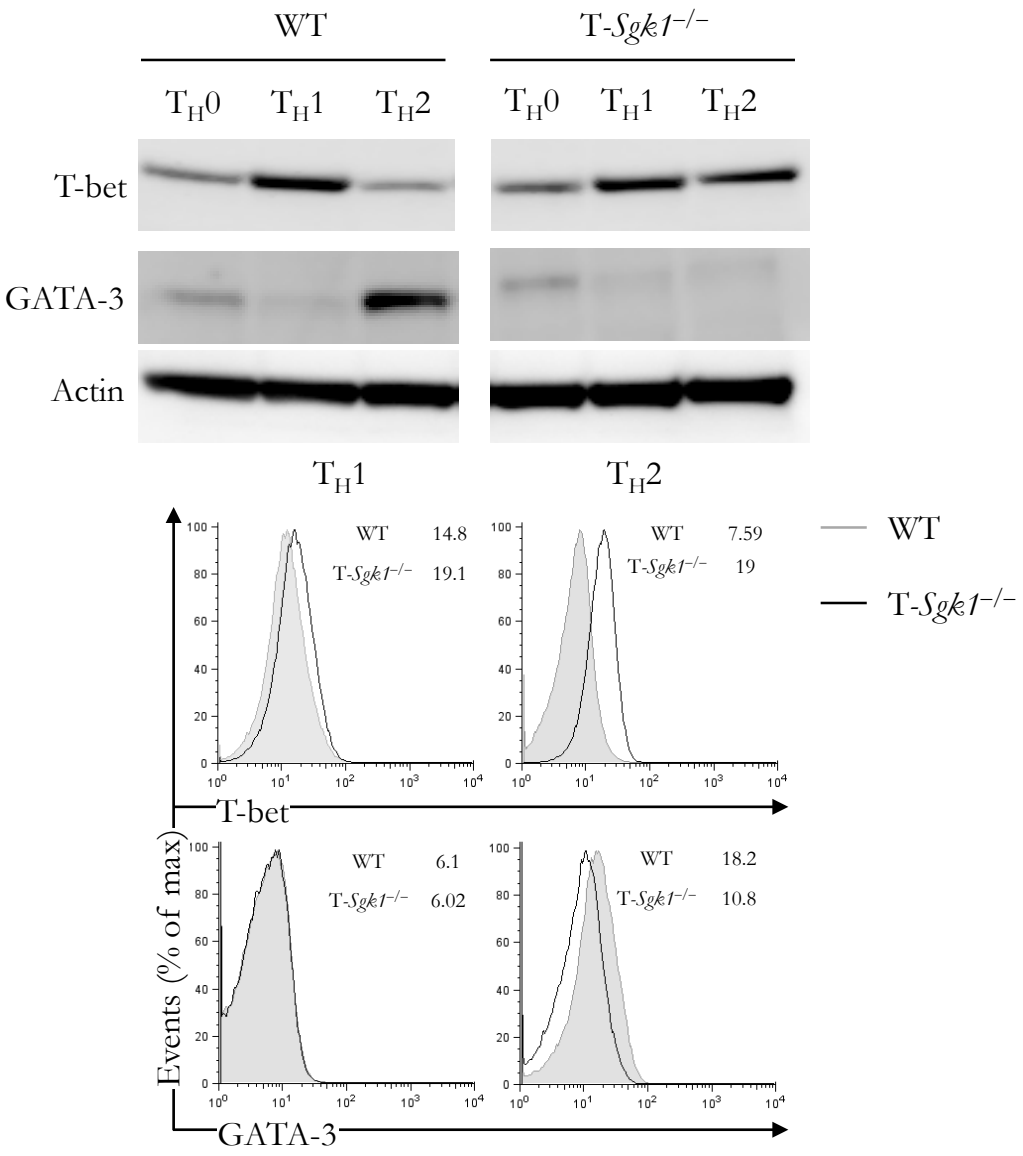

Figure 4

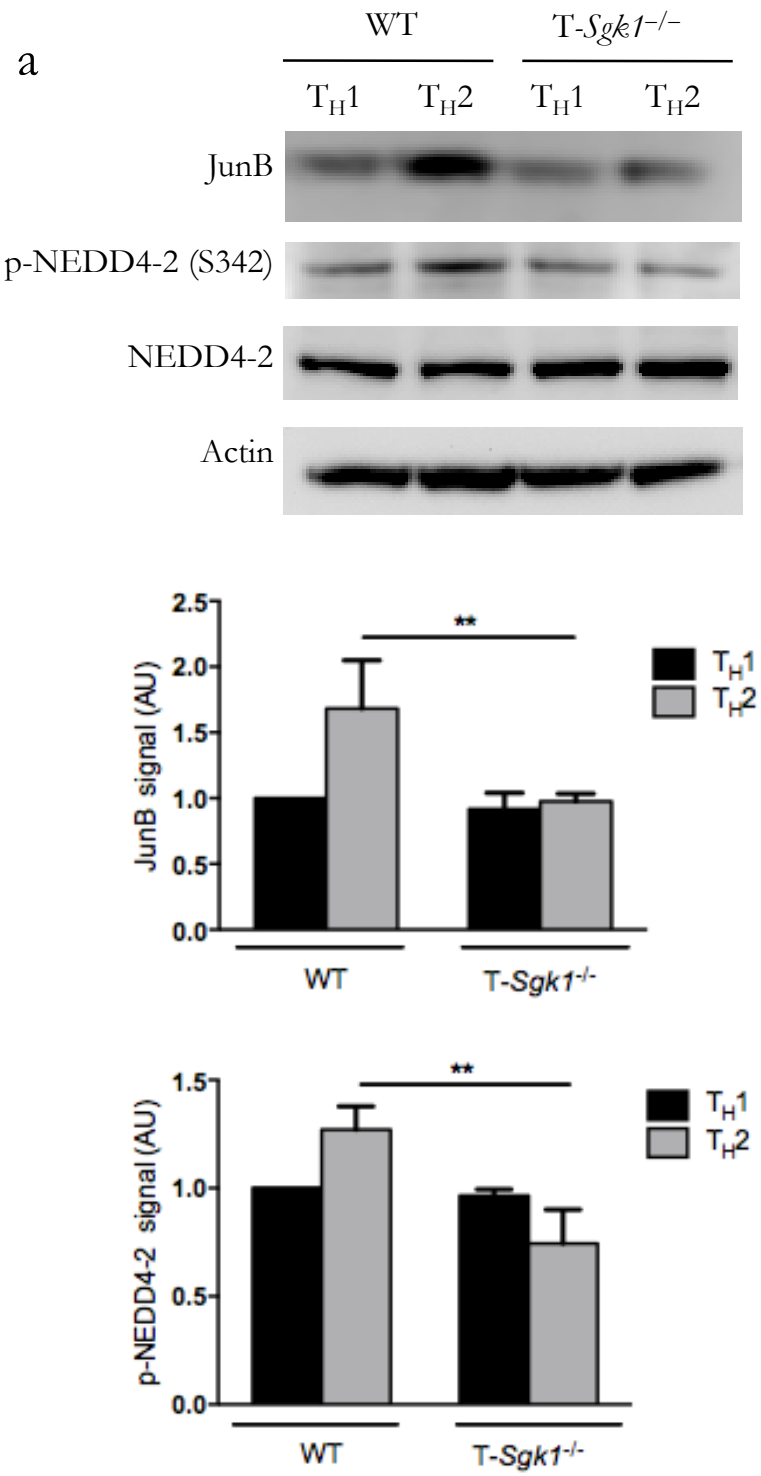
a
WT
T-Sgk1−/−
TH1
TH2
TH1
TH2
JunB
p-NEDD4-2 (S342)
NEDD4-2
Actin
JunB signal (AU)
2.5
2.0
1.5
1.0
0.5
0.0
**
TH1
TH2
WT
T-Sgk1-/-
p-NEDD4-2 signal (AU)
1.5
1.0
0.5
0.0
**
TH1
TH2
WT
T-Sgk1-/-

Figure 4, cont'd

b

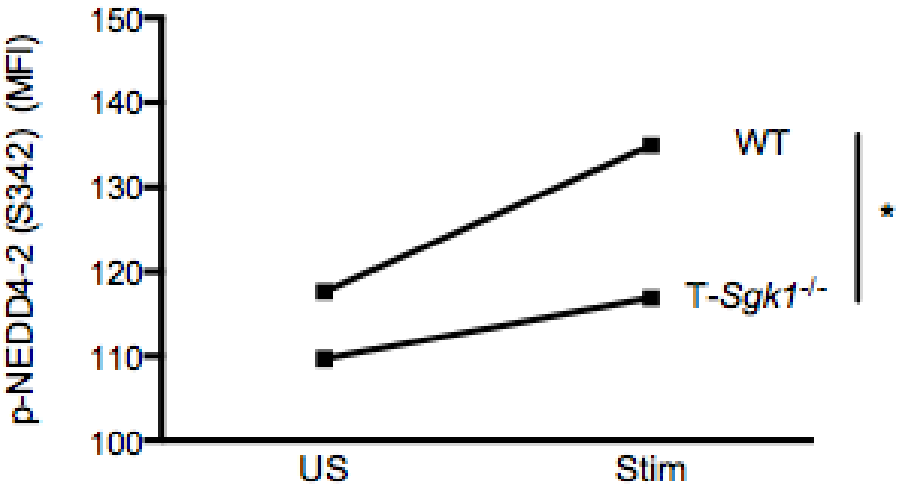

c

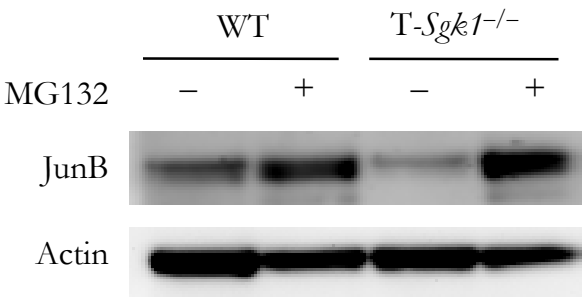

Figure 4, cont'd

d

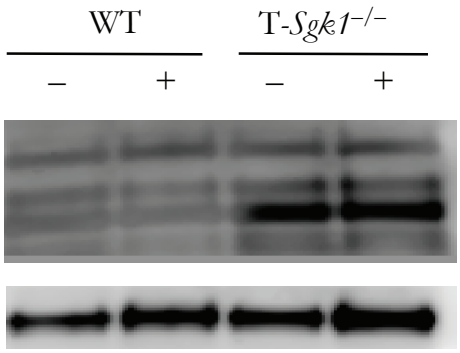

e

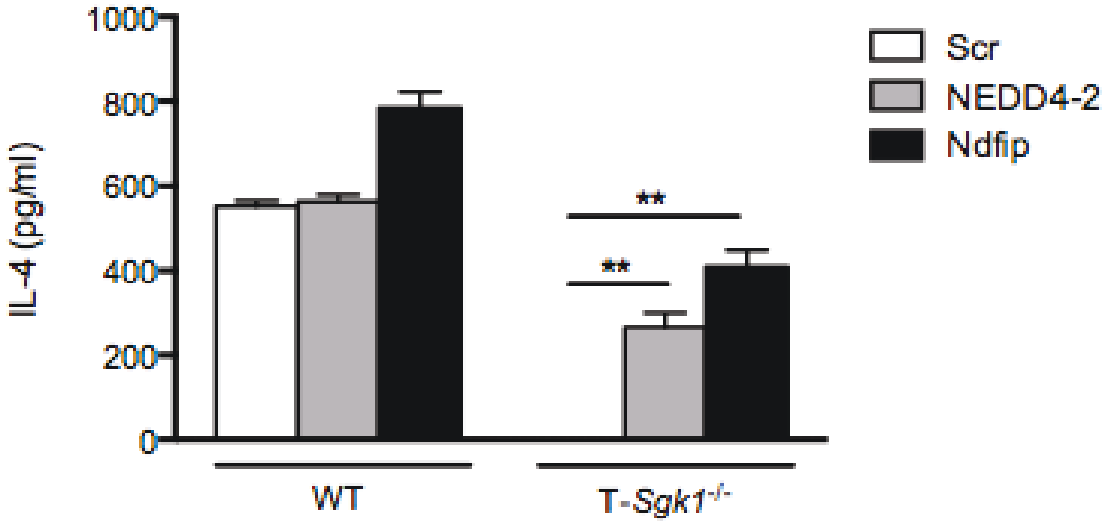

f

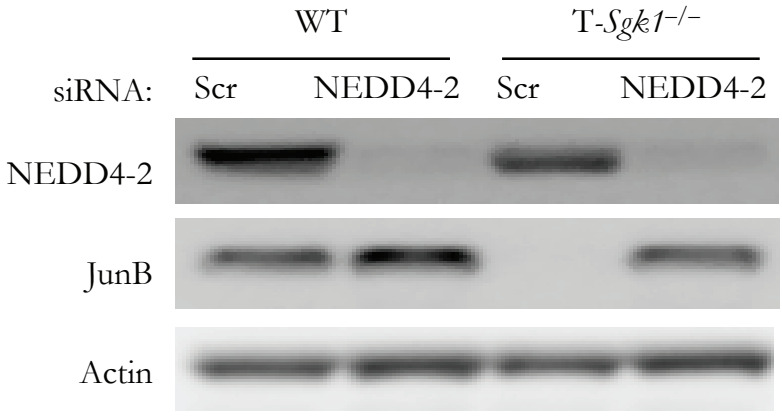

Figure 5

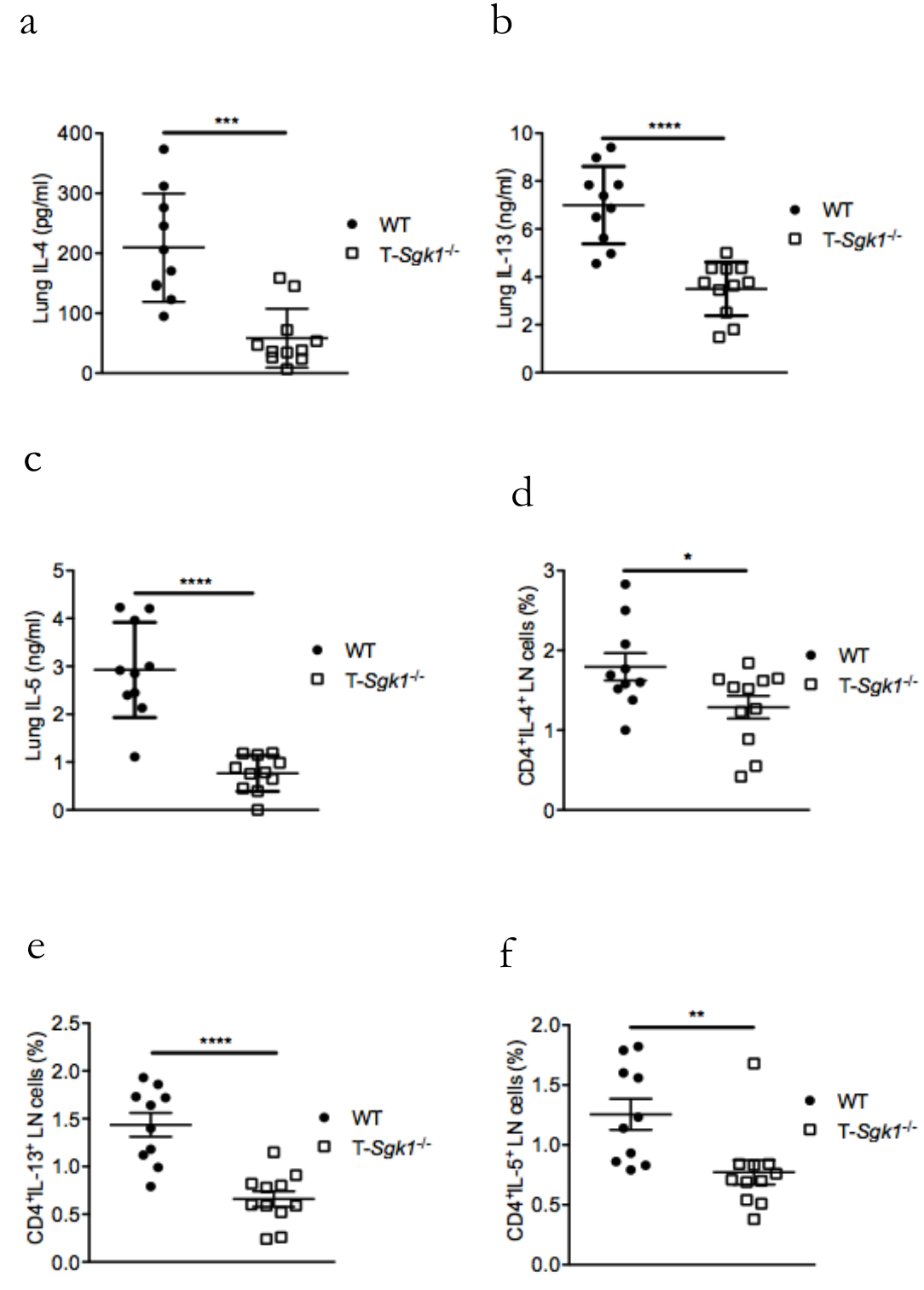
a
b
c
d
e
f
Lung IL-4 (pg/ml)
Lung IL-13 (ng/ml)
Lung IL-5 (ng/ml)
CD4+IL-4+ LN cells (%)
CD4+IL-13+ LN cells (%)
CD4+IL-5+ LN cells (%)
WT
T-Sgk1-/-
***
****
*
**

Figure 5, cont'd

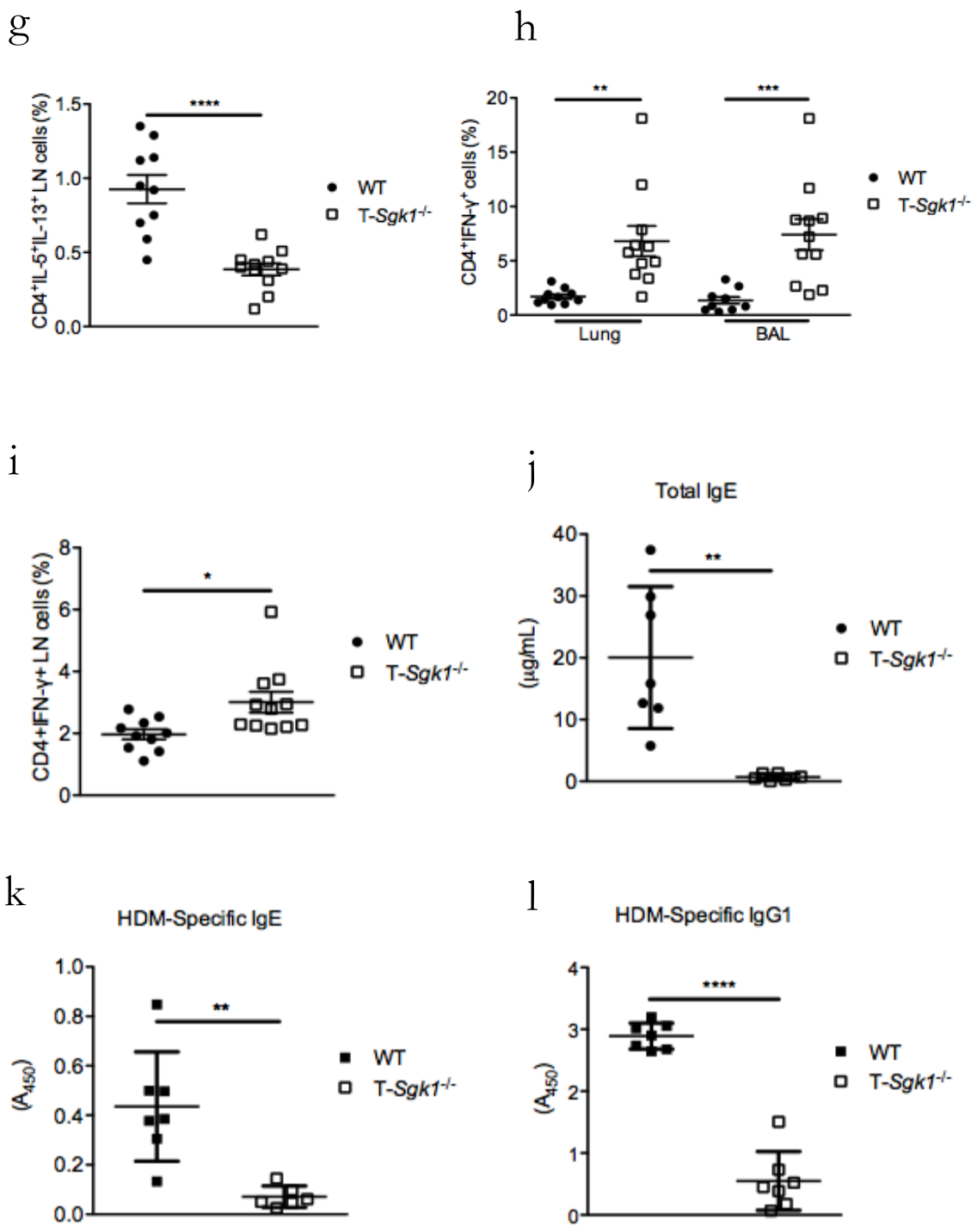

Figure 5, cont'd

m

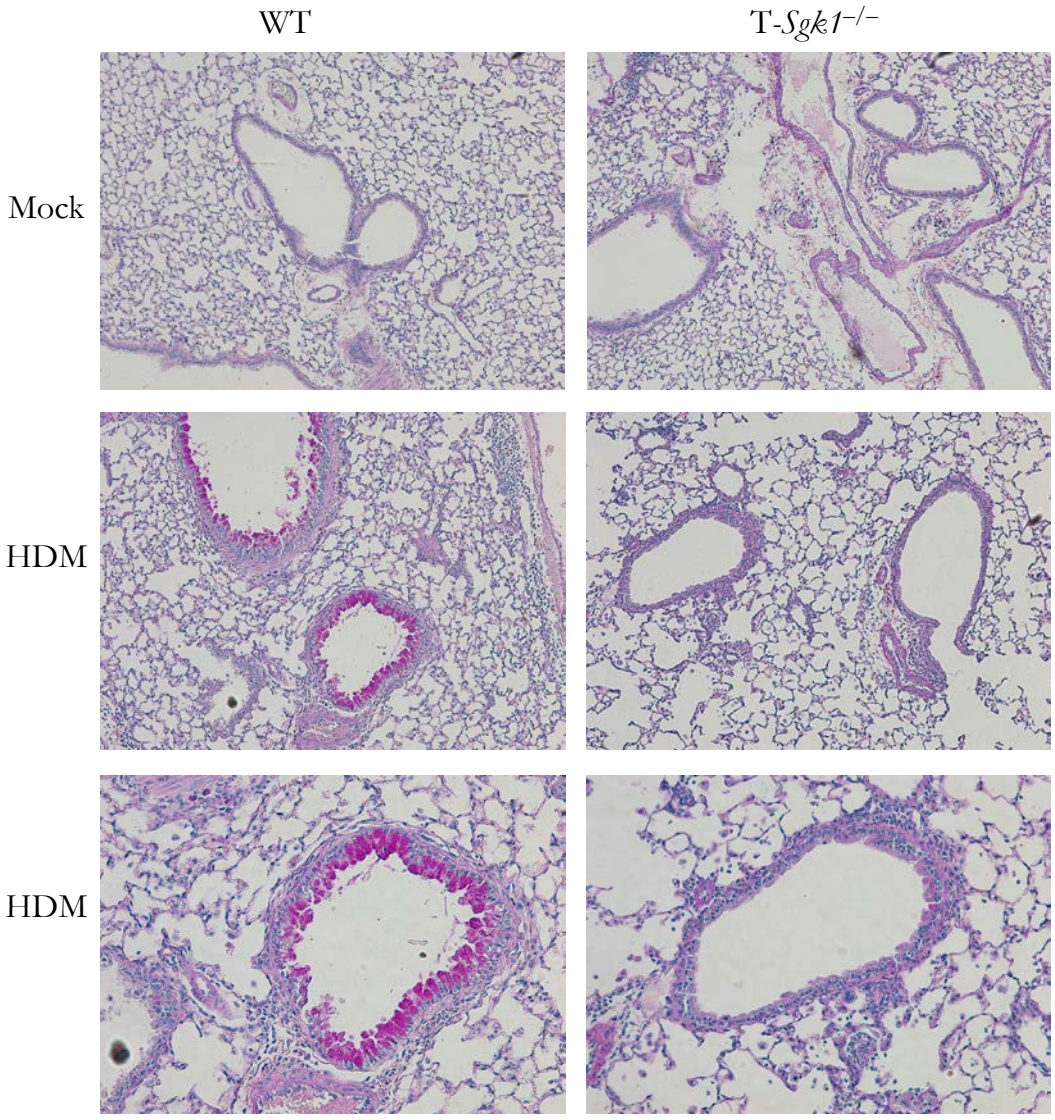

Figure 5, cont'd

n

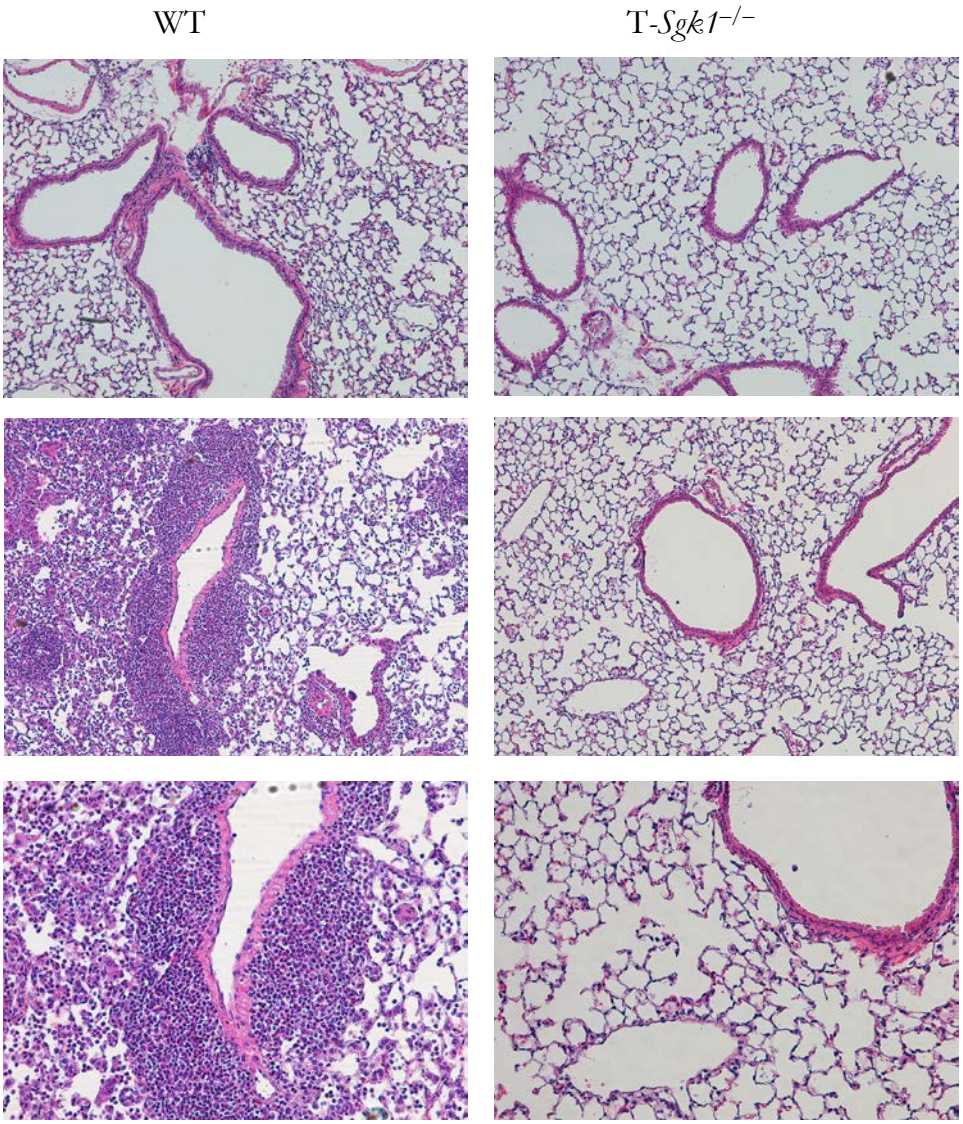

Figure 5, cont'd

o

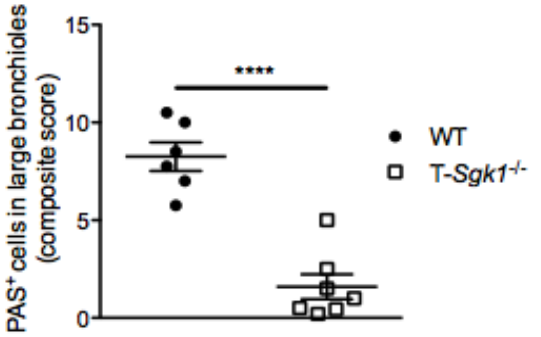

p

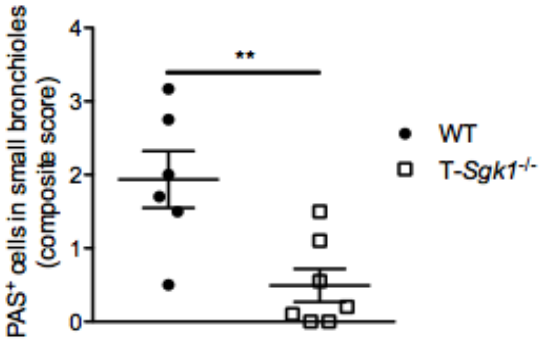

q

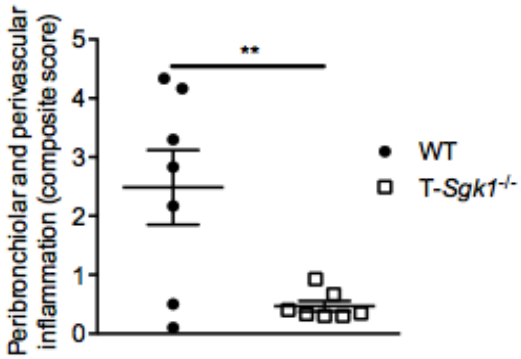

Figure 6

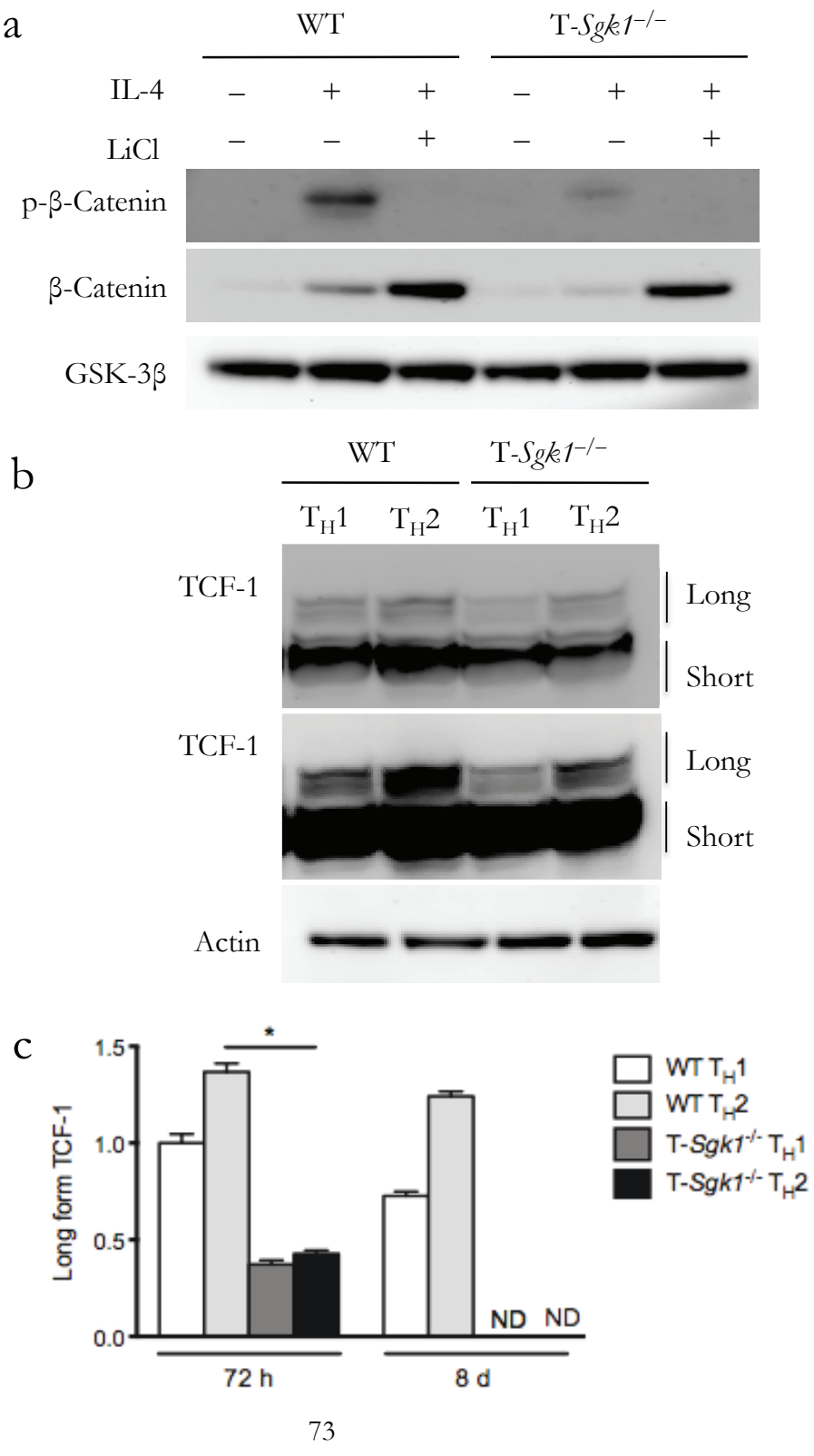
a
WT
T-Sgk1−/−
IL-4
LiCl
p-β-Catenin
β-Catenin
GSK-3β
b
WT
T-Sgk1−/−
TH1
TH2
TH1
TH2
TCF-1
Long
Short
TCF-1
Long
Short
Actin
c
Long form TCF-1
1.5
1.0
0.5
0.0
*
ND
ND
72 h
8 d
WT TH1
WT TH2
T-Sgk1-/- TH1
T-Sgk1-/- TH2

Figure 6, cont'd

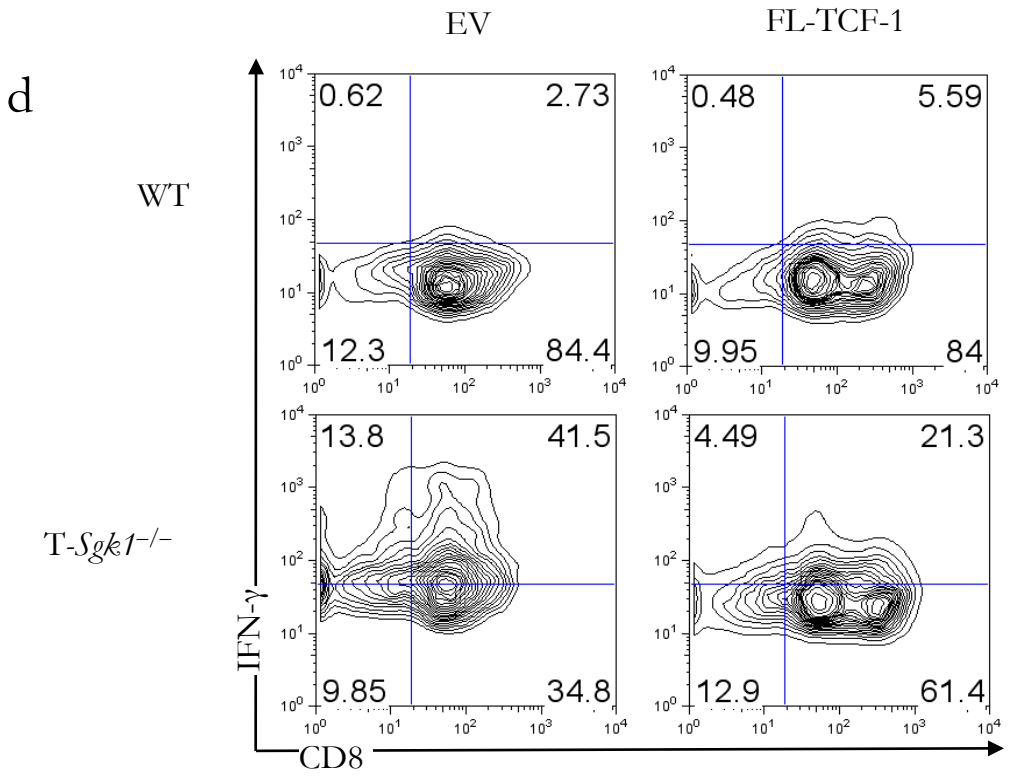

Figure 6, cont'd

d

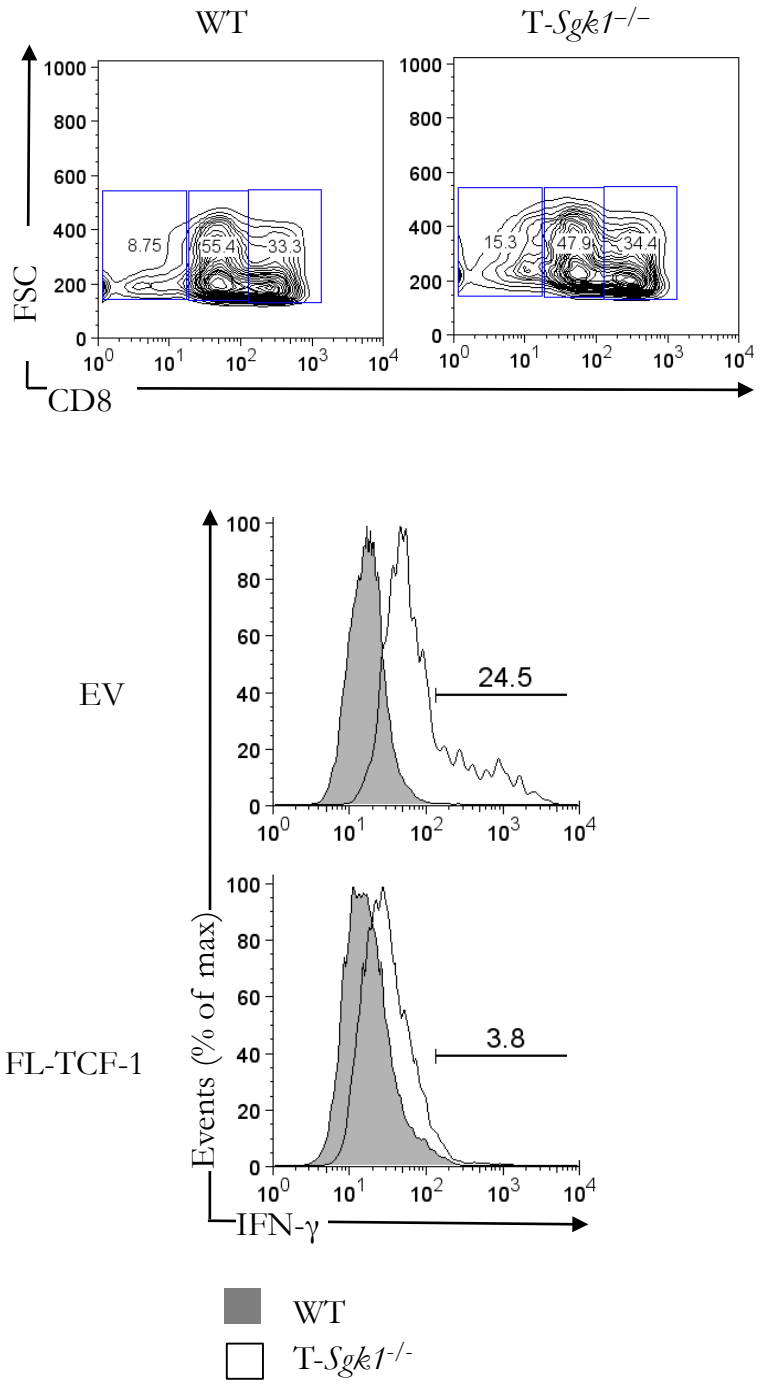

Figure 7

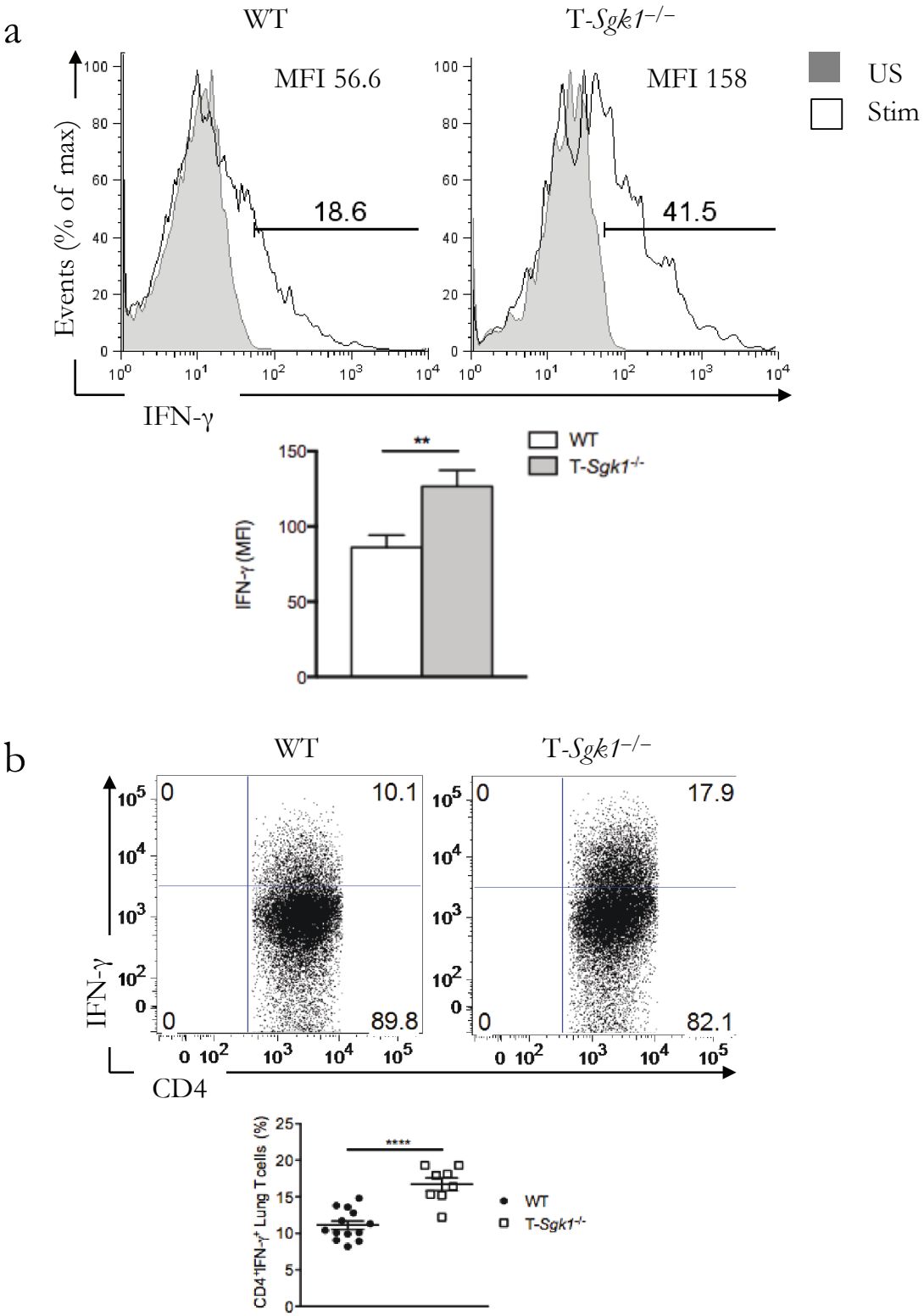
a
WT
T-Sgk1−/−
MFI 56.6
MFI 158
18.6
41.5
US
Stim
Events (% of max)
IFN-γ
IFN-γ (MFI)
WT
T-Sgk1-/-
**
b
WT
T-Sgk1−/−
10.1
89.8
17.9
82.1
IFN-γ
CD4
CD4+IFN-γ+ Lung T cells (%)
****
WT
T-Sgk1-/-

Figure 7, cont'd

c

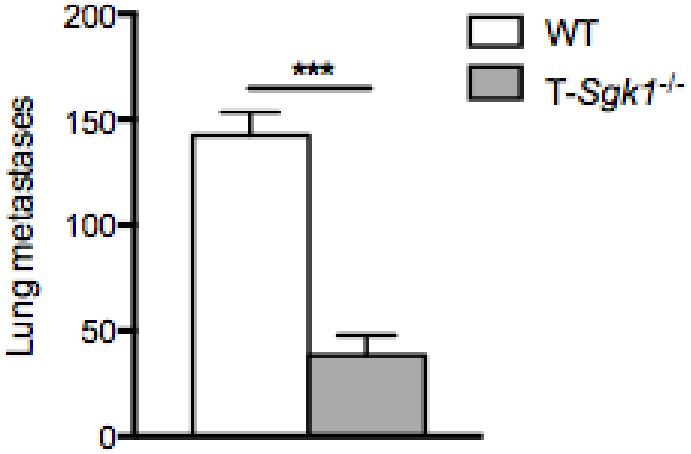

d

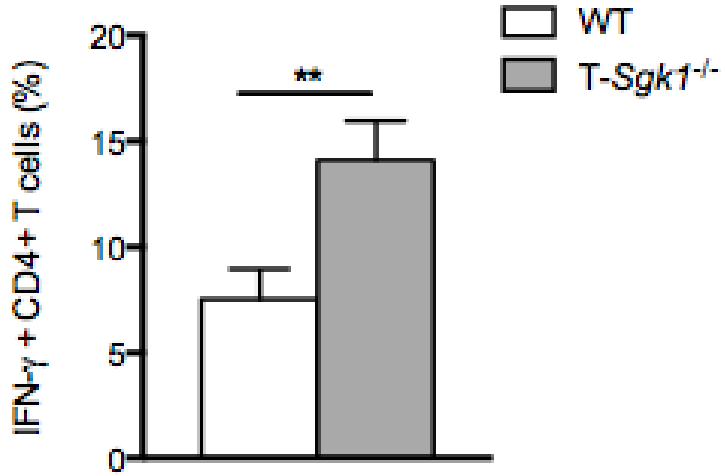

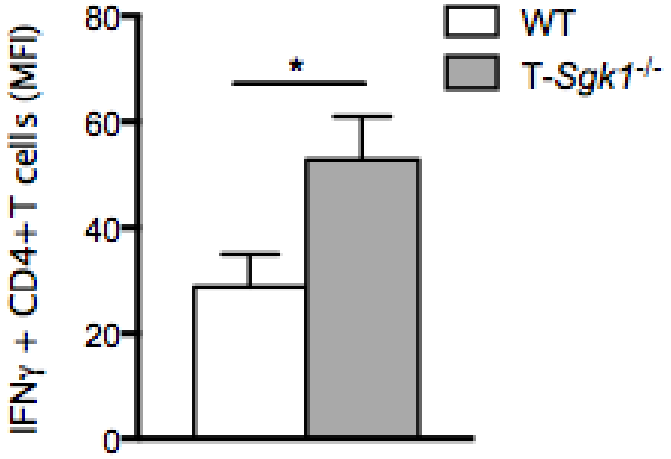

Figure 7, cont'd

e

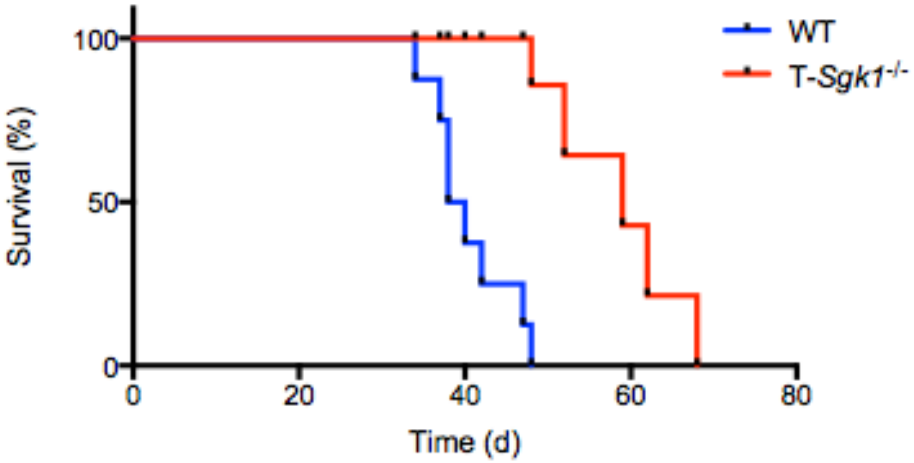

Supplementary Figure 1

a

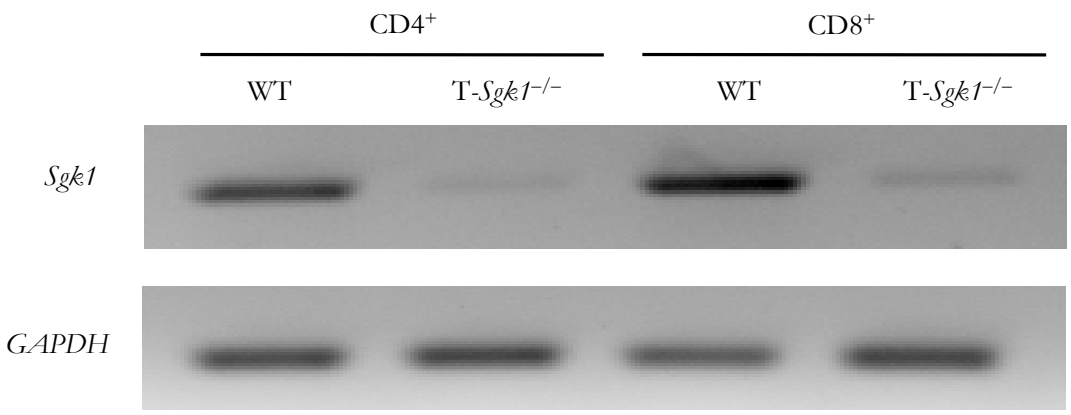

b

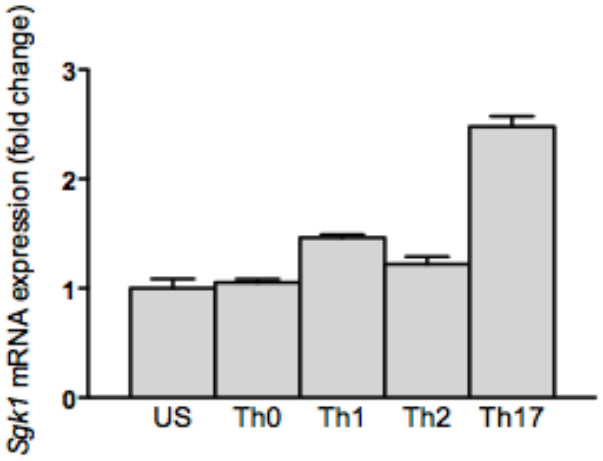

Supplementary Figure 2

a

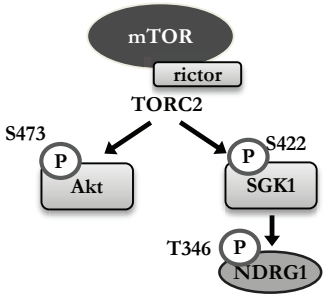

b

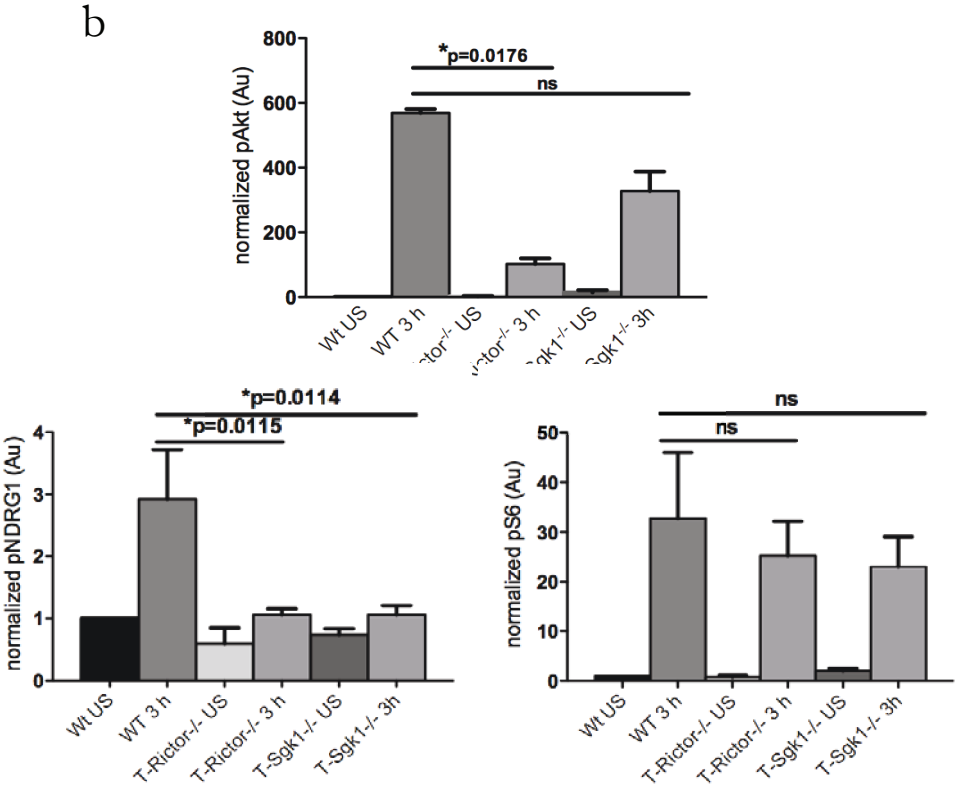

Supplementary Figure 2, cont'd

c

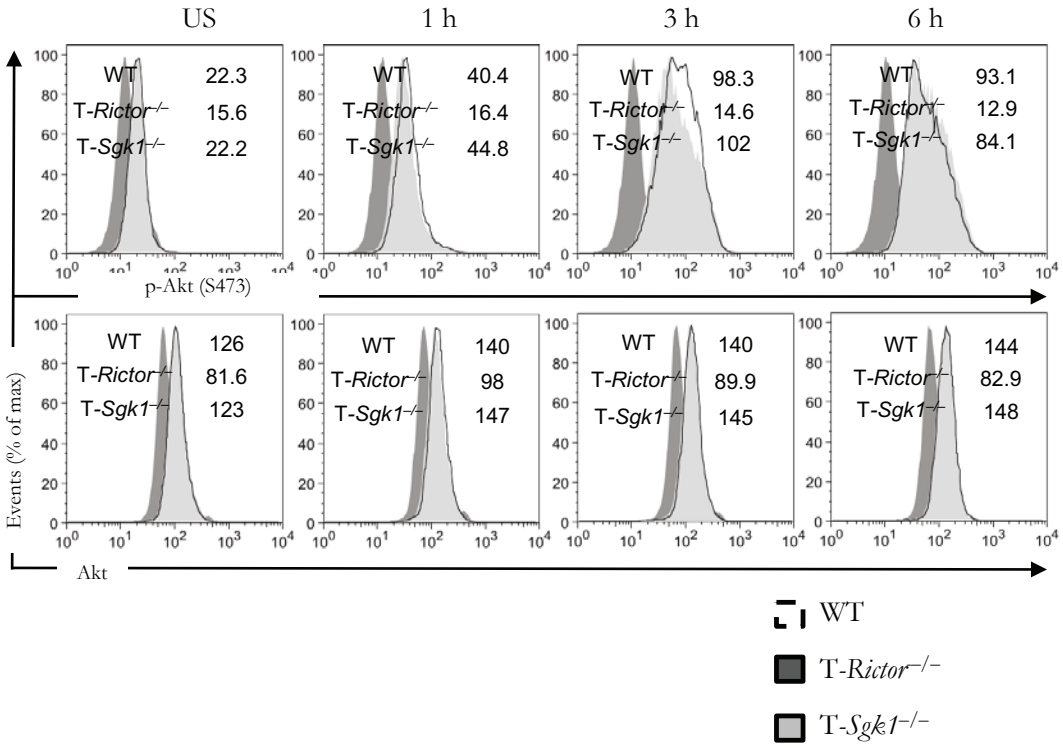

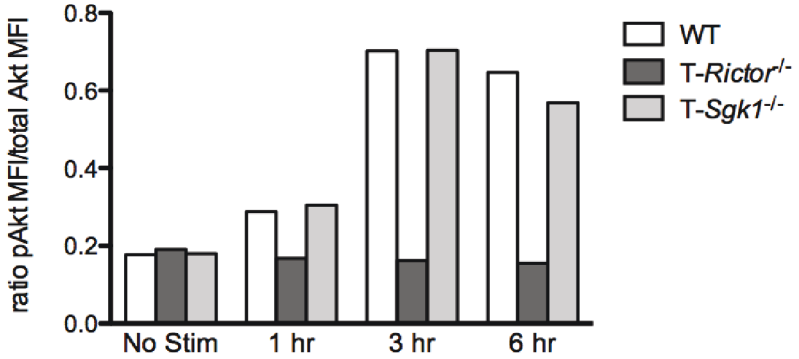

Supplementary Figure 3

a

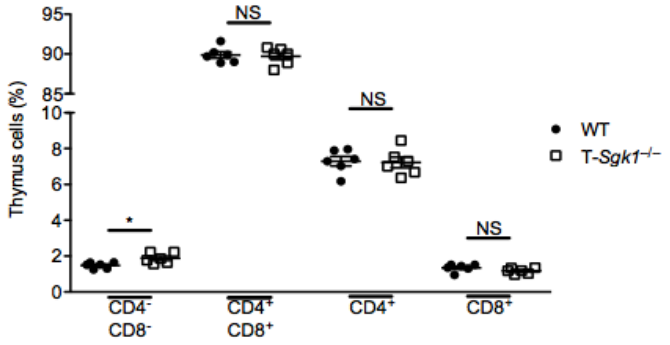

b

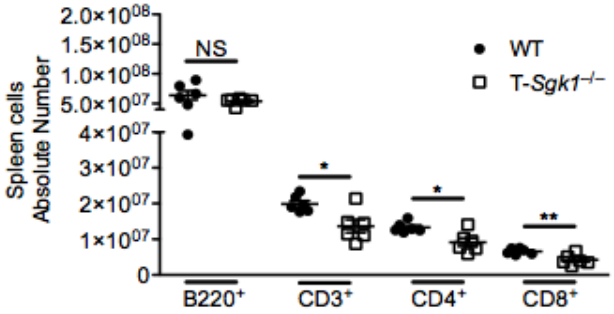

c

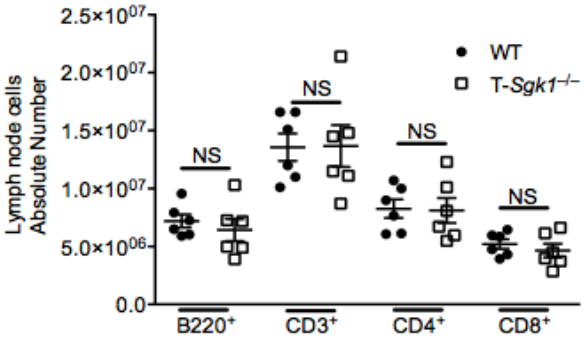

d

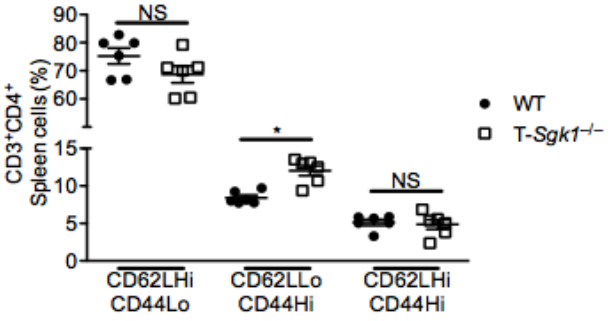

Supplementary Figure 3, cont'd

e

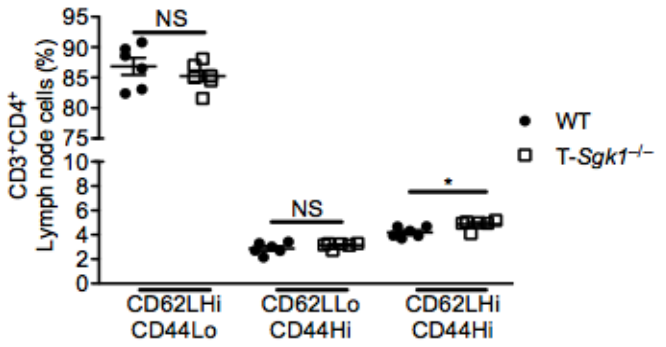

f

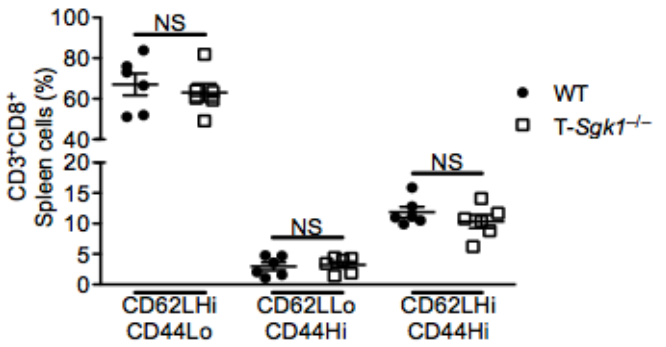

g

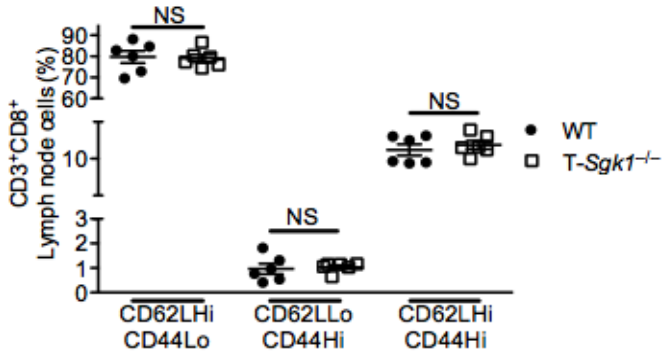

h

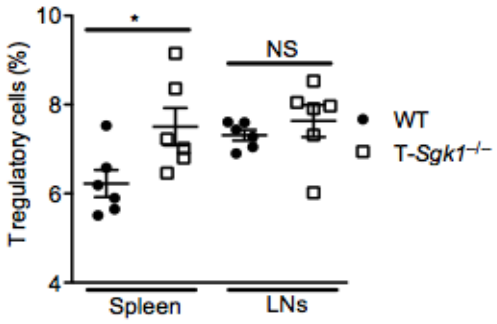

Supplementary Figure 4

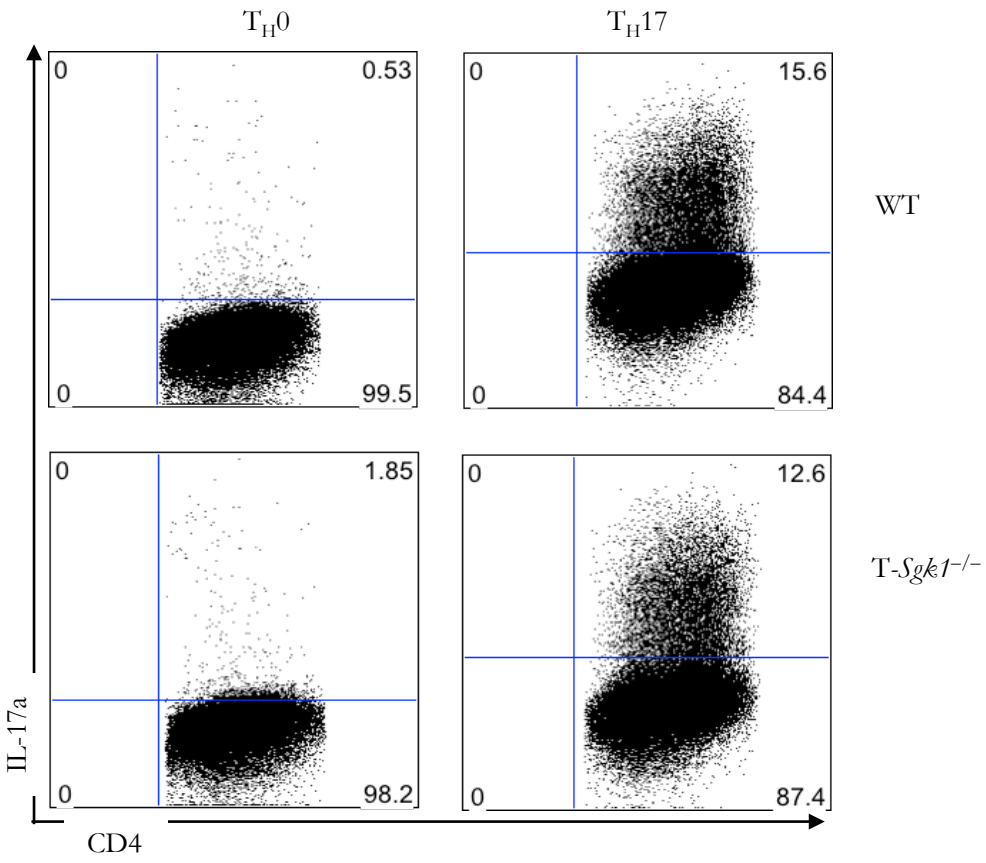

Supplementary Figure 5

a

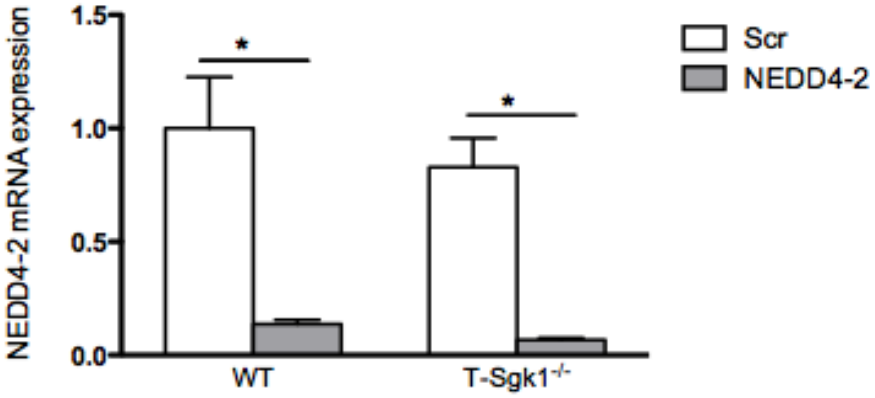

b

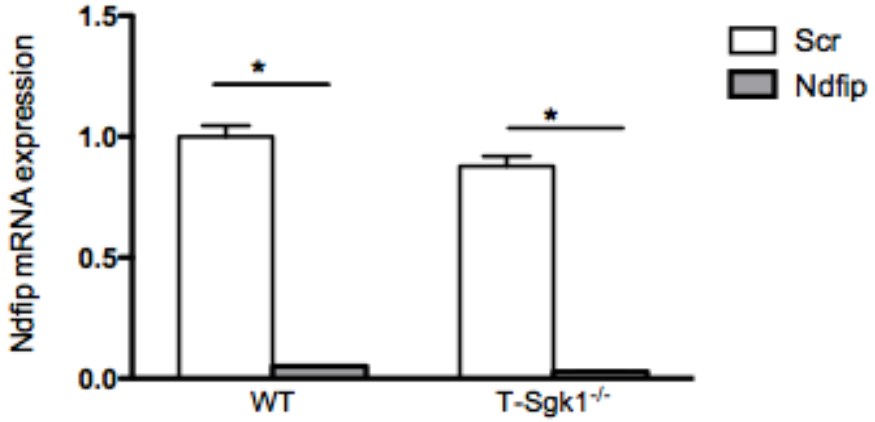

Supplementary Figure 6

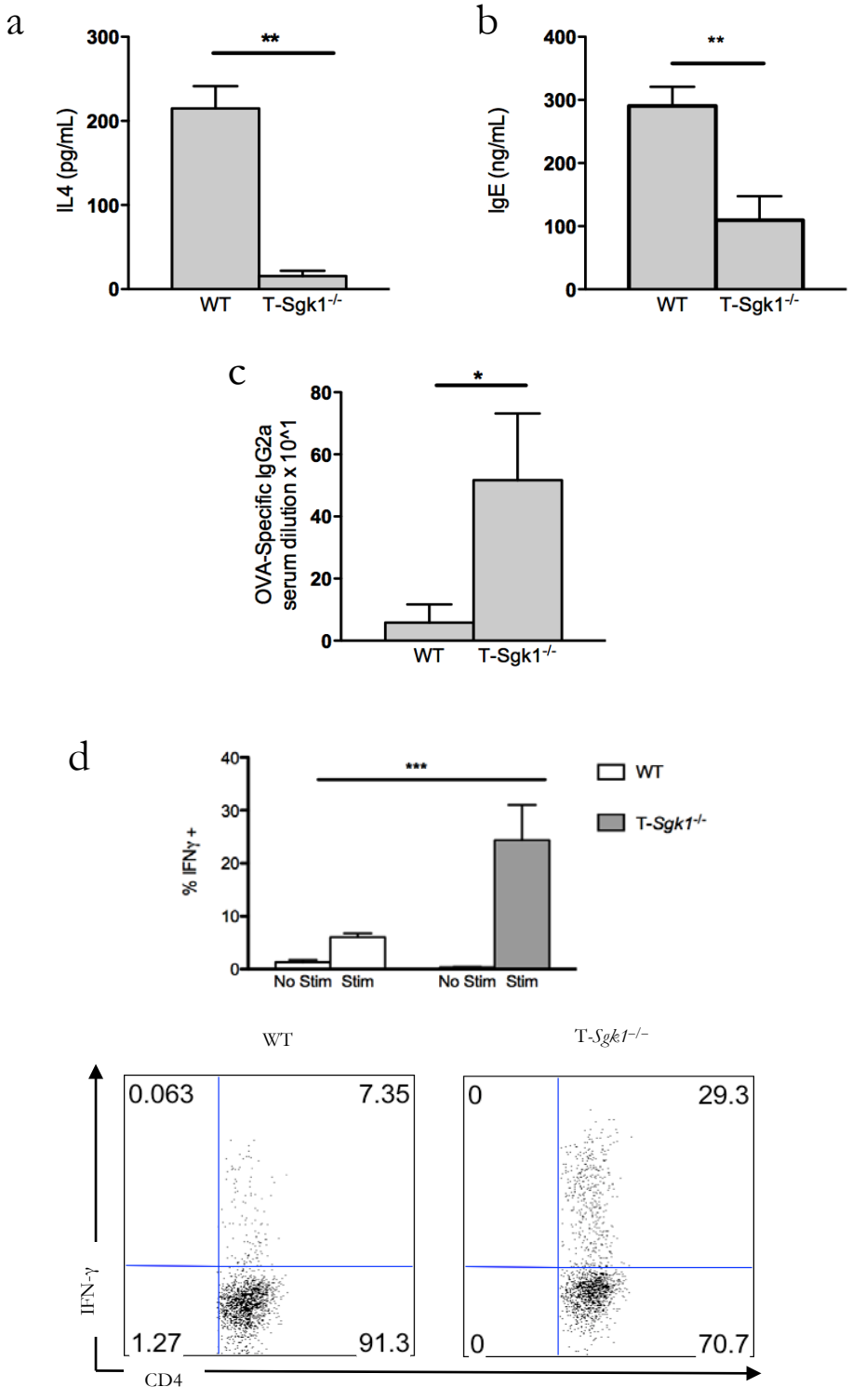

Supplementary Figure 6, cont'd

e

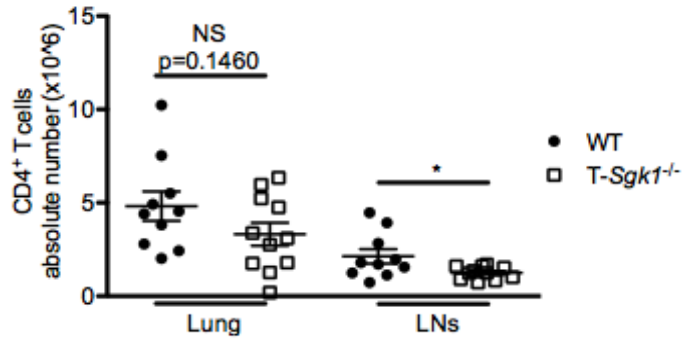

f

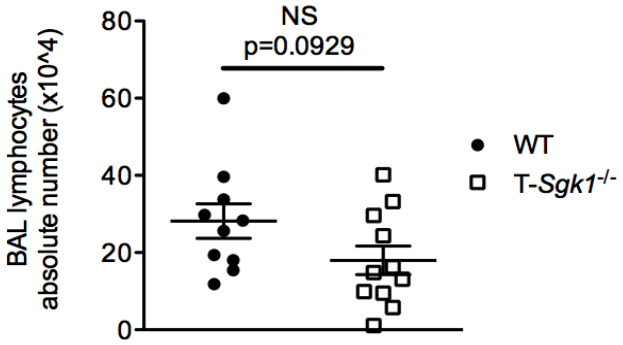

Supplementary Figure 7

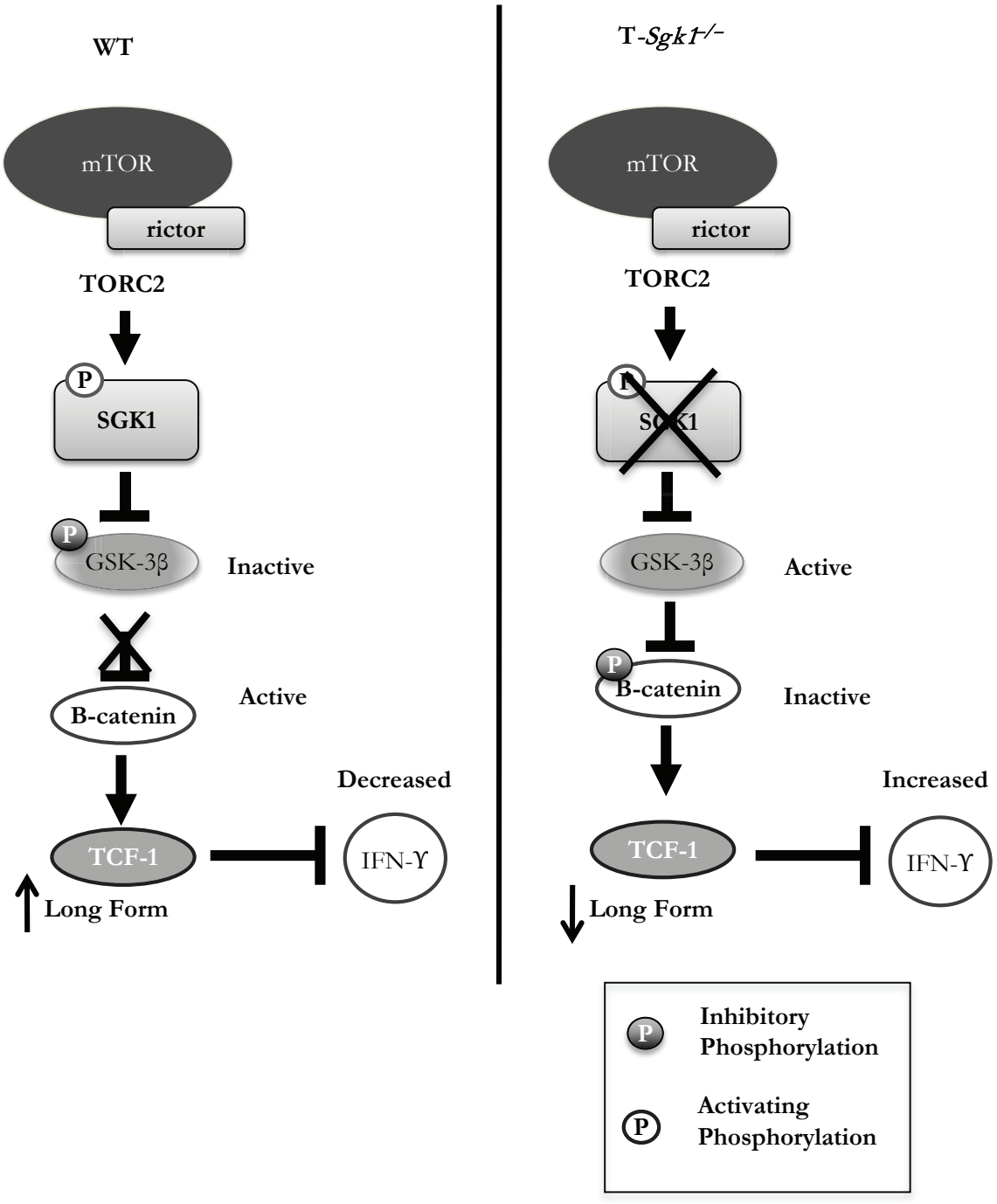

Supplementary Figure 8

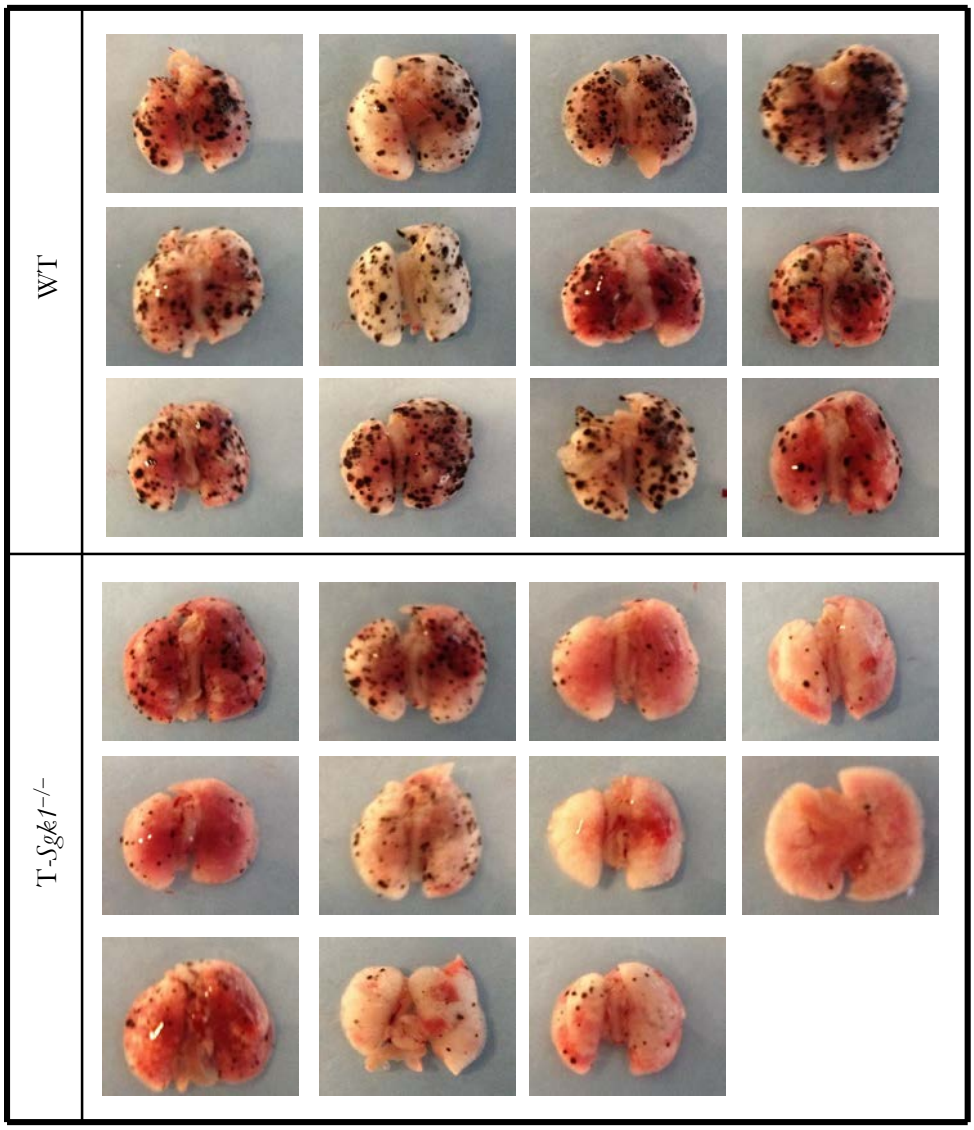

CHAPTER 3: SGK1 controls CD8+ memory differentiation by regulating Foxo1

Introduction

During an acute viral infection, antigen-specific CD8+ T cells expand rapidly, undergoing one cell division every 4 hours[1]. Two distinct subsets of CD8+ T cells arise during the course of an anti-viral immune response: cytotoxic effector cells and memory cells. The pool of CD8+ T cells at the height of the effector response can be divided into at least 2 subsets based on expression of the IL-7 receptor (IL-7R/CD127) and killer cell lectin-like receptor subfamily G, member 1 (KLRG1). Short-lived effector cells are $CD127^{LO}$ and $KLRG1^{HI}$, whereas memory precursor cells are $CD127^{HI}$ and $KLRG1^{LO}$ [2-4]. Effector and memory cells display also differences in their ability to survive, which underscores their unique roles in the immune response. Cytotoxic effector cells can proliferate rapidly to kill virally infected targets, but most of these cells undergo apoptosis during the contraction phase of the immune response. By contrast, memory cells divide slowly but have enhanced longevity compared to effector cells[5]. If rechallenged by a virus expressing the same antigen, memory cells can expand rapidly in a burst of proliferation that characterizes the secondary immune response[6].

Once a pathogen is cleared, memory cells are maintained in an antigen-independent, cytokine-dependent manner[2,7]. Memory cells are exquisitely sensitive to and dependent upon homeostatic cytokines such as IL-7 and IL-15 for their survival and self-renewal[2,8]. Thus, memory cells are characterized by high surface expression of the IL-7 and IL-15 cytokine receptors (IL-7R/CD127 and IL-15R/CD215)[9]. The basal rate of proliferation that is required for maintenance of memory cells is referred to as homeostatic proliferation[10,11].

Expression of CD127 alone, however, is not sufficient to enforce memory differentiation[12]. Rather, memory cells require a distinct transcriptional program to deliver instructive signals for proliferation and survival.

In addition to a distinct surface receptor phenotype, memory cells are also distinguished by their expression of the T-box transcription factor eomesodermin (EOMES)[13]. The expression of EOMES seems to be reciprocally regulated with Tbet, another T-Box transcription factor that predominates in effector cells[14,15]. Although it is expressed in effector cells albeit at low levels, EOMES is necessary for memory differentiation. Loss of EOMES in CD8+ T cells results in an inability to generate memory cells that display homeostatic proliferation and homing to lymph nodes and bone marrow[13]. It has recently been appreciated that the ratio of Tbet and EOMES is in part regulated by mTOR[16]. Thus, a model is emerging whereby mTOR regulates the balance of effector versus memory potential of CD8+ T cells via its regulation of downstream transcriptional networks.

Much like mTOR controls the differentiation of helper CD4+ T cells, there is new evidence to suggest that mTOR controls the effector to memory transition in CD8+ T cells[16-18]. Several studies have shown that inhibition of mTOR can lead to enhanced memory T cell differentiation[16,17,19]. Based on the divergent metabolic demands of effector and memory cells this is not surprising. However, it suggests that rapamycin, initially described as an immunosuppressive agent, may also be employed to enhance CD8+ memory generation. Indeed, in a mouse model of Lymphocytic Choriomeningitis Virus (LCMV) rapamycin was shown to increase the number of virus-specific CD8+ T cells by promoting

survival of memory T cells during the contraction phase of the immune response[17]. The observed decrease in attrition was due to upregulation of the anti-apoptotic factor Bcl-2[17]. Furthermore, it has been shown that rapamycin can promote CD8+ memory cell generation by inhibiting T-bet activation and enhancing EOMES activity[16]. In this model, treating mice with rapamycin during vaccination led to enhanced anti-tumor immunity. These studies suggest that mTOR is a critical regulator of downstream transcriptional networks that drive CD8+ T cell differentiation during an immune response. However, it is unclear what is the precise role of TORC1 versus TORC2 in regulating effector and memory differentiation.

Because of the emerging role of mTOR in regulating CD8 T cell responses, we hypothesized that SGK1 might also be an important regulator of effector and memory differentiation. Unpublished work from our laboratory has shown that loss of TORC2 activity (using *T-Rictor*-/- mice) is not necessary for effector differentiation. There is some evidence to suggest, however, that loss of TORC2 results in enhanced memory differentiation, characterized by decreased attrition of cells during the contraction phase of the immune response. Since SGK1 is a critical node downstream of mTORC2, we hypothesized that SGK1 might be responsible for the enhanced memory phenotype that we observe in *T-Rictor*-/- mice. To this end, we utilized our *T-SGK1*-/- mice to study the role of SGK1 in CD8+ effector and memory differentiation.

Methods

Mice. Mice were kept in accordance with guidelines of the Johns Hopkins University Institutional Animal Care and Use Committee. Mice with *lox*P-flanked *SGK1* alleles were

generated in the Fejes-Tóth laboratory, and mice with *lox*P-flanked *Rictor* alleles were provided by M. Magnuson. C57BL/6, *Cd4*-Cre, RAG2-/- and OT-I mice were obtained from Jackson Laboratories and bred to Thy-1.1 backgrounds. 5C.C7 mice were from Taconic Farms.

T cell stimulation. CD8+ T cells were purified by negative selection using a CD8+ isolation kit and MACS Cell Separation (Miltenyi Biotec). For immunoblot analysis of mTOR substrates, T cells were stimulated with mouse T activator magnetic Dynabeads coated with antiCD3/antiCD28 (Life technologies) for 1 or 3 hours. For coculture experiments, T cells were stimulated with activator beads for 48 hours, then expanded in IL-7 (Peprotech).

Vaccinia model. Mice were immunized with 1e6 pfu VAC-OVA by either retroorbital injection or intraperitoneal injection. For adoptive transfer experiments, 1e6 naïve CD8+ T cells specific for the OVA Class I epitope (OVA 257 - 264) congenically marked with Thy1.1 were transferred intravenously to Thy1.2 C57/BL6 recipients by retroorbital injection.

Homeostatic proliferation model. 1e6 naïve CD8+ T cells congenically marked with Thy1.1 were labeled with 5.0 uM CFSE and transferred intravenously to RAG2-/- recipients via retroorbital injection. Spleens were harvested on day 5 and analyzed by flow cytometry for CFSE dilution and expression of CD127.

Chromatin immunoprecipitation. Chromatin immunoprecipitation assays were done using the MAGnify chromatin immunoprecipitation kit (Applied Biosystems) according to

the manufacturer's instructions. Briefly, 10e6 Thy1.1+ adoptively transferred and sorted cells were fixed with 1% formaldehyde in PBS for 10 min at 25°C. Following fixation, cells were lysed for 5 minutes at 4 °C. Chromatin was sheared by sonication using a Biorupter UCD 200 on high power for 16 cycles of 30 seconds on, 30 seconds off. Sheared chomatin lysates were centrifuged, diluted, and divided into two equal fractions for incubation overnight at 4 °C with 5.0 μg of rabbit anti-mouse Foxo1 antibody (Cell Signaling, 2880) or rabbit IgG bound to magnetic beads. Immunoprecipitated chromatin was washed and eluted from the beads, and reverse crosslinked. After treatment with proteinase K, DNA was isolated using magnetic beads and resuspended in Tris-EDTA buffer. Immunoprecipitates and input fraction were analyzed in triplicate by qPCR using SYBR green PCR Master Mix (Applied Biosystems), and the following primers:

CD127 forward: 5′- ACCTCATCAGCCTTTCATGG -3′,

CD127 reverse: 5'-ATCCCCTGAGCAAACTAGCA-3'

Eomesodermin forward 5'- CAAAGAGGGCTCGTTGAGAG -3'

Eomesodermin reverse 5'- CCTAATTCGCGTGCTTCTTT -3'

Antibodies and reagents. The following antibodies for flow cytometry were from BD Biosciences: CD8, CD90.1/Thy1.1, CD90.2/Thy1.2, and CD62L (559772). The following antibodies for flow cytometry were from eBioscience: CD127 (17-1271), CD122 (12-1221), and eomesodermin (51-4875).

Class I iTAG tetramers bearing the OVA epitope (SIINFEKL) were from Beckman Coulter.

The following antibodies for immunoblotting were from Cell Signaling Technologies: pNDRG1 T346 (3217), pAkt S473 (4060), pS6K1 T389 (9204), pS6 S235/236 (4858), total S6 (2217), total S6 (2211), pFoxo1 S256 (9461), total Foxo1, clone C29H4 (2880), pSTAT5 Y694, clone C11C5 (9359), and total STAT5, clone 3H7 (9358).

Cytokines were from Peprotech, CFSE was from Invitrogen, and pp242 was from ChemDea.

Intracellular staining. Cells were stained for surface antigens, fixed and made permeable with the eBioscience Fixation/Permeabilization kit, then stained for transcription factors. Annexin V antibodies and binding buffer were from BD Biosciences.

Flow Cytometric Analysis. Flow cytometric data was acquired using a BD FACS Calibur, and analyzed using FlowJo7.6 (Tree Star Inc, Ashland, OR). Gates were determined by using unstimulated controls or isotype controls where appropriate.

Cells were sorted using a BD FACS Aria at the Flow Cytometry Core at the Sidney Kimmel Comprehensive Cancer Center, JHMI.

Immunoblot analysis. For immunoblot analysis, T cells were harvested by centrifugation and resuspended in ice-cold lysis buffer (20 mM Tris (pH 7.5), 150 mM NaCl, 1 mM EDTA, 1 mM EGTA, 1% Triton X-100, 2.5 mM sodium pyrophosphate, 1 mM β-glycerolphosphate (glycerol-2-phosphate), 1 mM sodium orthovanadate, 1 mM PMSF, 1× protease inhibitors (Roche, Basel, Switzerland)) and lysed at 4 °C for 30 min. Lysates were

cleared of debris by high speed centrifugation. Equal protein mass from each condition was mixed with 4× LDS buffer (Invitrogen, Carlsbad, CA) and boiled for 10 min. Lysates were then loaded into NuPAGE gels (4-12% Bis–Tris gels, Invitrogen) and run at 150 V for 90 min. Protein was transferred to polyvinylidene fluoride (*PVDF*) membranes with transfer buffer (1× NuPAGE Transfer Buffer (Invitrogen) with 20% methanol) at 30 V for 90 min. Membranes were blocked in 5% nonfat dry milk (NFDM) for 60 min, washed briefly with Tris-buffered saline + 0.1% Tween-20 (TBST) and probed with primary antibody in 4% NFDM in TBST overnight at 4°C. Membranes were washed with TBST three times for 10 min and probed with secondary antibody conjugated to HRP in NFDM. Membranes were washed 2 times in TBST for 5 min, and then once in Tris-buffered saline once for 5 min. Enhanced chemiluminescent plus substrate (GE Healthcare) was used to detect HRP-labeled antibodies. Blots were developed using a Biospectrum Multispectrum Imaging System and images were acquired and analyzed using VisionWorks, LS Image Acquisition and Analysis software (UVP, Upland, CA).

Real-time qPCR. RNA was isolated and reverse transcribed into cDNA using the SuperScript III First-Strand Synthesis System for RT-PCR (Invitrogen) according to the manufacturer's protocol. Primer and probe sets used to detect CD127, eomesodermin, and 18S rRNA were from Applied Biosystems. Taqman Universal Master Mix II, no UNG was used for qPCR. RT qPCR was performed using a Step One Plus Real Time PCR System (Applied Biosystems).

Statistical analysis. Prism version 5.0 (GraphPad Software) was used to perform statistical analyses, including unpaired Student's t-test and 2-way Analysis of Variance (ANOVA). A p value <0.05 was considered to be statistically significant.

Results

SGK1 is activated downstream of mTORC2 in CD8 T cells.

We have previously shown that SGK1 is activated downstream of TCR signaling in CD4 T cells (**Chapter 2**), so we sought to determine whether SGK1 was similarly regulated in CD8 T cells. Naïve RAG2-/- OT1 CD8 T cells were stimulated with anti-CD3 and anti-CD28 to measure the phosphorylation of the SGK1 substrate N-myc downregulated gene 1 (NDRG1). As we observed in CD8 T cells, activity of SGK1 as measured by pNDRG1 T346 increased upon TCR stimulation and was inhibited by the dual mTOR kinase inhibitor pp242, in a similar manner to the mTORC1 and mTORC2 substrates, pS6 S235/236 and pAkt S473, respectively (**Fig 1A**).

We have previously shown that SGK1 is activated in an mTORC2 dependent manner in CD4 T cells (**Chapter 2**). To determine whether SGK1 was downstream of mTORC2 in CD8 T cells, *T-SGK1*-/- CD8 T cells were activated *in vitro* and the phosphorylation of mTORC2 substrates was measured by immunoblot. *T-Rictor*-/- mice completely lack mTORC2 activity and exhibit loss of Akt activity and SGK1 activity (**Fig 1B**), suggesting that both Akt and SGK1 are downstream of mTORC2. In *T-SGK1*-/- mice,

however, selective loss of pNDRG1 T346 was observed, but Akt S473 phosphorylation remained intact. Therefore, we have placed SGK1 downstream of mTORC2 in a pathway that is parallel to Akt in CD8+ T cells.

SGK1 regulates expression of CD127 and survival in response to homeostatic cytokines.

CD8+ T cells from *T-SGK1-/-* cultured in IL-7 *in vitro* proliferate to a similar degree compared to Wt cells (**Supplementary Figure 1**). However, we wanted to determine if Wt and *T-SGK1-/-* CD8+ T cells would demonstrate differences in survival, particularly in the context of limiting concentrations of homeostatic cytokines and competition for growth factors. To address this question, Wt (Thy1.2) and T-SGK1-/- (Thy1.1) CD8 T cells were cocultured *in vitro* in limiting concentrations of IL7 following 48 hours of stimulation. *T-SGK1-/-* CD8 T cells demonstrated enhanced survival, particularly when the concentration of homeostatic cytokine was limiting (1.0 pg/ml IL-7) (**Fig 1C**). Accordingly, *T-SGK1-/-* cells constitutively upregulate CD127 when forced to compete with Wt cells for IL-7 (**Fig 1D**). This enhanced expression of CD127 was correlated with no change in proliferation, but this effect was correlated with enhanced survival of *T-SGK1-/-* CD8+ T cells that was most pronounced at the lowest concentration of IL7 (**Fig 1C**). Of note, there were no differences in the ability of naïve CD8+ T cells from *T-SGK1-/-* mice to signal through CD127, as measured by phosphorylation of STAT5 in response to IL-7 (**Supplementary Figure 2**).

Loss of SGK1 results in aberrant expression of memory markers on effector T cells.

Next, we sought to determine if SGK1 regulated survival and expression of CD127 *in vivo* in CD8+ T cells in a model of vaccination. Wt and *T-SGK1-/-* mice were immunized with vaccinia virus expressing the model antigen ovalbumin (VAC-OVA) and the fate of antigen specific T cells was followed over the course of the immune response. Consistent with our *in vitro* data, Wt and *T-SGK1-/-* OVA specific T cells proliferated similarly during the effector phase of the immune response (Day 0-7) (**Fig 2A**). These results suggest that SGK1 is not required for effector differentiation. Furthermore, there was no difference in the ability of *T-SGK1-/-* effector cells to kill antigen-loaded targets in an *in vivo* CTL assay (**Supplementary Figure 3**).

Although SGK1 is not required for effector differentiation, our data suggest that loss of SGK1 may enhance memory differentiation. In the VAC-OVA model, loss of SGK1 lead to decreased attrition of OVA-specific T cells during the contraction phase of the immune response (Day 8-32), suggesting that SGK1 represses memory differentiation (**Fig 2A**). Upon antigen recognition, Wt CD8 T cells downregulate the memory marker CD127 and upregulate KLRG1, a marker of effector cells. Similar to what we observed *in vitro*, OVA-specific *T-SGK1-/-* cells were unable to downregulate CD127 and expressed high levels of this memory marker at the height of the effector response on day 7.

Since SGK1 is deleted in both CD4 and CD8 subsets in *T-SGK1-/-* mice, we performed an adoptive transfer of OT1 Thy1.1 CD8 T cells from *T-SGK1-/-* mice into Wt recipients, who were simultaneously immunized with VAC-OVA. Similar to our results on the endogenous response to VAC-OVA, adoptively transferred cells from *T-SGK1-/-* mice proliferated similarly to Wt on day 6. There was no difference in the number of Thy1.1+

adoptively transferred cells from Wt and *T-SGK1-/-* donors (**Fig 2B**). However, adoptively transferred effector cells from *T-SGK1-/-* mice displayed aberrant expression of CD127 (**Fig 2B**). Furthermore, loss of SGK1 also lead to aberrant expression of the memory associated transcription factor EOMES (**Fig 2B**).

SGK1 is not required for homeostatic proliferation

Because loss of SGK1 leads to upregulation of CD127, we hypothesized that CD8+ T cells from T-SGK1-/- mice would demonstrate enhanced homeostatic proliferation. To address this question, CD8+ Thy1.1+ T cells from Wt or *T-SGK1-/-* mice that had been labeled with CFSE were adoptively transferred into RAG2-/- Thy1.2+ recipients. Unexpectedly, there was no difference in the number of cell divisions that occurred in response to lymphopenia when comparing Wt and *T-SGK1-/-* cells (**Fig 2C**). (Note: this observation may be due to lack of competition for IL-7 since this experiment was not performed as a co-adoptive transfer.) Interestingly, there was marked upregulation of CD127 on the adoptively transferred cells from *T-SGK1-/-* mice, whereas CD127 was downregulated on the Wt adoptively transferred cells. Lymphopenia in the setting of RAG deficiency leads to high serum concentrations of IL-7, which should lead to downregulation of CD127[20]. These results suggest that expression of CD127 remains (inappropriately) constitutively high in the absence of SGK1 signaling.

SGK1 regulates CD127 and Eomesodermin expression via phosphorylation of Foxo1.

Next, we sought to determine the mechanism by which SGK1 was regulating expression of CD127 and EOMES. Both CD127 and EOMES are transcriptional targets of the forkhead box transcription factor Foxo1, which has been shown to promote survival and memory differentiation in CD8+ T cells[21,22]. Upon T cell activation, the Foxo transcription factors are phosphorylated, resulting in their translocation from the nucleus to the cytoplasm. Phosphorylation and sequestration of Foxo in the cytoplasm ensures that these transcription factors are held in an inactive state by association with 14-3-3 scaffolding proteins[23-25].

It has previously been reported in HEK293 cells that SGK1 directly phosphorylates Foxo1[26]. In naïve CD8 T cells, Foxo1 is dephosphorylated and thus active in the nucleus[21,27]. Not surprisingly, there was no difference in phosphorylation of Foxo1 in naïve CD8+ T cells from Wt and *T-SGK1*-/- mice (**Fig 3A**). Furthermore, there were no differences in the expression of several Foxo1 target genes (CD122, CD127, and CD62L) in naïve cells from Wt versus *T-SGK1*-/- mice (**Supplementary Figure 4**). These results are consistent with previously published results that Foxo1 is active in naïve T cells, where it promotes survival and homeostatic turnover[21,27].

In effector CD8+ T cells, Foxo1 is phosphorylated and thus sequestered in the cytoplasm where is it kept inactive. We predicted that loss of SGK1 would result in loss of Foxo1 phosphorylation, and inappropriately high Foxo1 activity in effector CD8+ T cells. To this end, OT1 Thy1.1+ CD8+T cells from Wt or *T-SGK1*-/- were adoptively transferred into naïve recipients who were simultaneously immunized with VAC-OVA. On Day 6 post infection, the adoptively transferred cells were sorted and assayed for the activity of Foxo1

by immunoblot. On day 6 post infection, phosphorylation of Foxo1 increased in Wt adoptively transferred cells, which correlated with decreased Foxo1 activity (**Fig 3A**). By contrast, Foxo1 was not phosphorylated in adoptively transferred cells from *T-SGK1-/-* mice.

We hypothesized that the increased expression of CD127 and EOMES that were observed *in vivo* in *T-SGK1-/-* was due to increased activity of Foxo1. Since these genes are transcriptional targets of Foxo1[21,22], mRNA expression of CD127 and EOMES was measured in day 6 adoptively transferred cells. Loss of SGK1 lead to marked upregulation of CD127 and EOMES transcripts in *T-SGK1-/-* cells compared to Wt (**Fig 3B**). To confirm that increased expression of CD127 and EOMES was due to Foxo1, we performed chromatin immunoprecipitation of Foxo1 from Day 6 adoptively transferred cells. CHiP revealed binding of Foxo1 to enhancer elements in the CD127 and EOMES promoters in *T-SGK1-/-* mice, but not Wt mice (**Fig 3C, D**). These data are consistent with previously published reports of Foxo1 binding to enhancer elements in the promoters of these genes in naïve and memory cells. In the absence of SGK1, however, Foxo1 promotes transcription of these genes by constitutively binding to enhancer elements, even in effector CD8 T cells where Foxo1 should be inactive.

Discussion

A model is emerging whereby mTOR regulates AGC kinases (such as SGK1 and Akt), which in turn regulate a transcriptional program that leads to either effector or memory

differentiation (**Fig 4**). At the center of the transcriptional network that drives memory differentiation is the forkhead box (FOXO) family of transcription factors. In resting or naïve T cells where mTOR/SGK1/Akt are not active, the FOXO proteins reside in the nucleus where they promote expression of downstream targets. Upon T cell activation, however, SGK1 and Akt phosphorylate the FOXOs, resulting in their translocation from the nucleus to the cytoplasm, where they are held in an inactive state by association with 14-3-3 scaffolding proteins[23-25]. SGK1 has previously been shown to phosphorylate Foxo1 in CCL39 fibroblasts and HEK 293T cells[26]. For the first time, our data establish a role for SGK1 in regulating Foxo1 in CD8 T cells.

The subcellular localization of the FOXO transcription factors is controlled by phosphorylation at several sites. In studies on HEK293 cells, both Akt and SGK1 can phosphorylate Foxo1, but these kinases have preferences for different sites[26]. For example, Akt seems to favor phosphorylation at serine 253, while SGK1 favors serine 315[26]. On the other hand, both Akt and SGK1 readily phosphorylate threonine 32 in Foxo1[26]. Transfection of HEK293 cells with kinase inactive mutants of SGK1 or Akt resulted in inappropriate retention of Foxo1 in the nucleus upon growth factor stimulation[26]. By contrast, constitutively active Akt or SGK1 resulted in inappropriate retention of Foxo1 in the cytoplasm upon growth factor withdrawal, leading to apoptosis[26]. These findings suggest that SGK1 and Akt have partially overlapping but nonredundant roles in controlling subcellular localization and thus Foxo1 activity. Thus, the regulation of Foxo1 by both Akt and SGK1 is critical to promoting survival upon growth factor withdrawal, such as that which occurs during the contraction phase of the immune response.

Recently, several reports have suggested that Foxo1 plays a critical role in regulating CD8 memory cell differentiation downstream of Akt[22,28]. Strong TCR signaling in the context of IL-12 promotes activation of mTOR, which in turn activates Akt and drives differentiation of terminal effector cells[22]. Sustained Akt activity results in enhanced effector differentiation[28]. However, decreased expression of CD127, EOMES, and the anti-apoptotic transcription factor Bcl2 results in an inability to mount a memory response for long-term protective immunity[28]. By contrast, inhibition of Akt results in enhanced memory differentiation[28]. Mechanistically, decreased Akt activity leads to an increase in Foxo1 activity, which allows Foxo1 to bind to the enhancer regions of CD127 and EOMES to promote expression of these memory markers[22]. Thus, Akt and SGK1 are critical in fine-tuning the balance of effector versus memory differentiation in CD8 T cells. Taken together, our data supports a model whereby mTORC2 regulates downstream AGC kinases to control transcriptional programs that promote effector or memory differentiation in CD8+ T cells.

Figure Legends

Figure 1. SGK1 regulates survival in response to homeostatic cytokines in CD8 T cells. (A) Immunoblot (IB) of naïve lymphocytes from 5C.C7 mice that were serum starved for 1 hour prior to stimulation with anti-CD3 and anti-CD28. Cells were lysed, and the activity of SGK1 was measured by blotting for phosphorylated NDRG1 (T346). The activity of mTORC1 and mTORC2 was measured by blotting for phosphorylated S6 (S235/236) activity downstream of TORC1, and for Akt activity downstream of TORC2 (S473). Total protein levels and actin are included as loading controls. **(B)** IB of WT, *T-Rictor-/-*, and *T-SGK1-/-* CD4+ T cells that were stimulated as in A. Cells were lysed and the activity of

mTORC2 and SGK1 was measured as above. Actin is included as a loading control. **(C)** Flow cytometry plots of WT and *T-SGK1*-/- CD8 T cells cocultured *in vitro*. CD8 T cells from WT (Thy1.2) and T-SGK1-/- (Thy1.1) were stained with 0.5 uM CFSE and stimulated *in vitro* with anti-CD3 and anti-CD28 for 48 hours, then expanded in limiting concentrations of IL-7 (10.0 pg/ml, 2.0 pg/ml, or 1.0 pg/ml). At 96 hours, proliferation was measured by CFSE dilution, and death was measured by Annexin V staining. **(D)** As in 1C, cultures were stained and analyzed by flow cytometry for the ratio of Thy1.1 to Thy1.2 positive cells and expression of CD127. Where indicated, values represent the percent of cells in each quadrant, mean fluorescent index (MFI) of CD127 expression.

Figure 2. Loss of SGK1 results in aberrant expression of CD127 on CD8 effector T cells in response to Vaccinia virus. (A) Percent of antigen-specific CD8 T cells during an immune response to VAC-OVA. WT and *T-SGK1*-/- mice were immunized with 1e6 pfu vaccina virus expressing the model antigen OVA (VAC-OVA) by intraperitoneal (i.p.) injection on day 0. The number of OVA-specific CD8 T cells was monitored at interval timepoints over 30 days post infection by serial cheek bleed. Graph depicts the percentage of antigen specific T cells as meausured by flow cytometry using MHC I tetramers loaded with the OVA epitope SIINFEKL (OVA 257-264). Histogram depicts expression of CD127 on tetramer positive cells on day 7. **(B)** Response of adoptively transferred OT1 cells to VAC-OVA. 1e6 OT1 Thy1.1 cells from WT or T-SGK1-/- mice were adoptively transferred to WT recipients, who were simultaneously immunized with 1e6 pfu VAC-OVA i.p. Graphs depict the percentage of Thy1.1 positive cells among CD8+ splenocytes as measured by flow cytometry on Day 6 post adoptive transfer & immunization. Expression of CD127 and eomesodermin in adoptively transferred cells was measured by flow cytometry, and plotted

as MFI. **(C)** Number of cell divisions measured by CFSE dilution in a homeostatic proliferation model. 1e6 Thy1.1+ CD8+ T cells were CFSE labeled and adoptively transferred into RAG2-/- recipients. Splenocytes were harvested on day 7 post-adoptive transfer and analyzed by flow cytometry for dilution of CFSE and expression of CD127.

Figure 3. SGK1 controls expression of CD127 and Eomesodermin by regulating Foxo1. (A) IB of naïve and adoptively transferred cells sorted from splenocytes of mice immunized with VAC-OVA. WT Thy1.2 mice were immunized with 1e6 pfu VAC-OVA and simultaneously received 1e6 OT1 Thy1.1 T cells. Spleenocytes were harvested 6 days later and sorted based on a CD8+Thy1.1+. Sorted cells were lysed and immunoblotted, and naïve OT1 cells are included as a control. Total Foxo1 protein and actin are shown as loading controls. **(B)** mRNA expression of CD127 and eomesodermin in adoptively transferred cells. Mice were immunized and received adoptive transfer of OT1 Thy1.1 T cells as in A. Cells were sorted and RNA was harvested and reverse transcribed. Graphs depict quantitative PCR results for expression of CD127 and eomesodermin, relative to 18s rRNA control. **(C)** Foxo binding sites in the CD127 and eomesodermin promoters. Conserved Foxo responsive elements are located at -3.5 kb and -150 bp in the CD127 and eomesodermin promoters, respectively. Arrows depict primer binding sites for chromatin immunoprecipitation in D. **(D)** Chromatin immunoprecipitation of Foxo1 at the CD127 and eomesodermin promoters. CD8+Thy1.1+ cells were sorted as in A, and lysates were subject to shearing and chromatin immunoprecipitation with Foxo1 antibody. qPCR was used to measure abundance of CD127 and eomesodermin promoter sequences that were bound to Foxo1 or IgG control. Graphs depict fold enrichment of Foxo1 at the sites indicated on the CD127 and eomesodermin promoters, normalized to IgG control and input control.

Figure 4. Model depicting regulation of CD127 and eomesodermin by Foxo1 and SGK1. In effector CD8 T cells, high mTOR activity leads to phosphorylation and activation of SGK1. In turn, SGK1 phosphorylates Foxo1 which leads to its exclusion from the nucleus and sequestration in the cytoplasm by binding 14-3-3 proteins. In memory CD8 T cells, low mTOR activity is not sufficient to phosphorylate and activate SGK1. As a result, the Foxo transcription factors are not phosphorylated and held in the cytoplasm, but rather translocate to the nucleus where they bind to Foxo responsive elements in target genes such as CD127 and eomesodermin, which promote a memory phenotype.

Supplemental Figures.

Supplementary Figure 1. Proliferation of WT and *T-SGK1-/-* CD8 T cells *in vitro*. CD8 T cells from WT (Thy1.2) and T-SGK1-/- (Thy1.1) were labeled with 0.5 uM CFSE and stimulated in vitro with anti-CD3 and anti-CD28 magnetic stimulator beads for 48 hours, then expanded in limiting concentrations of IL-7 (10.0 pg/ml, 2.0 pg/ml, or 1.0 pg/ml).

Supplementary Figure 2. IB of CD8 T cells for phosphorylated STAT5 in response to a dose curve of IL-7. CD8+ T cells were isolated from WT and *T-SGK1-/-* (KO) mice and cultured with IL-7 (1.0 ng/ml, 0.1 ng/ml, or 0.01 ng/ml) for 30 minutes. Cells were lysed and immunoblotted for pSTAT5 (Tyr 694). Total STAT5 protein is included as a loading control.

Supplementary Figure 3. In vivo CTL killing assay. WT and T-SGK1-/- mice were immunized with VAC-OVA, then challenged on day 6 with efluor labeled targets that were pulsed with OVA peptide or no peptide as a control. Histograms depict the percentages of cells among the no peptide control (efluor low) or OVA pulsed targets (efluor high) at 4 and 6 hours post challenge from representative mice.

Supplementary Figure 4. Expression of Foxo target genes on naïve CD8 T cells. Splenocytes were harvested from WT and *T-SGK1-/-* mice and analyzed by flow cytometry for the expression of the Foxo transcriptional targets CD122, CD127, and CD62L.

References

1 Kaech, S. M. & Cui, W. Transcriptional control of effector and memory CD8+ T cell differentiation. *Nat Rev Immunol* **12**, 749-761, doi:10.1038/nri3307 nri3307 [pii] (2012).

2 Kaech, S. M. *et al.* Selective expression of the interleukin 7 receptor identifies effector CD8 T cells that give rise to long-lived memory cells. *Nat Immunol* **4**, 1191-1198, doi:10.1038/ni1009 ni1009 [pii] (2003).

3 Joshi, N. S. *et al.* Inflammation directs memory precursor and short-lived effector CD8(+) T cell fates via the graded expression of T-bet transcription factor. *Immunity* **27**, 281-295, doi:S1074-7613(07)00371-8 [pii] 10.1016/j.immuni.2007.07.010 (2007).

4 Sarkar, S. *et al.* Functional and genomic profiling of effector CD8 T cell subsets with distinct memory fates. *J Exp Med* **205**, 625-640, doi:10.1084/jem.20071641 jem.20071641 [pii] (2008).

5 Surh, C. D. & Sprent, J. Homeostasis of naive and memory T cells. *Immunity* **29**, 848-862, doi:10.1016/j.immuni.2008.11.002 S1074-7613(08)00506-2 [pii] (2008).

6 Jameson, S. C. & Masopust, D. Diversity in T cell memory: an embarrassment of riches. *Immunity* **31**, 859-871, doi:10.1016/j.immuni.2009.11.007 S1074-7613(09)00507-X [pii] (2009).

7 Lau, L. L., Jamieson, B. D., Somasundaram, T. & Ahmed, R. Cytotoxic T-cell memory without antigen. *Nature* **369**, 648-652, doi:10.1038/369648a0 (1994).

8 Schluns, K. S., Williams, K., Ma, A., Zheng, X. X. & Lefrancois, L. Cutting edge: requirement for IL-15 in the generation of primary and memory antigen-specific CD8 T cells. *J Immunol* **168**, 4827-4831 (2002).

9 Prlic, M., Lefrancois, L. & Jameson, S. C. Multiple choices: regulation of memory CD8 T cell generation and homeostasis by interleukin (IL)-7 and IL-15. *J Exp Med* **195**, F49-52 (2002).

10 Tan, J. T. *et al.* Interleukin (IL)-15 and IL-7 jointly regulate homeostatic proliferation of memory phenotype CD8+ cells but are not required for memory phenotype CD4+ cells. *J Exp Med* **195**, 1523-1532 (2002).

11 Goldrath, A. W. *et al.* Cytokine requirements for acute and Basal homeostatic proliferation of naive and memory CD8+ T cells. *J Exp Med* **195**, 1515-1522 (2002).

12 Hand, T. W., Morre, M. & Kaech, S. M. Expression of IL-7 receptor alpha is necessary but not sufficient for the formation of memory CD8 T cells during viral infection. *Proc Natl Acad Sci U S A* **104**, 11730-11735, doi:0705007104 [pii]
10.1073/pnas.0705007104 (2007).

13 Banerjee, A. *et al.* Cutting edge: The transcription factor eomesodermin enables CD8+ T cells to compete for the memory cell niche. *J Immunol* **185**, 4988-4992, doi:10.4049/jimmunol.1002042
jimmunol.1002042 [pii] (2010).

14 Takemoto, N., Intlekofer, A. M., Northrup, J. T., Wherry, E. J. & Reiner, S. L. Cutting Edge: IL-12 inversely regulates T-bet and eomesodermin expression during pathogen-induced CD8+ T cell differentiation. *J Immunol* **177**, 7515-7519, doi:177/11/7515 [pii] (2006).

15 Intlekofer, A. M. *et al.* Effector and memory CD8+ T cell fate coupled by T-bet and eomesodermin. *Nat Immunol* **6**, 1236-1244, doi:ni1268 [pii]
10.1038/ni1268 (2005).

16 Rao, R. R., Li, Q., Odunsi, K. & Shrikant, P. A. The mTOR kinase determines effector versus memory CD8+ T cell fate by regulating the expression of transcription factors T-bet and Eomesodermin. *Immunity* **32**, 67-78, doi:S1074-7613(09)00545-7 [pii]
10.1016/j.immuni.2009.10.010 (2010).

17 Araki, K. *et al.* mTOR regulates memory CD8 T-cell differentiation. *Nature* **460**, 108-112, doi:nature08155 [pii]
10.1038/nature08155 (2009).

18 He, S. *et al.* Characterization of the metabolic phenotype of rapamycin-treated CD8+ T cells with augmented ability to generate long-lasting memory cells. *PLoS One* **6**, e20107, doi:10.1371/journal.pone.0020107
PONE-D-10-04534 [pii] (2011).

19 Pearce, E. L. *et al.* Enhancing CD8 T-cell memory by modulating fatty acid metabolism. *Nature* **460**, 103-107, doi:nature08097 [pii]
10.1038/nature08097 (2009).

20 Mackall, C. L., Fry, T. J. & Gress, R. E. Harnessing the biology of IL-7 for therapeutic application. *Nat Rev Immunol* **11**, 330-342, doi:10.1038/nri2970
nri2970 [pii] (2011).

21 Kerdiles, Y. M. *et al.* Foxo1 links homing and survival of naive T cells by regulating L-selectin, CCR7 and interleukin 7 receptor. *Nat Immunol* **10**, 176-184, doi:ni.1689 [pii]
10.1038/ni.1689 (2009).

22 Rao, R. R., Li, Q., Gubbels Bupp, M. R. & Shrikant, P. A. Transcription factor Foxo1 represses T-bet-mediated effector functions and promotes memory CD8(+) T cell differentiation. *Immunity* **36**, 374-387, doi:10.1016/j.immuni.2012.01.015
S1074-7613(12)00088-X [pii] (2012).

23 Rena, G., Prescott, A. R., Guo, S., Cohen, P. & Unterman, T. G. Roles of the forkhead in rhabdomyosarcoma (FKHR) phosphorylation sites in regulating 14-3-3 binding, transactivation and nuclear targetting. *Biochem J* **354**, 605-612 (2001).

24 Brunet, A. *et al.* 14-3-3 transits to the nucleus and participates in dynamic nucleocytoplasmic transport. *J Cell Biol* **156**, 817-828, doi:10.1083/jcb.200112059
jcb.200112059 [pii] (2002).

25 Hedrick, S. M. The cunning little vixen: Foxo and the cycle of life and death. *Nat Immunol* **10**, 1057-1063, doi:ni.1784 [pii]
10.1038/ni.1784 (2009).

26 Brunet, A. *et al.* Protein kinase SGK mediates survival signals by phosphorylating the forkhead transcription factor FKHRL1 (FOXO3a). *Mol Cell Biol* **21**, 952-965, doi:10.1128/MCB.21.3.952-965.2001 (2001).

27 Hess Michelini, R., Doedens, A. L., Goldrath, A. W. & Hedrick, S. M. Differentiation of CD8 memory T cells depends on Foxo1. *J Exp Med* **210**, 1189-1200, doi:10.1084/jem.20130392
jem.20130392 [pii] (2013).

28 Kim, E. H. *et al.* Signal integration by Akt regulates CD8 T cell effector and memory differentiation. *J Immunol* **188**, 4305-4314, doi:10.4049/jimmunol.1103568
jimmunol.1103568 [pii] (2012).

Figure 1

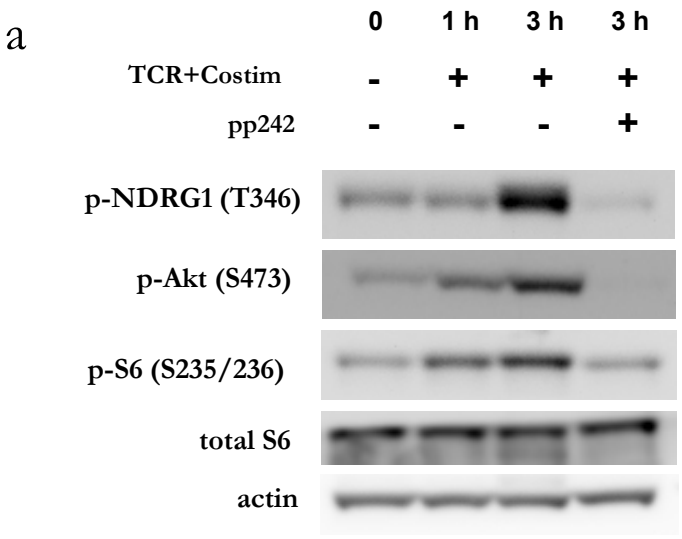
a
0
1 h
3 h
3 h
TCR+Costim
- + + +
pp242
- - - +
p-NDRG1 (T346)
p-Akt (S473)
p-S6 (S235/236)
total S6
actin

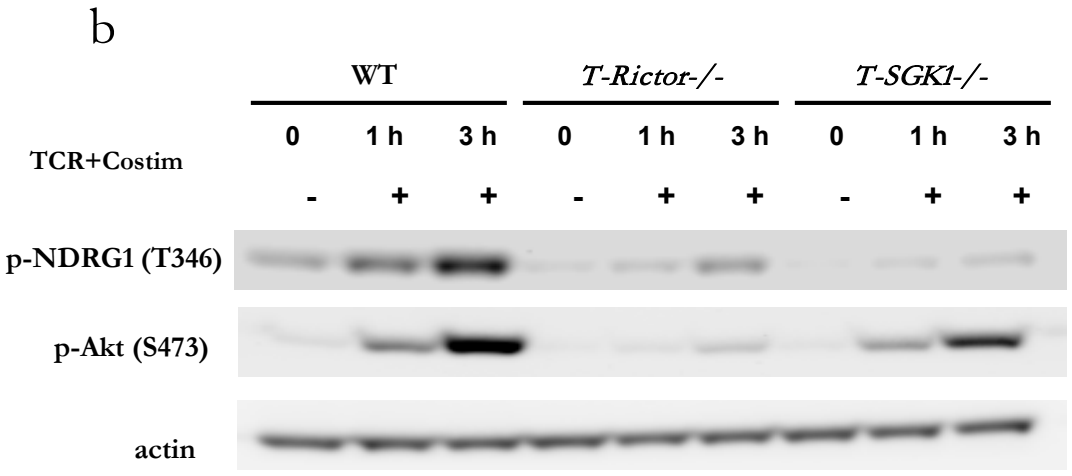
b
WT
T-Rictor-/-
T-SGK1-/-
TCR+Costim
0 1 h 3 h 0 1 h 3 h 0 1 h 3 h
- + + - + + - + +
p-NDRG1 (T346)
p-Akt (S473)
actin

Figure 1, cont'd

c

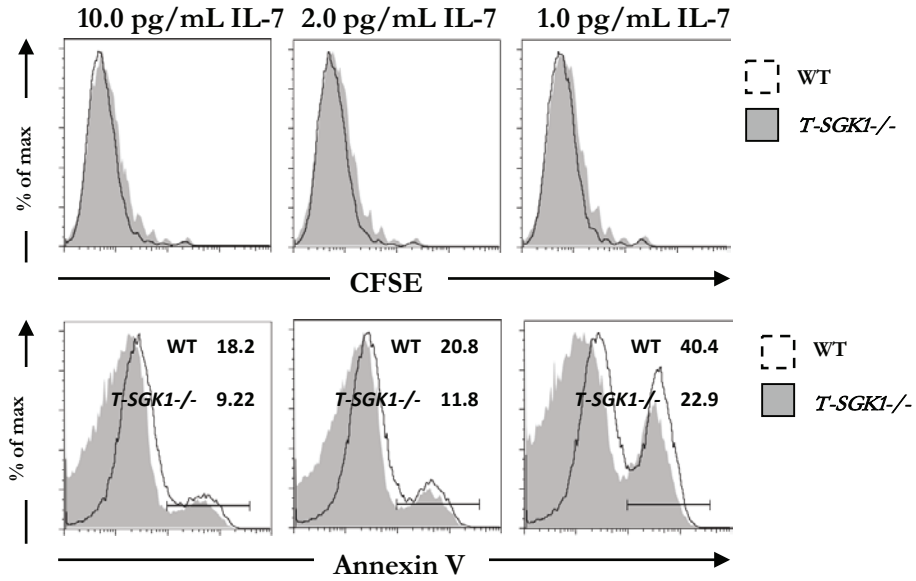

d

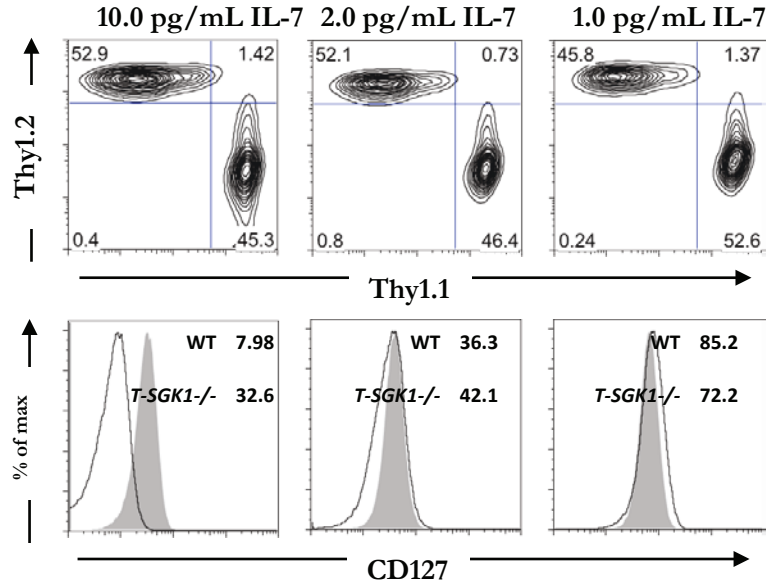

Figure 2

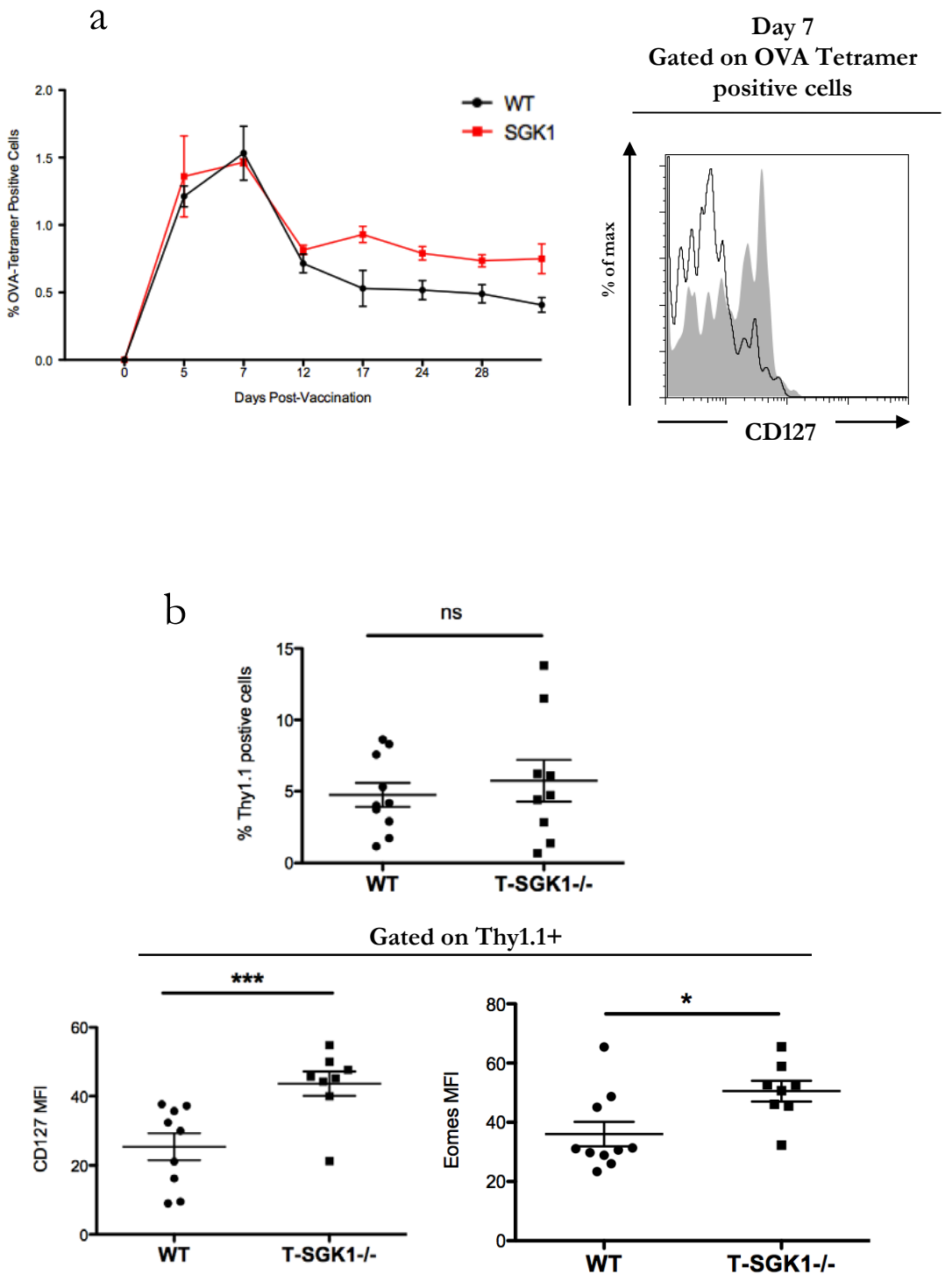
a
Day 7
Gated on OVA Tetramer positive cells
% OVA-Tetramer Positive Cells
Days Post-Vaccination
WT
SGK1
% of max
CD127
b
ns
% Thy1.1 postive cells
WT
T-SGK1-/-
Gated on Thy1.1+
***
CD127 MFI
*
Eomes MFI

Figure 2, cont'd

c

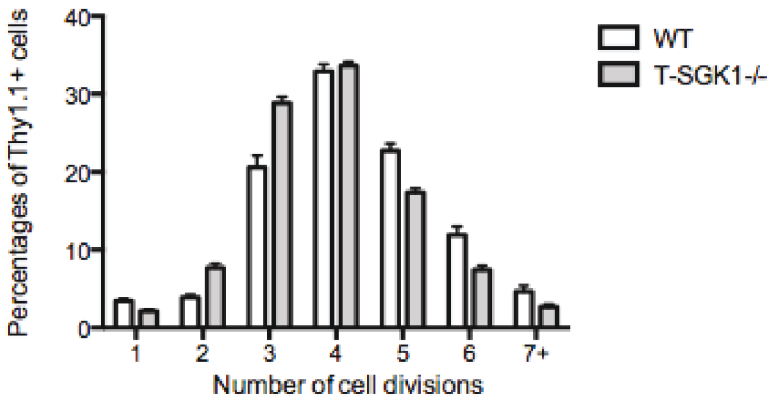

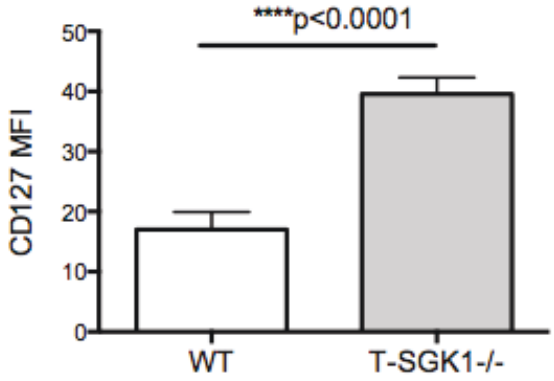

Figure 3

a

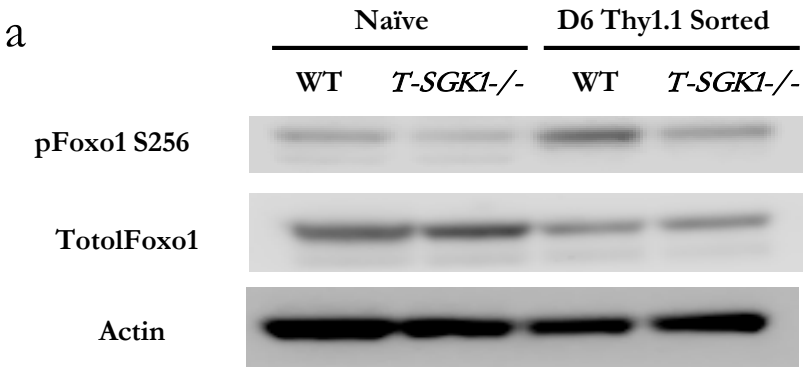
Naïve
D6 Thy1.1 Sorted
WT
T-SGK1-/-
WT
T-SGK1-/-
pFoxo1 S256
TotolFoxo1
Actin

b

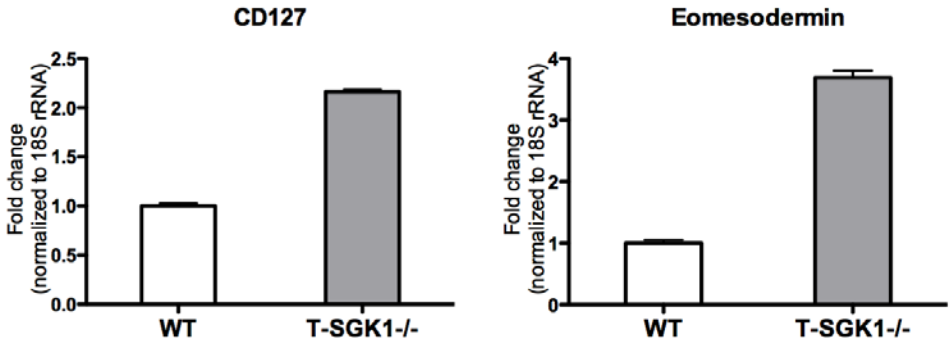
CD127
Fold change (normalized to 18S rRNA)
2.5
2.0
1.5
1.0
0.5
0.0
WT
T-SGK1-/-
Eomesodermin
Fold change (normalized to 18S rRNA)
4
3
2
1
0
WT
T-SGK1-/-

Figure 3, cont'd

c

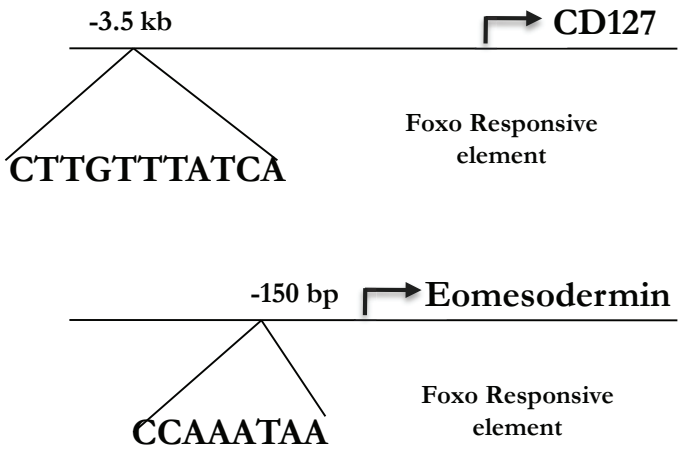

d

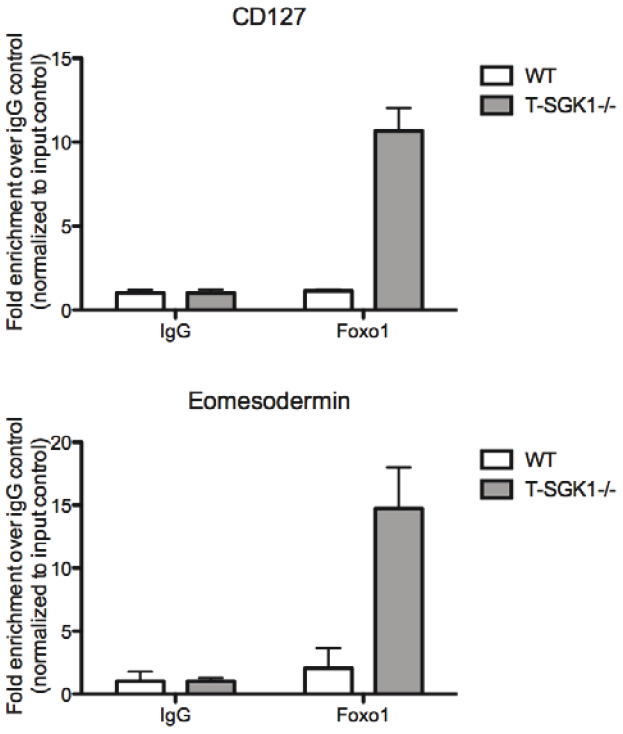

Figure 4

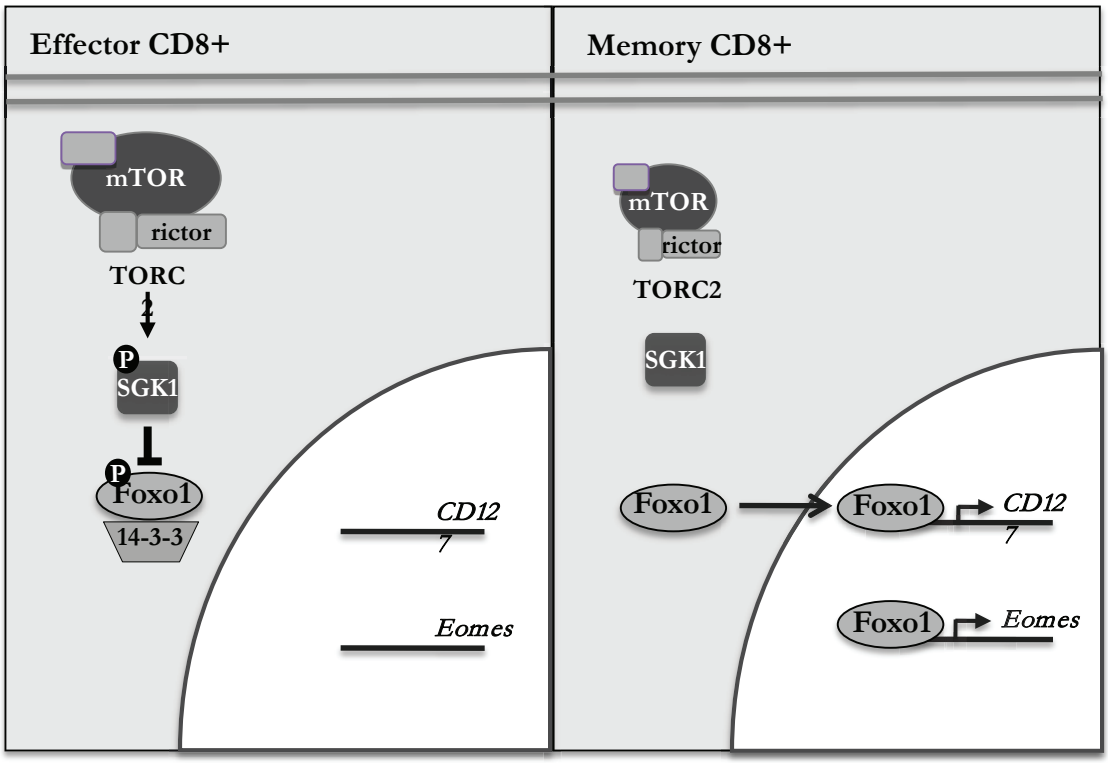
Effector CD8+
Memory CD8+
mTOR
rictor
TORC
2
P
SGK1
P
Foxo1
14-3-3
CD12
7
Eomes
mTOR
rictor
TORC2
SGK1
Foxo1
Foxo1
CD12
7
Foxo1
Eomes

Supplementary Figure 1

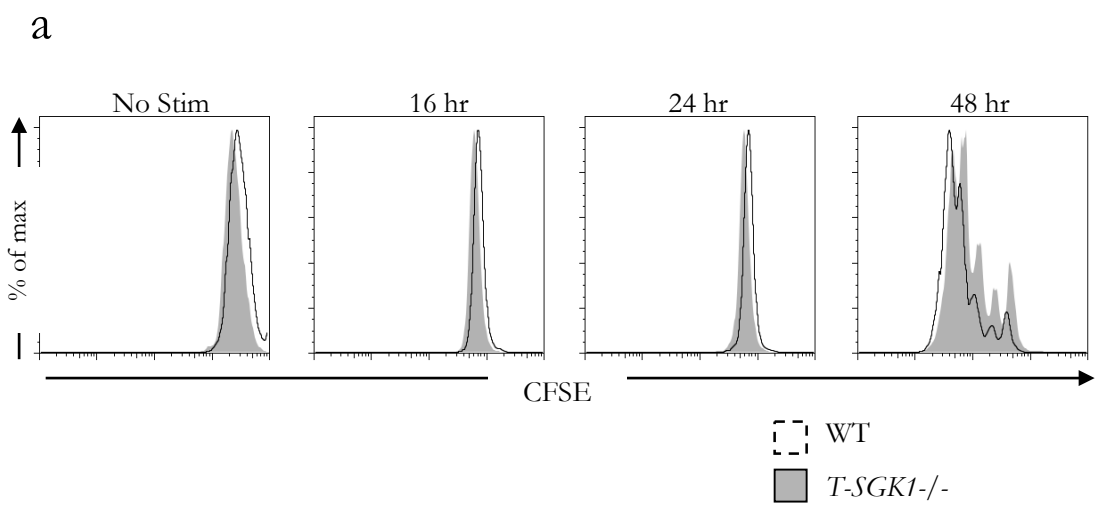

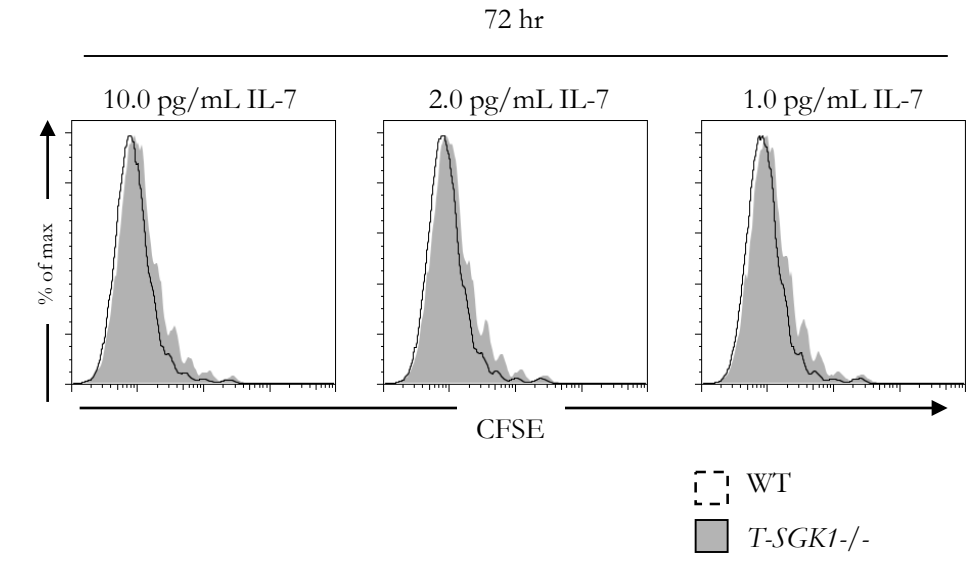

Supplementary Figure 2

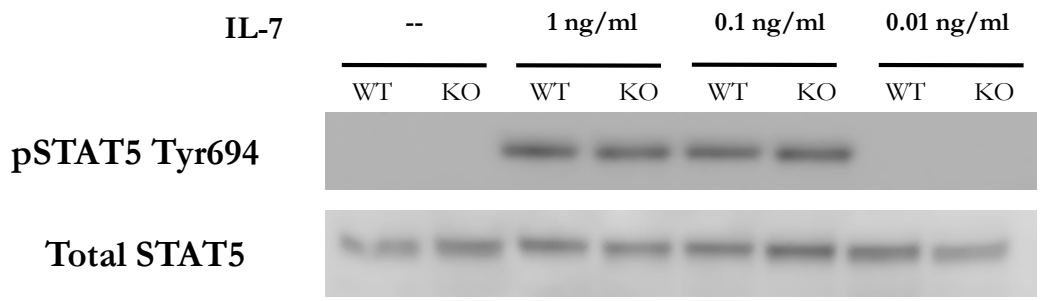

Supplementary Figure 3

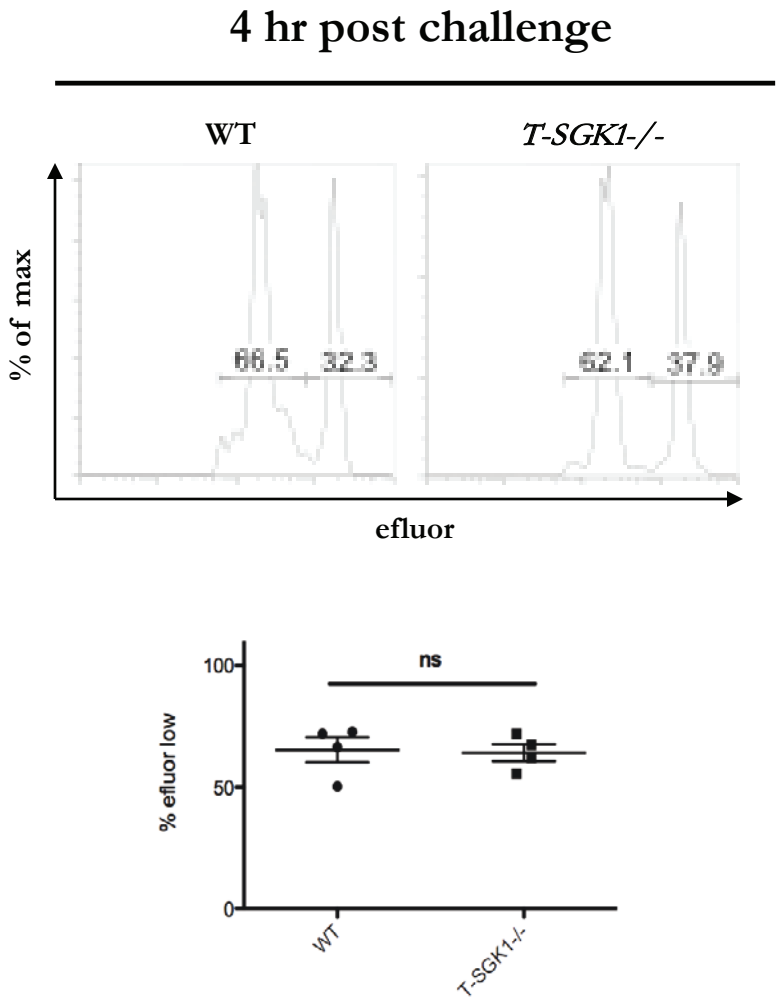

Supplementary Figure 3, cont'd

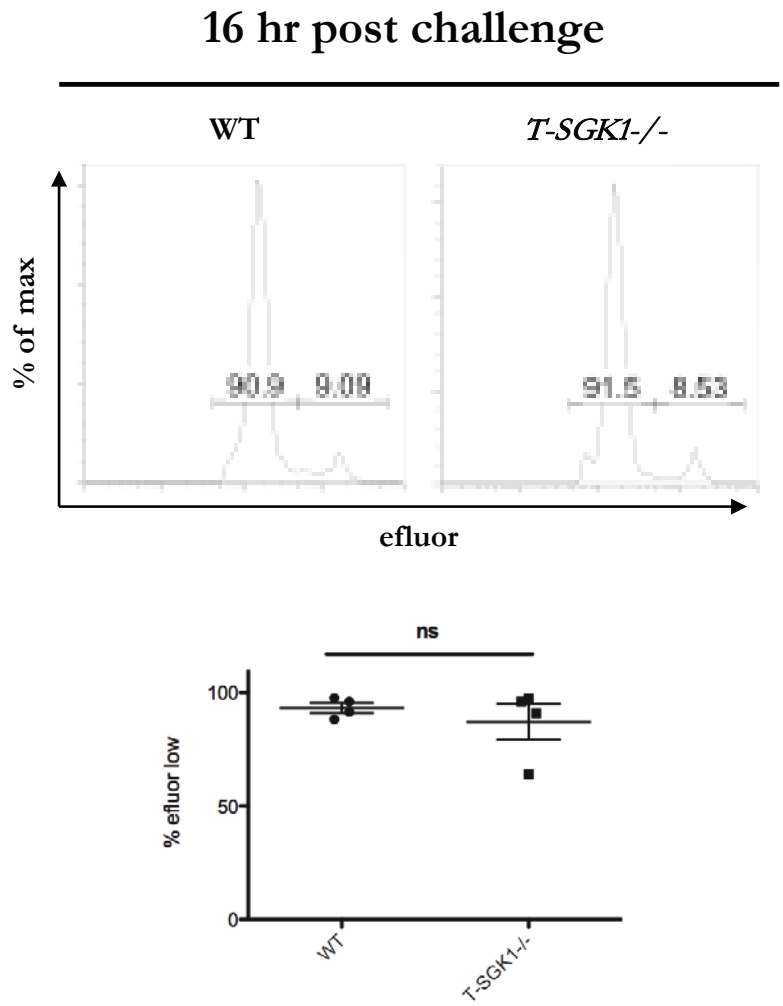

Supplementary Figure 4

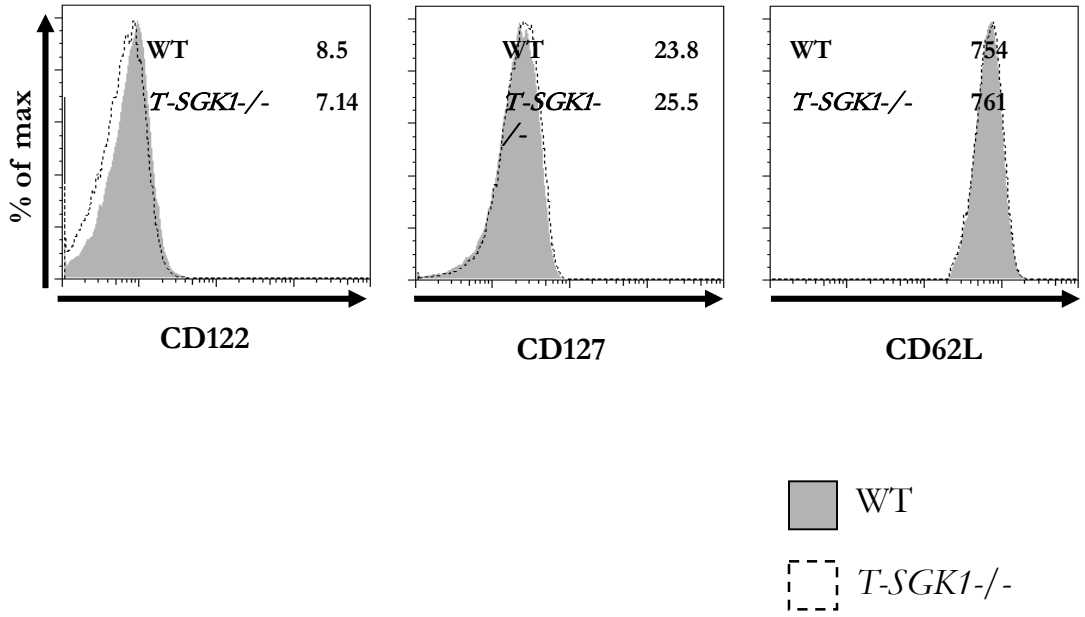

CHAPTER 4: Discussion and Future Directions

Summary of Findings in CD4+ T cells

In summary, these results demonstrate a previously unappreciated role for SGK1 in both CD4+ and CD8+ T cells. SGK1 is a key mediator downstream of TORC2 that is involved in influencing T cell differentiation in both lineages. In CD4+ T cells, loss of SGK1 leads to a constitutive IFNγ-producing, Th1 phenotype, while Th2 differentiation is impaired. Mechanistically, loss of SGK1 leads to increased ubiquitination and destruction of JunB via the E3 ligase NEDD4-2. This results in decreased IL-4 production and impaired Th2 differentiation in *T-SGK1-/-* mice. Furthermore, loss of SGK1 leads to a decrease in expression of the long isoforms of TCF-1, resulting in enhanced IFNγ production and a constitutive Th1 phenotype.

Our mechanistic studies on the role of SGK1 in CD4+ T cells have been strengthened by our *in vivo* observations in various disease models using *T-SGK1-/-* mice. We have shown that these mice are resistant to Th2-mediated disease, such as allergic asthma, since CD4+ T cells from these mice inappropriately produce IFN-γ and thus mount a protective Th1 response. In a melanoma model, we have shown that enhanced IFN-γ production in *T-SGK1-/-* mice leads to robust rejection of tumors and prolonged survival. Altogether, these results suggest that inhibition of SGK1 may be a useful target for immunomodulatory therapies that seek to enhance a Th1 immune response.

Summary of Findings in CD8+ T cells

In CD8+ T cells, we have shown that loss of SGK1 may lead to an enhanced memory phenotype. In a model of infection with vaccinia virus expressing OVA, we have shown that loss of SGK1 results in inappropriate expression of memory markers, such as CD127 and EOMES, on effector cells. Decreased attrition of antigen-specific T cells in T-SGK1-/- mice during the contraction phase of the immune response suggests that these mice may have an enhanced memory phenotype.

We hypothesized that the mechanism of decreased attrition in *T-SGK1-/-* mice might be due to increased activity of the FOXO transcription factors. It has been shown that FOXO transcription factors lead to increased expression of the IL-7 receptor (CD127), which is associated with survival of long-lived memory cells due to their ability to proliferate in response to homeostatic cytokines like IL-7[1,2]. Foxo1 has also been shown to bind to enhancer regions of the EOMES promoter. Indeed, antigen-specific CD8+ T cells from *T-SGK1-/-* mice show increased expression of CD127 and EOMES, even at the height of the effector phase of the viral immune response.

Future Directions and Applications

The mTOR pathway is an ideal target for new therapies that specifically and potently inhibit a particular arm of the T effector response. Our work has previously established that mTORC1 is necessary for Th1 and Th17 development, while TORC2 is necessary for Th2 development[3]. This dissertation advances our understanding of how mTOR reciprocally regulates Th1 and Th2 differentiation via SGK1. By defining the downstream components

of this signaling pathway, we have identified targets that can be manipulated to more precisely control T cell differentiation.

Immunomodulatory drugs that are currently in clinical use are non-selective and globally suppress T cell responses. For example, rapamycin and mTOR kinase inhibitors globally inhibit differentiation of effector T cells and promote regulatory T cell development. However, complete immunosuppression is not always desirable, particularly in autoimmune disease. In some disease settings, such as asthma for example, a particular subset of T effector cell is responsible for disease pathogenesis. Atopic/allergic asthma seems to be driven by a Th2 response, but Th1 and Th17 subsets are largely not involved in the immune response[4]. Thus, it is desirable to specifically inhibit autoreactive Th2 cells in asthma, while leaving other helper T cell subsets untouched, in order to preserve immunity to foreign pathogens. Therefore, SGK1 may be a particularly promising target in treating allergic/atopic asthma, where Th2 subsets are primarily involved in promoting disease pathogenesis.

It has been well established that CD4+ and CD8+ effector and memory T cells are necessary for developing long-lasting immunity against tumors[5,6] Since loss of SGK1 lead to robust rejection of tumors, these results suggest that SGK1 may be a good target for anti-tumor immunomodulatory therapies. Furthermore, since loss of SGK1 in CD8+ T cells leads to enhanced memory differentiation, inhibiting SGK1 in T cells may also promote lasting tumor immunity. Finally, inhibition of SGK1 may also have an anti-proliferative effect on cancer cells directly, as several groups have reported that TORC2 signaling is

upregulated in certain cancers and tumor cells lines[7-9]. We propose that inhibitors of SGK1 may be used as chemotherapy or as adjuvant therapy to boost the efficacy of tumor vaccines.

In WT mice that fail to reject their tumors, we predict that tumor infiltrating lymphocytes become tolerant and fail to proliferate, resulting in few tumor antigen-specific T cells that make little IFNγ. However, we hypothesize that loss of SGK1 in T cells will lead to a robust CD4+ and CD8+ effector response characterized by a high numbers of antigen-specific, IFNγ-secreting T cells. To further enhance the anti-tumor immune response in *T-SGK1-/-* mice, we propose that combining deletion of SGK1 with inhibition of PD-1 will lead to complete tumor regression. In WT mice that fail to reject their tumors, we hypothesize that the anti-tumor immune response is ineffective because Teff become exhausted. Tumors express high levels of ligands for the PD-1 receptor, which is a marker of exhausted T cells. Even though *T-SGK1-/-* mice may mount a robust effector T cell response to tumor antigens, we cannot rule out the possibility that IFNγ-producing Teff become exhausted and thus ineffectual within the tumor microenvironment. This phenomenon could explain our observation that *T-SGK1-/-* mice have reduced tumor burden, but they cannot completely eliminate their tumors. Therefore, one future direction of this work might be to study the effects of loss SGK1 on tumor growth in combination with an antibody that inhibits PD-1. Monoclonal antibodies targeting PD-1 are commercially available and are currently being tested in clinical trials for treating melanoma, where they have demonstrated efficacy even in patients with advanced metastatic disease[10].

Our findings on the role of SGK1 in promoting anti-tumor immunity provide a therapeutic rationale for how inhibitors of SGK1 might be used in combination with

chemotherapy or other immunomodulatory agents like anti-PD1 in the treatment of neoplastic diseases. Notably, several small molecule inhibitors of SGK1 have been developed. One compound (GSK650394) is commercially available, and we plan to synthesize another compound that was recently published[11]. In future work, we would like to extend our tumor studies of *T-SGK1-/-* by treating WT mice with these inhibitors of SGK1.

Figure Legends

Figure 1. Summary of Findings. SGK1 represents a central node in a signaling complex downstream of mTORC2 that regulates CD4+ and CD8+ T cell differentiation. In CD4+ T cells, SGK1 phosphorylates and inhibits the E3 ligase NEDD4-2, resulting in decreased destruction of JunB. SGK1 also phosphorylates and inhibits GSK-3β, which phosphorylates and targets β-catenin for destruction. B-catenin upregulates transcription of its transcriptional co-activator, TCF-1, which represses IFN-γ. In CD8+ T cells, SGK1 phosphorylates Foxo1, which results in sequestration of this transcription factor in the cytoplasm. When Foxo1 is dephosphorylated, it translocates to the nucleus to bind to the enhancers of genes that promote memory differentiation, such as CD127 and eomesodermin.

References

1 Kerdiles, Y. M. *et al.* Foxo1 links homing and survival of naive T cells by regulating L-selectin, CCR7 and interleukin 7 receptor. *Nat Immunol* **10**, 176-184, doi:ni.1689 [pii] 10.1038/ni.1689 (2009).

2 Rao, R. R., Li, Q., Gubbels Bupp, M. R. & Shrikant, P. A. Transcription factor Foxo1 represses T-bet-mediated effector functions and promotes memory CD8(+) T cell differentiation. *Immunity* **36**, 374-387, doi:10.1016/j.immuni.2012.01.015 S1074-7613(12)00088-X [pii] (2012).

3 Delgoffe, G. M. *et al.* The kinase mTOR regulates the differentiation of helper T cells through the selective activation of signaling by mTORC1 and mTORC2. *Nat Immunol* **12**, 295-303, doi:ni.2005 [pii] 10.1038/ni.2005 (2011).

4 Galli, S. J., Tsai, M. & Piliponsky, A. M. The development of allergic inflammation. *Nature* **454**, 445-454, doi:10.1038/nature07204 nature07204 [pii] (2008).

5 Pardoll, D. M. & Topalian, S. L. The role of CD4+ T cell responses in antitumor immunity. *Curr Opin Immunol* **10**, 588-594, doi:S0952-7915(98)80228-8 [pii] (1998).

6 Klebanoff, C. A. *et al.* Central memory self/tumor-reactive CD8+ T cells confer superior antitumor immunity compared with effector memory T cells. *Proc Natl Acad Sci U S A* **102**, 9571-9576, doi:0503726102 [pii] 10.1073/pnas.0503726102 (2005).

7 Guertin, D. A. *et al.* mTOR complex 2 is required for the development of prostate cancer induced by Pten loss in mice. *Cancer Cell* **15**, 148-159, doi:S1535-6108(08)00436-4 [pii] 10.1016/j.ccr.2008.12.017 (2009).

8 Hietakangas, V. & Cohen, S. M. TOR complex 2 is needed for cell cycle progression and anchorage-independent growth of MCF7 and PC3 tumor cells. *BMC Cancer* **8**, 282, doi:1471-2407-8-282 [pii] 10.1186/1471-2407-8-282 (2008).

9 Masri, J. *et al.* mTORC2 activity is elevated in gliomas and promotes growth and cell motility via overexpression of rictor. *Cancer Res* **67**, 11712-11720, doi:67/24/11712 [pii] 10.1158/0008-5472.CAN-07-2223 (2007).

10 Brahmer, J. R. *et al.* Phase I study of single-agent anti-programmed death-1 (MDX-1106) in refractory solid tumors: safety, clinical activity, pharmacodynamics, and immunologic correlates. *J Clin Oncol* **28**, 3167-3175, doi:JCO.2009.26.7609 [pii] 10.1200/JCO.2009.26.7609 (2010).

11 Ackermann, T. F. *et al.* EMD638683, a novel SGK inhibitor with antihypertensive potency. *Cell Physiol Biochem* **28**, 137-146, doi:000331722 [pii] 10.1159/000331722 (2011).

Figure 1

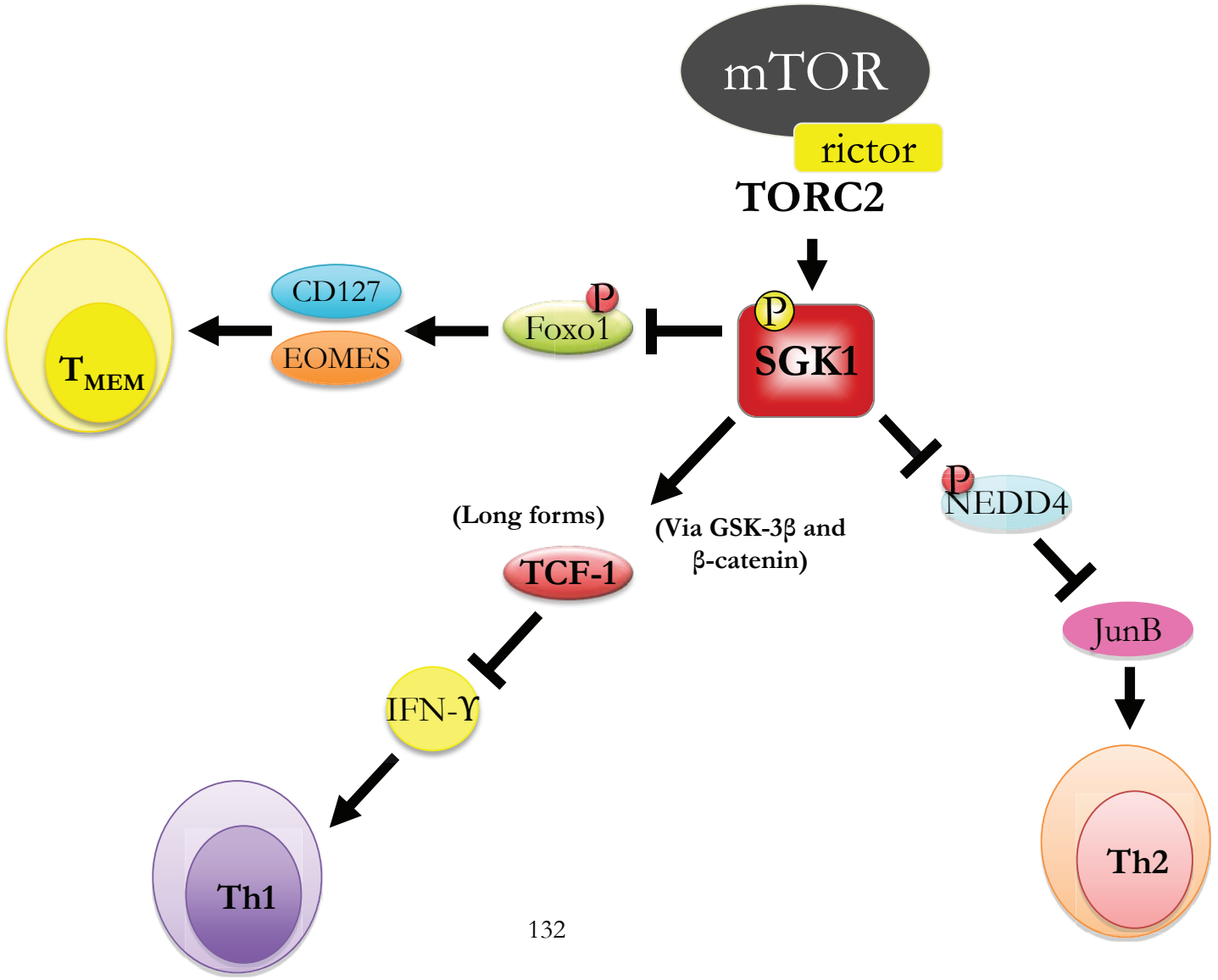
mTOR
rictor
TORC2
P
SGK1
P
Foxo1
CD127
EOMES
T MEM
(Long forms)
TCF-1
IFN-γ
Th1
(Via GSK-3β and
β-catenin)
P
NEDD4
JunB
Th2

CURRICULUM VITAE FOR Ph.D. CANDIDATES
Johns Hopkins University School of Medicine

Emily Heikamp **March 9, 2015**

Date and Place of Birth: October 2, 1983, New Orleans, Louisiana

Educational History

Ph.D.	2015	Program in Immunology	Johns Hopkins
expected		Mentor: Jonathan Powell, M.D., Ph.D.	School of Medicine
M.Sc.	2008	Medical Oncology	Oxford University
B.S.	2005	Biology	Duke University

Other Professional Experience

M.Sc. Thesis Research	2005-2007	Lab of Dr. Adrian Harris, Oxford University, Department of Medical Oncology
Undergraduate Research	2002-2005	Lab of Dr. Garnett Kelsoe, Duke University, Department of Immunology
Summer Research	2004	Lab of Dr. Vivek Mittal, Cold Spring Harbor Laboratory Undergraduate Research Program
Summer Research	2003	Lab of Dr. Alex Betz, Cambridge University, Department of Immunology

Scholarships, fellowships, and external funding

Medical Scientist Training Program, Johns Hopkins University School of Medicine. (2007-2015)

American Medical Association Seed Grant Award. (2012)

Academic Honors

2005 Marshall Scholarship. The Marshall Scholarship is a full scholarship for 2 years of graduate study at any British university. In 2005, I was among 44 students in the United States to be awarded the Marshall Scholarship.

2005 Faculty Scholar Award. The Faculty Scholar Award is awarded annually by the Duke University Academic Council to four of the most outstanding undergraduates in their respective fields.

2004 Barry M. Goldwater Scholarship. The Barry M. Goldwater Scholarship is a merit-based scholarship for undergraduate leaders in science, mathematics, and engineering. In 2004, I was among 310 students in the United States to receive this award.

2001 Angier B. Duke Memorial Scholarship. The Angier B. Duke Memorial Scholarship is a full-tuition merit scholarship for four years of undergraduate study at Duke University. In 2001, I was among 15 students in the United States to receive this award.

Publications

Heikamp EB, Patel CH, Collins S, Waickman A, Oh MH, Sun IH, Illei P, Sharma A, Naray-Fejes-Toth A, Fejes-Toth G, Misra-Sen J, Horton MR, Powell JD. (2014) The AGC kinase SGK1 regulates TH1 and TH2 differentiation downstream of the mTORC2 complex. Nature Immunology 15(5):457-64.

Powell JD, **Heikamp EB,** Pollizzi KN, Waickman AT. (2013) A Modified Model of T-Cell Differentiation Based on mTOR Activity and Metabolism. Cold Spring Harbor Symp Quant Biol 78:125-30

Heikamp EB, Powell JD. (2012) Sensing the immune microenvironment to coordinate T cell metabolism, differentiation & function. Seminars in immunology 24(6):414-20.

Delgoffe GM, Pollizzi KN, Waickman AT, **Heikamp E,** Meyers DJ, Horton MR, Xiao B, Worley PF, Powell JD. (2011) The kinase mTOR regulates the differentiation of helper T cells through the selective activation of signaling by mTORC1 and mTORC2. Nature Immunology. 12(4):295-303.

Powell JD, Pollizzi KN, **Heikamp EB**, Horton MR. (2012) Regulation of immune responses by mTOR. Annual Reviews in Immunology 30:39-68.

Sheldon H, **Heikamp E,** Turley H, Dragovic R, Thomas P, Oon CE, Leek R, Edelmann M, Kessler B, Sainson RC, Sargent I, Li JL, Harris AL. (2010) New mechanism for Notch signaling to endothelium at a distance by Delta-like 4 incorporation into exosomes. Blood 30;116(13):2385-94.

Li JL, Sainson RC, Shi W, Leek R, Harrington LS, Preusser M, Biswas S, Turley H, **Heikamp E,** Hainfellner JA, Harris AL. (2007) Delta-like 4 Notch ligand regulates tumor angiogenesis, improves tumor vascular function, and promotes tumor growth in vivo. Cancer Research 67(23):11244-53.

Davila M, Liu F, Cowell LG, Lieberman AE, **Heikamp E,** Patel A, Kelsoe G. (2007) Multiple, conserved cryptic recombination signals in VH gene segments: detection of cleavage products only in pro B cells. Journal of Experimental Medicine. 204(13):3195-208.

Nolan DJ, Ciarrocchi A, Mellick AS, Jaggi JS, Bambino K, Gupta S, **Heikamp E,** McDevitt MR, Scheinberg DA, Benezra R, Mittal V. (2007) Bone marrow-derived endothelial progenitor cells are a major determinant of nascent tumor neovascularization. Genes and Development. 21(12):1546-58. PMID: 17575055

Conferences & Presentations

Invited Talks

Heikamp, EB, Powell, JD. (2013) American Association of Immunologists (AAI) Annual Meeting, "mTOR regulates CD4 and CD8 effector T cell differentiation via serum- and glucocorticoid-regulated kinase 1 (SGK1)"

Heikamp, EB. (2012) Keynote Address, State of North Carolina Undergraduate Research & Creativity Symposium, "Lessons from an undergraduate education through the lens of research"

Heikamp, EB, Powell, JD. (2012) American Physician Scientist Association Annual Meeting, Oral Presentation & Travel Award. (Joint meeting of ASCI & AAP) "mTOR regulated CD4 T cell differentiation via SGK1"

Poster Presentations

Heikamp, EB, Powell, JD. (2011) FASEB Conference on Signal Transduction in the Immune System, Poster Presentation. "A novel role for serum- and glucocorticoid-regulated kinase 1 (SGK1) in T cell differentiation"

Heikamp, EB, Powell, JD. Keystone Conference on Cytokine Signaling, February 2012, Poster Presentation. "mTOR regulates CD4 and CD8 effector T cell differentiation via serum- and glucocorticoid-regulated kinase 1 (SGK1)"

Inventions, Patents, Copyrights

U.S. Patent Application Serial Number: 14/118,261
Filing Date: January 13, 2014
Authors: Emily Heikamp & Jonathan Powell
"TREATMENT OF AUTOIMMUNE DISORDERS AND INFECTIONS USING ANTAGONISTS OF SGK1 ACTIVITY"

Service and Leadership

Camp Sunrise Pediatric Oncology Volunteer (2012-present).

Camp Sunrise Gala Planning Committee (2012-present).

Founded Association of Women Student MD-PhDs (AWSM) at Hopkins (May 2012)

Founded MD-PhD Advising Program at Hopkins (September 2012)

Founded Triangle Undergraduate Research Symposium (2003), now the State of North Carolina Undergraduate Research and Creativity Symposium (2004-present)